2017

Constraint relaxation and cascading contingency monitoring: A risk-based approach

Xian Guo
Iowa State University

Constraint relaxation and cascading contingency monitoring:

A risk-based approach

by

Xian Guo

A dissertation submitted to the graduate faculty

in partial fulfillment of the requirements for the degree of

DOCTOR OF PHILOSOPHY

Major: Electrical Engineering

Program of Study Committee:
James McCalley, Major Professor
Venkataramana Ajjarapu
Ian Dobson
Cameron A. MacKenzie
Sunanda Roy

The student author, whose presentation of the scholarship herein was approved by the program of study committee, is solely responsible for the content of this dissertation. The Graduate College will ensure this dissertation is globally accessible and will not permit alterations after a degree is conferred.

Iowa State University

Ames, Iowa

2017

TABLE OF CONTENTS

Page

LIST OF FIGURES vi
LIST OF TABLES viii
NOMENCLATURE ix
ACKNOWLEDGMENTS xii
ABSTRACT xiv
CHAPTER 1. INTRODUCTION 16
1.1 Motivation and Problem Statement 16
1.1.1 Infeasibility in security constrained economic dispatch 16
1.1.2 Risk-based constraint relaxation for security constrained economic dispatch 17
1.1.3 Predictive risk-based constraint relaxation 18
1.1.4 Integration of renewables into risk-based constraint relaxation 18
1.1.5 Risk-based stress monitoring for cascading contingencies 19
1.2 Summary of contribution 19
1.3 Structure of dissertation 21
CHAPTER 2. BACKGROUND 23
2.1 Security constrained economic dispatch 23
2.2 Unmanageable constraints and infeasibility in SCED 24
2.3 Application of constraint relaxation in handling infeasibility of SCED 25
2.4 Risk-based optimal power flow 26
2.5 Summary 27
CHAPTER 3. CONSTRAINT RELAXATION AND INDUSTRY PRACTICE 28
3.1 ISO market mechanisms 28
3.2 Congestion management and constraint relaxation 31
3.3 State of art of constraint relaxation practice in ISOs 34

3.3.1 Constraint relaxation practice in the MISO 34
3.3.2 Constraint relaxation practice in the NYISO 35
3.3.3 Constraint relaxation in California ISO 37
3.3.4 Constraint relaxation in ERCOT 38
3.3.5 Constraint relaxation practices in other ISOs 40
3.4 Statistics of constraint relaxation practices in industry 41
3.5 Summary 47
CHAPTER 4. DETERMINISTIC RISK-BASED CONSTRAINT RELAXATION 48
4.1 Introduction 48
4.2 Literature review 48
4.2.1 Constraint relaxation of SCED in academic area 48
4.2.2 Constraint relaxation of SCED in industry 50
4.3 Formulation of industry-based constraint relaxation (A-CR) 51
4.3.1 Formulation 52
4.3.2 Determination of penalty price 53
4.4 Methodology of deterministic risk-based constraint relaxation 55
4.4.1 Definition and calculation of risk metric 55
4.4.2 Definition of risk indices 64
4.4.3 Risk Limits and Risk Table 65
4.4.4 Formulation of deterministic risk-based constraint relaxation 67
4.5 Case Study—IEEE test system 71
4.5.1 IEEE test system and parameter determination 71
4.5.2 Constraint relaxation results 72
4.6 Summary 75
CHAPTER 5. PREDICTIVE RISK-BASED CONSTRAINT RELAXATION 76
5.1 Introduction 76
5.2 Literature review 77

5.2.1 Look-ahead power scheduling in power system 77
5.2.2 Dynamic thermal ratings in power system 77
5.3 Dynamic heat balance equation 79
5.4 Conceptual illustration 82
5.5 Methodology of predictive risk-based constraint relaxation 85
5.5.1 Risk assessment 85
5.5.2 Formulation 86
5.5.3 Solving approach 89
5.6 Case Study on a representative IEEE test system 91
5.6.1 Parameter and data preparation for IEEE test system 91
5.6.2 Risk-based predictive constraint relaxation results 94
5.7 Case Study on contrived NYISO system 98
5.7.1 Evaluation of the mini-NYISO system 98
5.7.2 Constraint relaxation results 100
5.8 Summary 102
CHAPTER 6. STOCHASTIC RISK-BASED CONSTRAINT RELAXATION 103
6.1 Introduction 103
6.2 Literature review 103
6.3 Methodology of stochastic risk-based constraint relaxation 104
6.3.1 Relaxation margin determination 104
6.3.2 Risk assessment–Conditional value at risk 106
6.3.3 Scenario reduction of stochastic factors—Uncertainty set 108
6.3.4 Formulation and solving algorithm 110
6.4 Case Study 113
6.4.1 Relaxation margin determination 114
6.4.2 Two-stage RBCR 115
6.4.3 Analysis and comparsions 116
6.5 Summary 118

CHAPTER 7. RISK-BASED STRESS MONITORING FOR CASCADING CONTINGENCIES 119
7.1 Introduction 119
7.2 Literature review 120
7.3 Risk-based stress indicator 120
7.3.1 Definition and calculation of risk indicators 121
7.3.2 Power flow calculation based on successive line outage distribution factor (SLODF) 127
7.4 Development of risk-based stress indicator for cascading contingencies 129
7.4.1 Contingency selection 129
7.4.2 Procedure of developing cascading tree 130
7.5 Numerical example–a representative IEEE test system 131
7.5.1 Cascading tree development 133
7.5.2 Risk mitigation 136
7.6 Summary 138
CHAPTER 8. SUMMARY 139
8.1 Summary of contributions and work 139
8.2 Future work 141
REFERENCES 143
APPENDIX A. LMP CALCULATION 150
A.1. LMP calculation in A-CR 150
A.2. LMP calculation in optimality stage of the P-RBCR 152
APPENDIX B. DEVELOPMENT OF CONTRIVED NYISO SYSTEM 155
B.1. Transmission grid 155
B.2. Generator attributes 158
B.3. LSE attributes 160
B.4. Reserve requirements 160

LIST OF FIGURES

Page

Fig. 3.1. Energy market timeline in NYISO 29
Fig. 3.2. Day-ahead market process in the MISO 31
Fig. 3.3. GTDC in the NYISO market 36
Fig. 3.4. Updated Process for CR methodology in the NYISO 36
Fig. 3.5. The SCED optimization model in ERCOT 39
Fig. 3.6. Plot of CR occurrences for each violation category 42
Fig. 3.7. Distribution of shadow price for contingency cases with high CR occurrences 43
Fig. 3.8. Distribution of shadow price for transmission lines with high occurrences 44
Fig. 3.9. Example for investigating relationship between LMPs and transmission congestion ... 47
Fig. 4.1. Market operation timeline 57
Fig. 4.2. Severity function of circuit overloading 59
Fig. 4.3. Piecewise linear function for severity calculation 60
Fig. 4.4. Relationship between severity and overloading (circuit flow/conductor temperature).. 61
Fig. 4.5. Piece-wise linear severity function 62
Fig. 4.6. Flowchart of deterministic risk-based constraint relaxation 70
Fig. 4.7. Single-line diagram for the representative IEEE test network 72
Fig. 4.8. Overflow distribution ($\geq 0.9LTE$) 72
Fig. 5.1. Structure of the Predictive RBCR 77
Fig. 5.2. Relationship between the circuit current and the conductor temperature 81
Fig. 5.3. Change of the load and conductor temperature 83
Fig. 5.4. Flow chart of the P-RBCR solution procedure 90
Fig. 5.5. Simplified optimization formulations for solution procedure in the P-RBCR 90
Fig. 5.6. Network topology of a representative IEEE test system 91
Fig. 5.7. Relationship between current flow and conductor temperature 93
Fig. 5.8. Flow/Temperature change for line 24 under contingency 2 94
Fig. 5.9. Breakdown and comparisons of LMP between the A-CR and the P-RBCR 98
Fig. 5.10. Flow/temperature change for the Dunwoodie-NYC line 100
Fig. 5.11. LMP plots for the A-CR v.s. the P-RBCR 101
Fig. 6.1. The thermal rating characteristic as a function of loading duration 105

Fig. 6.2. Probability density function of the circuit flow 107
Fig. 6.3. A typical two-dimensional uncertainty set ($\gamma = 1.4$) 109
Fig. 6.4. Diagram of heavily-loading flows 117
Fig. 7.1. Illustration of the application of propagation risk 121
Fig. 7.2. The probability function of circuit trip 122
Fig. 7.3. Two-segment severity function 123
Fig. 7.4. Identified high-risk cascading tree 126
Fig. 7.5. Detection of isolated system 130
Fig. 7.6. High-level representation of network topology for RTS-96 system 133
Fig. 7.7. Flow change rate between normal and 'N-1' contingency 134
Fig. 7.8. Visualization of circuit risk 136
Fig. 7.9. Visualization of circuit risk (after risk mitigation) 137

LIST OF TABLES

Page
Table 3.1. Contingency list and CR occurrences 43
Table 3.2. Congested line list and CR occurrences 45
Table 4.1. MVL values of the MISO 54
Table 4.2. Demand curve for transmission constraints 55
Table 4.3. Illustration of Risk Table 67
Table 4.4. 'N-1' contingency probability 71
Table 4.5. Risk Table for IEEE test network 72
Table 4.6. Dispatch decision, costs and risk 74
Table 4.7. LMP at each bus 74
Table 5.1. Generator attributes 92
Table 5.2. Load attributes 92
Table 5.3. Transmission circuits parameters 92
Table 5.4. Comparisons on cost and risk 96
Table 5.5. Breakdown of LMP for A-CR and P-RBCR 96
Table 5.6. Limiting facilities 99
Table 5.7. Breakdown of LMP in A-CR 99
Table 5.8. Comparisons on production cost and risk 101
Table 6.1. Parameters of conventional generators 114
Table 6.2. Wind output scenarios 114
Table 6.3. Event probabilities 114
Table 6.4. The ATR for each circuit 115
Table 6.5. Constraint relaxation decisions 115
Table 6.6. Generation dispatch decisions 116
Table 6.7. CVaR and dispatch costs 118
Table 7.1. Circuit data in RTS-96 test system 131
Table 7.2. Cascading tree development 134
Table 7.3. Circuits with top 10 circuit risk 135
Table 7.4. Cascading tree after risk mitigation 137
Table 7.5. Circuits with top 10 circuit risk 137

NOMENCLATURE

ACRONYM

ATR	Adaptive transmission ratings
BMS	Business management system
CAISO	California ISO
CR	Constraint relaxation
CRM	Constraint reliability margin
CVaR	The conditional value at risk
DAL	Drastic action limit
DAM	Day-ahead market
DHBE	Dynamic heat balance equation
DLR	Dynamic line rating
ED	Economic dispatch
GTDC	Graduated transmission demand curve
IMM	Independent market monitor
ISOs	Independent system operators
LMP(s)	Locational marginal prices
LSEs	Load serving entities
LTE	Long time emergency ratings
MISO	Mid-continent ISO
MVLs	Marginal value limits
NYISO	New York ISO
OMCs	Out-of-market corrections
OPF	Optimal power flow
RA	Risk assessment
RAC	Reliability assessment commitment
RCPF	Reserve constraint penalty factors
RTC	Real-time commitment
RTD	Real-time dispatch
RTM	Real-time market

RUC	Residual unit commitment
SCED	Security constrained economic dispatch
SCUC	Security-constrained unit commitment
SLR	Static line rating
STE	Short-time emergency ratings
S-PS	Stochastic power scheduling
SPP	Southwest Power Pool
TCDC	Transmission constraint demand curve
VRLs	Violation relaxation limits

Index

i	Generator unit i
m	Bus m
a_{il}, b_{il}	The coefficients for piece-wise linear severity function
$k = 0$	Pre-contingency condition, i.e., normal condition
k	Post-contingency condition, $1, \dots, NC$
l	The l th circuit/ line/ branch, $1, \dots, NL$
s	The scenario for stochastic programming, $1, \dots, NS$
T	Time-period for look-ahead horizon, $1, \dots, NI$
ND	Total number of nodal load
N	Total number of buses
NG	Total number of conventional generator units
NS	Total number of scenarios
NW	Total number of generator units with variable output

Parameters

ρ_{Ctg}^{k}	The probability of event k
ρ_s	The occurrence probability of scenario s
$c_{G,i}$	Production costs of unit i, \$/MWh
$c_{W\_C,j}$	Wind curtailment cost, \$/MWh
D_m	Nodal loads at bus m
$D_{m,T}$	Nodal load of bus m at time period T

$Limit_l^k$	Transmission thermal limit of circuit l under event k, MW, $k = 0$, normal condition.
$P_{G,i,min}, P_{G,i,max}, P_{i,min}, P_{i,max}$	Generation output limits for conventional unit i
$P_{W,j,s,T}$	The output from variable unit j for scenario s at time-period T
$PTDF_{l,i}^k$	Power transfer distribution factor
$REG_{req,T}^{up}, REG_{req,T}^{down}$	Regulation reserve requirement, MW
$RMP_{G,i}^{up}, RMP_{G,i}^{down}$	Ramping capability of conventional unit, MW/min

Set

CCS	The set of critical contingencies
COCS	The set of critical overloaded circuit
CR	The set of candidate circuits that can be used for constraint relaxation, 'soft' constraints
NCR	The set of candidate circuits that are not allowable for constraint relaxation, 'hard' constraints

Variables

$\alpha_{l,s,T}^k$	The slack variable for circuit flow constraints
h_l^k	Power flow on circuit l at event k
$h_{l,s,T}^k$	Power flow on circuit l at event k of scenario s at time-period T
$P_{G,i,T}$	Generation output from conventional unit i at time-period T
$P_{i,T}$	Generation output from unit i at time-period T
P_m	Total generation output level at bus m
$P_{W\_C,j,s,T}$	Output curtailment from variable unit j
$REG_{G,i,T}^{up}, REG_{G,i,T}^{down}$	Regulation up and down provided by conventional unit i, MW
sev_l^k	Overload severity of circuit l at event k
sev_P, sev_C	Overload severity and conductor over-heating severity

ACKNOWLEDGMENTS

It is a fantastic journey with precious memories to accomplish this Ph.D. program and produce this dissertation. I would have never finished it without the prompt guidance from my major professor and other fellow faculties, the kind support from my dear friends and strong support from my family.

I would like to express the deepest appreciation to my major Professor, Dr. James McCalley, who has profound knowledge in power system and strict attitudes on scientific research. He offers me customized guidance and timely assistance through all periods of my PhD study. He is always patient to my puzzles and always encourages me with my achievements. Nevertheless, He continually and convincingly conveys the approaches to learn knowledge and conduct creative research. His guidance and help are indispensable for making this dissertation possible.

I would like to thank the rest of my committee, Dr. Ian Dobson, Dr. Venkataramana Ajjarapu, Dr. Cameron A. MacKenzie and Dr. Sunanda Roy, who devote significant time and efforts to the development of my dissertation. Thank you for your encouragement, insight comments to motivate the enhancement on my research.

My sincere thanks go to the fellow PhD candidate, Shiyang Li, and Dr. Guangyuan Zhang, who are great friends and always generous and ready to help with my research. Their timely advices and comments are very valuable to enhance my research. I also would like to thank other fellow students, Qian Zhang, Dr. Ali Jahanbani, and Dr. Hussam Nosair, who offer me valuable comments and kind help on various aspects of my research. My sincere thanks also go to faculty and staff members in Electrical and Computer Engineering department of Iowa State University for offering such a great environment for power system study and research. I would like to thank the other fellow students for all the great times we have shared.

I would like to thank Dr. Vladimir Koritarov and Dr. Muhammad Marwali, who is the advisor for my internship in Argonne National Lab and NYISO, respectively, where I built up my professional abilities and combined industry experiences with academic research. I also would like to thank Dr. Haozhong Cheng from Shanghai Jiao Tong University, who is my major professor for my M.S. program; he guided me to the power system research, and helped improve my research capabilities and potentials. My sincere thanks also go to the fellow students in Dr. Cheng's research group, for the kind help and great moments we have experienced.

Finally, I am deeply thankful to my grandmother from father's side, my parents, my elder brother, He Guo, who encourage me to start the PhD study and always cheer me up. Their strong support and endless love provide me strength to overcome all the obstacles and challenges during this PhD program, and they help me live through the most tough moments. I dedicate this dissertation to the memory of my grandma from mother's side, who was always proud of my achievements and continuously performed supports on my study.

The last word of the acknowledgement is saved for Guangyuan Zhang. Thank you for your continuous understanding, love, caring and support.

ABSTRACT

Transmission constraint violation can cause the infeasibility in security constrained economic dispatch (SCED) due to insufficient control flexibility. To eliminate this infeasibility, the approach of constraint relaxation (CR) is applied to expand the feasibility region of SCED problem. The current general industrial practice for solving the infeasibility of SCED is by adding the slack variable to relax the infeasible transmission constraint and penalize the slack variable with penalty cost in objective function. The deficiency of industrial method is that the penalty cost of slack variable is determined based on heuristic which does not reflect its effect on system security. In this dissertation, a risk-based constraint relaxation (RBCR) model is proposed for overcoming the deficiencies of the industry approach. RBCR produces feasible solutions via constraint relaxation with controlled risk exposed to the system. In this approach, the thermal limits of individual circuits are relaxed while the exposed risk is controlled simultaneously; this approach prevents the artificial selection of penalty prices, therefore reduces the tendency of locational marginal prices (LMPs) spike in the electricity market.

To reflect the inter-temporal effect of CR, the multi-interval look-ahead SCED, which simultaneously optimizes the binding interval and several look-ahead advisory intervals, is applied to co-optimize the production cost and system risk in the multi-interval SCED model. Based on the initial system condition and time variant effects of transmission thermal limit, the methodology of predictive risk-based constraint relaxation is developed which is capable of utilizing inter-temporal effects, as well as managing conduct temperature. The risk metric is proposed, and it is used by constraining it so that the effects of constraint relaxation on system security can be controlled. The methodology of predictive risk-based constraint relaxation has been tested and investigated on both the representative IEEE test system and a contrived model of an actual

independent system operator (ISO) network. With the increasing penetration of variable energy resources, system operation incurs an increasing amount of uncertainty. In the framework of stochastic risk-based constraint relaxation, the concept of conditional value at risk (CVaR) is utilized to develop the alternative risk indices. Based on alternative risk metric, the methodology of two-stage stochastic constraint relaxation is formulated and tested on a representative network. The testing results indicate that the methodology of risk-based constraint relaxation has a better performance than that of industry model of constraint relaxation, in terms of operation cost and system risk. Furthermore, it can effectively reduce LMP spikes with maintain the appropriate congestion signal unmasked.

Nevertheless, not all circuits are available for constraint relaxation. To identify weak areas under an operating condition, actionable steady-state risk-indicators are developed for cascading contingency monitoring. The cascading tree is developed according to the propagation risk, and then the cascading tree risk is utilized to evaluate the propensity of cascading contingencies at the operating condition. Application of circuit risk is beneficial for system operator to identify abnormal condition and weak areas in current network topology. Finally, re-dispatch is recommended for risk mitigation on system exposure to cascading risk. The theory of risk-based stress monitoring for cascading contingency is examined on an IEEE test system.

CHAPTER 1. INTRODUCTION

1.1 Motivation and Problem Statement

1.1.1 Infeasibility in security constrained economic dispatch

The security constrained economic dispatch (SCED) has been widely used in power system electricity markets, to derive dispatch decisions and settlement for both day-ahead market (DAM) and real-time market (RTM). The objective is to minimize production costs while satisfying demand as well as the system security requirements. The system security requirements include both that under normal (pre-contingency) conditions and that under post-contingency conditions (NERC's class B contingencies, also known as, 'N-1' contingencies). The SCED also enforces other constraints such as minimum and maximum MW output for generators, as well as regulation and contingency reserve requirements.

The SCED is a linear program and is therefore a convex programming problem. Thus, if a solution is obtained by the optimization engine, it is certain that the solution is indeed optimal. However, there is no guarantee that the optimization engine will be able to identify a solution, because the problem may be infeasible[1]. An infeasible problem indicates that there is no solution can satisfy all eligible constraints simultaneously. The infeasible SCED is problematic because it means that the market has failed for that condition, which is an unacceptable outcome.

In general, the common sources for infeasible SCED include 1) over-generation or under-generation of generating units and 2) overloads on transmission line, either under normal or post-contingency conditions. Specifically, the most observed and frequently occurred infeasibilities are resulting from transmission line overloads. Thus, the scope of this dissertation is focused on the

[1] Such infeasible condition occurs quite frequently, as addressed in Section 2.2.

transmission overloading related infeasible SCED problem. The approach to handling such infeasible problems is to relax one or more eligible constraints (Constraint Relaxation, CR) for transmission flow limits. The reason why constraint relaxation for circuit flow limits can be considered is that it is possible to allow flows on circuits in excess of their modeled boundary within a limited time basis, since transmission thermal limits generally have some margins due to the fact that they are set under conservative conditions (such as cold winter and hot summer).

The deterrent to relaxing transmission limits is that it exposes the power system to increased stress on system security. The effects on system security should be controlled while conducting CR. This is the motivation for proposing the concept of risk metric. Based on this, the methodology of risk-based constraint relaxation (RBCR) is developed to solve infeasible SCED problems. Following the brief introduction about SCED and its infeasibilities, the state of art for CR practice in industry is investigated and summarized, and the industry-based CR methodology (the industry-based CR methodology is referred to as applied constraint relaxation with the acronym A-CR) is formulated as well. Then, the methodology of CR is explored in detail for three typically practical occasions: 1) single time-interval SCED (defined as deterministic RBCR, D-RBCR); 2) multi-interval look-ahead SCED (defined as predictive RBCR, P-RBCR) and 3) SCED with renewable sources (defined as stochastic RBCR, S-RBCR). Furthermore, the risk metric is applied to identify the high-risk cascading sequence under an operating point. This application can provide restrictions for CR actions. In other words, those weak circuits will not be relaxed, since their outage will impose relatively high cascading risk on the system.

1.1.2 Risk-based constraint relaxation for security constrained economic dispatch

This research starts with the most common and classic SCED problem—single time-interval dispatch. An overloading circuit survives until it reaches at a certain level within the

limited time basis (i.e., 5 minutes). The relaxation margin is determined by the adaptive transmission ratings (ATR). The set of risk indices, including the system risk, the contingency risk and the second contingency circuit risk are proposed to restrict the negative stress imposed on the system.

1.1.3 Predictive risk-based constraint relaxation

Under the situation of look-ahead SCED optimization problem, multiple time-intervals are involved. The methodology of deterministic RBCR, which is designed for single time-interval problem, is not applicable. Considering load change and the action of re-dispatch, overloading that exists in current time interval may disappear in the next time interval[2]. In addition, it is noted that the actual limitation for circuit flow is conductor temperature along that circuit. The maximum temperature that the conductor can withstand restricts the allowable flow over that circuit. Based on these observations and thoughts, the methodology of predictive RBCR is proposed, which considers conductor temperature instead of power flow management and allows for both pre-contingency overloads and post-contingency constraint violations being addressed. It can capture inter-temporal effects, as well as prepare current system with future operation conditions. Furthermore, the effects on system security level imposed by constraint relaxation are monitored and controlled by risk metrics, which is similar to that of the deterministic RBCR.

1.1.4 Integration of renewables into risk-based constraint relaxation

The stochastic power scheduling (S-PS) has been investigated to deal with increasing penetration of variable and uncertain resources, such as wind energy and solar energy. However, similar to the deterministic power scheduling problem, model infeasibilities are frequently observed, which result from thermal overloads on transmission lines, in which the transmission

[2] In general, the time-interval for SCED problem is five minutes in current market structure.

thermal limits are violated. A systematic way is proposed to handle the thermal overloading in S-PS, especially in stochastic look-ahead SCED problem. It solves the model by relaxing thermal limits with degraded effects being imposed on system security, which are evaluated and represented by stochastic risk metrics.

1.1.5 Risk-based stress monitoring for cascading contingencies

When constraint relaxation is conducted on overloaded circuits, severe consequences can be stimulated for overloading some circuits. Those consequences include incurring successive cascading contingency, even network blackout. Thus, the weak and sensitive area should be identified, which with the relaxation can expose the power system to severe cascading risk. Furthermore, it is necessary that specific stress indicators are active in continuously monitoring current power systems for its exposure to potential cascading events. This is the motivation for proposing risk-based stress indicators to monitor cascading contingencies, which can provide information for constraints that cannot be relaxed, as well as generate early warnings and provide situation awareness for the system operator to take immediate action, for the purpose of relieving the system stress.

1.2 Summary of contribution

The major contributions of the research work are summarized as follows:

- **Developed methodologies for constraint relaxation decision-making within the framework of SCED.**
    - Deterministic model: In the developed framework of risk-based constraint relaxation for deterministic SCED, risk indices are defined and proposed to evaluate the system security level, by which the conducting of constraint relaxation satisfies the

requirement that the effects on system security are under control by allowing the overloads along transmission circuits. ***(Chapter 4)***

- Predictive model: For the multi-interval look-ahead SCED, the framework of predictive risk-based constraint relaxation is developed, which utilizes inter-temporal effects with conductor temperature management and provides a relaxation solution more optimized and economic for the performance of control. (***Chapter 5***)
- With integration of high-penetration renewable energy resources, the RBCR methodology is extended and re-designed for cooperating with stochastic factors, which can address multiple dispatch conditions in a more economical and secure way. ***(Chapter 6)***

- **Proposed, illustrated and tested the methodology of cascading assessment**

  Based on the developed risk-based indicator for monitoring the steady-state stress, an approach is formulated for identifying propensity of cascading contingencies under an initial event (a steady-state operating point or an initial contingency). It can identify weak areas within a power system, which should not be applied with the methodology of constraint relaxation. Furthermore, it has observable benefits of guiding the system operation and improving situation awareness. ***(Chapter 7)***

The relationships among major contributions of the dissertation are indicated in Fig.1.1.

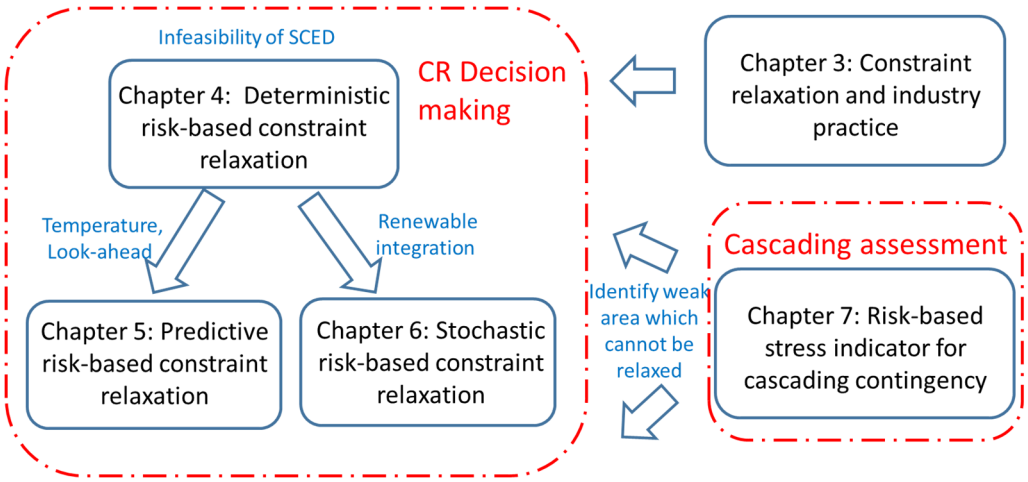

Fig1.1. Summary of major contributions

1.3 Structure of dissertation

This dissertation consists of eight chapters organized as follows.

- Chapter 1 is the introduction which describes the motivation and problem statement; it also summarizes major contributions.
- Chapter 2 provides the problem background, describing unmanageable constraints and introducing the risk-based optimal power flow.
- Chapter 3 is the summary of the CR practice in industry and the motivation for conducting CR-related research.
- Chapter 4 introduces the definition and calculation of risk metric and proposes the set of risk indices for conducting constraint relaxation; it also develops and formulates the methodology of risk-based constraint relaxation for the deterministic SCED problem.
- Chapter 5 describes the motivation for utilizing dynamic heat balance equation within the multi-interval look-ahead framework, and formulates the corresponding optimization model of RBCR for the predictive SCED problem.

- Chapter 6 extends the theory of risk-based constraint relaxation to the situation where there exists significant penetration of variable generation resources (e.g., wind and solar energy). The stochastic risk factors are explicitly modeled in this chapter.
- Chapter 7 develops the methodology of risk-based assessment for cascading contingencies, using K^{th} -order power flow by successive line outage distribution factor and investigates approaches of re-dispatch to mitigate the cascading risk.
- Chapter 8 summarizes and concludes the dissertation and provides suggestion for future work.

CHAPTER 2. BACKGROUND

Security constrained economic dispatch has been widely used in both system operation and electricity market settlement. However, unmanageable constraints and the resulting SCED infeasibility can occur under certain operating conditions. The necessary background associated with this problem is described and provided in this chapter.

2.1 Security constrained economic dispatch

The priority objective of modern electricity grids is that generation supply is guaranteed to satisfy load requirements. However, uncertain factors are observed frequently in objects of both generation side and demand side: 1) demand vary greatly over the time of a day, a week or a year; 2) the generation costs and ramping performance are different among various generator technology type; 3) the penetration of intermittent renewable energy, such as wind power and solar energy, increases significantly. Thus, the conventional optimal power flow (OPF), or economic dispatch (ED) cannot satisfy the requirements of reliable power supply. Furthermore, in the common applied concept of preventive operation, the network security constraints at both normal condition and contingency condition should be considered simultaneously, to construct preventive SCED. The solution of SCED provides dispatch decisions for real-time operation to minimize the production cost while maintaining the system reliability.

The SCED is widely deployed by independent system operators (ISOs) as the application within day-ahead electricity market and real-time electricity market for determining generator dispatch and locational marginal prices (LMPs, or LBMP). The SCED should satisfy generators related constraints (e.g., MW output and reserve requirements) and transmission related constraints, such as circuit thermal limits under both normal and ‘N-1’ contingency conditions.

2.2 Unmanageable constraints and infeasibility in SCED

Under some operating conditions, the SCED is unable to provide a feasible dispatch solution, since all the constraints cannot be satisfied simultaneously. Specifically, the overloads along transmission circuits is one of the most common factors.

The industry refers the term 'unmanageable constraint,' to the situation that a branch overloading cannot be decreased below its thermal limit within a five-minute time horizon with reallocation of all available resources. This is a significant issue in congestion management. According to the Independent Market Monitor (IMM) market status report of Mid-continent ISO (MISO) in 2007, about 25% of binding constraints cannot be managed on a five-minute basis [1]. The investigation in MISO indicates that the primary reasons for unmanageable constraints are: 1) generation inflexibility, i.e., limited re-dispatch capability among system generating units and 2) impropriate selection of parameter in market engine, which causes the misleading actions of market software (such as not re-dispatch insensitive resources for alleviating transmission congestion). However, the occurrence of unmanageable constraints does not necessarily mean that the system is in violation of NERC requirements, considering that such overflows can be mitigated within the operating horizon of 30 minutes.

Unmanageable cases include infeasible cases, which are generally due to the inability to resolve a transmission constraint violation. This is caused by insufficient control capability because that the constraints adjustments are related to ramping rate, regulation reserve and unit capacity. The research in this dissertation is focused on infeasible cases. Unmanageable cases are also frequently observed in other ISOs among system operations.

2.3 Application of constraint relaxation in handling infeasibility of SCED

From the mathematical point of view, the general approach for handling such infeasibilities is to apply constraint relaxation, where one or more constraints are relaxed to a certain level sufficient to obtain a feasible solution, thus eliminating the infeasibility. In electricity markets and infeasible SCED problem, this is considered as a reasonable approach because emergency thermal rates of conductors are evaluated with some margins so that they can withstand slightly higher loadings for a limited time basis [2]; for example, the actual loading can reach as high as 110% of the long-term emergency (LTE) rating if the time duration of the overload is short enough. This feature provides the foundation for the application of CR in obtaining an operating solution (and thus a market solution) for SCED problems that would otherwise be infeasible.

There are four common categories for CR actions. 1) Accepting a relaxed constraint 'as is' because it does not cause much risk of damage to the circuit or of additional cascading consequences to the system. This action is eligible to relax constraints imposed by contingency conditions; it should be cautious regarding using this approach to relax constraints imposed by normal conditions. 2) Accepting a relaxed constraint because it will be possible to take a corrective action to relieve the constraint if the contingency occurs. This action can be used only for constraints imposed by contingency conditions. 3) Utilizing monitoring equipment that reduces uncertainty associated with sagging and annealing of the circuit. This is essentially category 1), with the requirement that the investment in monitoring equipment has been made. This approach is very attractive for circuits that experience frequent constraint violations under normal conditions. 4) Utilizing load curtailment. In this dissertation, the focus is on category 1), emphasizing on the control of additional stress exposed to the system, which is evaluated and represented by risk metrics.

2.4 Risk-based optimal power flow

Risk assessment (RA) is a common methodology and has been widely implemented in other industries such as nuclear, aerospace, oil, food, public health, information technology and financial engineering. There is research work on exploring the application of risk assessment for thermal overload-related constraints; the implementation of risk assessment on security assessment is relatively new, with the first publication on this topic published in 2003 and many others published thereafter.

According to the IEEE standards, risk can be defined and calculated as the product of occurrence probability of a contingency multiply by the outcomes of that contingency. The obstacles and challenges are observed when quantifying both the occurrence probability and the outcomes of an event.

As a developing new research direction, risk-based approach has been explored in certain research area on power system. References [3] and [4] describe the application of risk metric in obtaining power system planning schemes; references [5] and [6] implement risk-based theory in power system maintenance. It can be noted that most of the previous work are focused on risk-based security assessment (RBSA). Until then, research on real-time applications of risk-based methodology is limited and none of them is applied for handling infeasibility in SCED problem. The framework of risk-based approach application for power grid is proposed in [7] and [8], but it does not cover detailed specifications and realizations of this risk-based framework. Reference [9] proposes the methodology of risk-limiting dispatch under the background of smart-grid. The risk-limiting methodology does cooperate with stochastic factors from renewable energy resources and demand response, however, the deployment to the ISOs system is relatively challenging. References [10] and [11] did significant work on exploring the application of the risk-based

optimal power flow, especially risk-based SCED and congestion management. Its work is oriented by embedding risk and the corresponding benefits to the real-time OPF software. The introduction and application of the coordinating parameters realize the trade-offs between system economy performance and system security level by conducting risk-based SCED. These studies and achievements have paved the way for implementing risk metric in handling infeasibility in SCED problems.

2.5 Summary

This chapter provides research background. It introduces the concept of unmanageable constraints, unmanageable cases and infeasible cases, and points out that the focus of the research in this dissertation is infeasibility in SCED. In addition, it describes the reason why the approach of constraint relaxation is critical and can be applied in handling infeasibility of SCED. Furthermore, it introduces the concept of risk-based optimal power flow. Thus, this chapter lays out the foundation for the remainders of this dissertation.

CHAPTER 3. CONSTRAINT RELAXATION AND INDUSTRY PRACTICE

The security constrained economic dispatch is the critical component of the electricity market engine (for example, this market engine is referred to as the Market Information System in the MISO and the Business Management System (BMS) in New York ISO, NYISO). The objective of SCED is to minimize production costs, subject to network and generation limitations. The model formulation itself is complex, including tens of thousands of nodes and hundreds of thousands of constraints. Slack variables are employed within the constraints with a pre-defined penalty price, to assure that the market software is always able to obtain a feasible market solution. This action is called constraint relaxation, as has been mentioned in previous sections.

3.1 ISO market mechanisms

The wholesale electricity market consists of two settlement systems–day-ahead market (or forward market) and real-time market (or spot market). Fig. 3.1 conveys the timeline of energy market process for the NYISO and is representative of timelines adopted by other market operators. The DAM is a financially binding market, in which the energy is purchased or sold one day prior to the operating day and accounts for around 94% of energy transactions. Based on the forecasting input data (such as load forecast, variable energy output, regulation and reserve procurement), the DAM schedules the available generators on an hourly basis for the next operating day, and it is optimized in terms of economic performance, i.e., total production costs of energy and reserves. The RTM is a balancing market, which balances the DAM schedule with the actual energy consumption during the operating day based on five-minute time intervals. Currently, both the security constrained unit commitment (SCUC) and the SCED algorithms utilized among all ISOs, to administer the competitive auction processes, are deterministic.

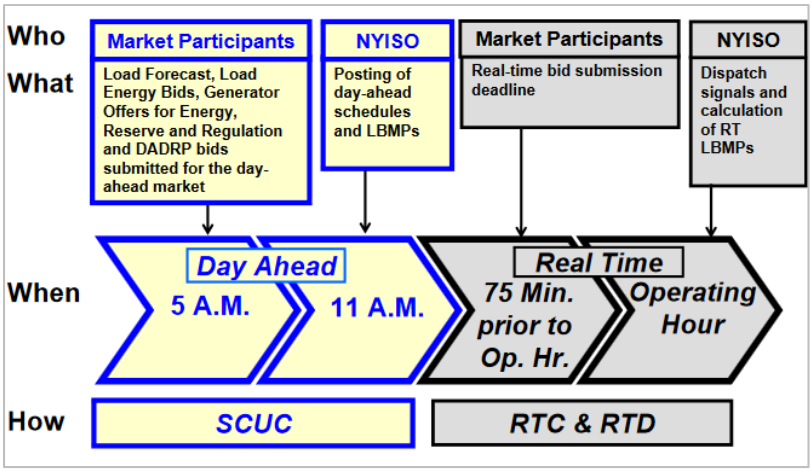

Fig. 3.1. Energy market timeline in NYISO [12]

Motivated by the varying market rules among the ISOs, customized functionalities have been added to this basic market structure. The NYISO employs the real-time commitment (RTC) approach, which allows commitment of available fast-response resources (such as gas-turbine units, GTs) and proposes advisory commitment-dispatch decisions for the reminder of the optimization period, before enforcing the real-time dispatch (RTD, which is conducted on 5-minutes time-interval) [13]. In addition, the NYISO energy market algorithm co-optimizes energy consumption and ancillary services, reflecting a feature that is common among most ISOs. The California ISO (CAISO) conducts market power mitigation tests to determine whether bids and offers are valid; the residual unit commitment (RUC) is established following the basic SCUC process. The RUC provides information about additional resources to stand by during the real-time operating stage [14]. MISO runs the reliability assessment commitment (RAC) after publishing the DAM results; the purpose of the RAC is to allocate generator scheduling motivated by reliability requirements [15].

Multiple passes (runs) are deployed in executing the RTD. In the NYISO market software, the RTD procedures consists of Physical Pass and Ideal Pass. Physical Pass is a mixed-integer optimization program which includes non-convex ramping products and quadratic production cost.

The purpose of Physical Pass is to simulate the system as realistic as possible to produce the base point for energy dispatching. Ideal pass is a linear program which approximates the complex non-linear modeling and is capable to compute LMPs. Specifically, fast-start GTs are treated distinctly in these passes: in Physical Pass, blocked bid limits are utilized for GTs; in Ideal Pass, GTs are dispatched across the entire operating range to set prices [16]. A similar mechanism is implemented in the CAISO market, which are referred to as Scheduling Run and Pricing Run. In Scheduling Run, self-schedule curtailment and relaxation of constraints can help market software arrive at a solution when simply considering the energy bid is not possible, subjecting to the system energy balance, congestion management and ancillary service requirements. The distinctive feature between the CAISO approach and the NYISO approach is that both dispatch schedules and price signals are provided in Scheduling Run and Pricing Run in the CAISO approach. However, for the settlement purposes, dispatch schedules are achieved from Scheduling Run, and nodal prices are taken from Pricing Run [17].

Out-of-market corrections (OMCs) refer to those actions necessary to adjust or correct market solutions, which cannot satisfy reliability or operational requirements. Those market solutions achieved by relaxation will be evaluated by the corresponding test and review procedures, and this guarantees that the solution is physical feasible. The review and resulting necessary OMCs ensure that the CR methodology is applicable to achieve a market solution. The terminology for OMCs among ISOs includes ‘uneconomic adjustments’ and ‘exceptional dispatches’ in the CAISO and ‘out-of-merit energy/capacity’ in the ERCOT [18]. Fig. 3.2 describes the DAM process in the MISO and how OMCs are integrated into the market process, which can be considered as a representative example. A deliverability test is performed to check the impacts on system reliability and stability; once the test fails, necessary adjustments and improvements will be

activated. No action is required if the market solution passes the testing and review procedures. Those solutions passing Operator Review are qualified for the submittal to the DAM postings.

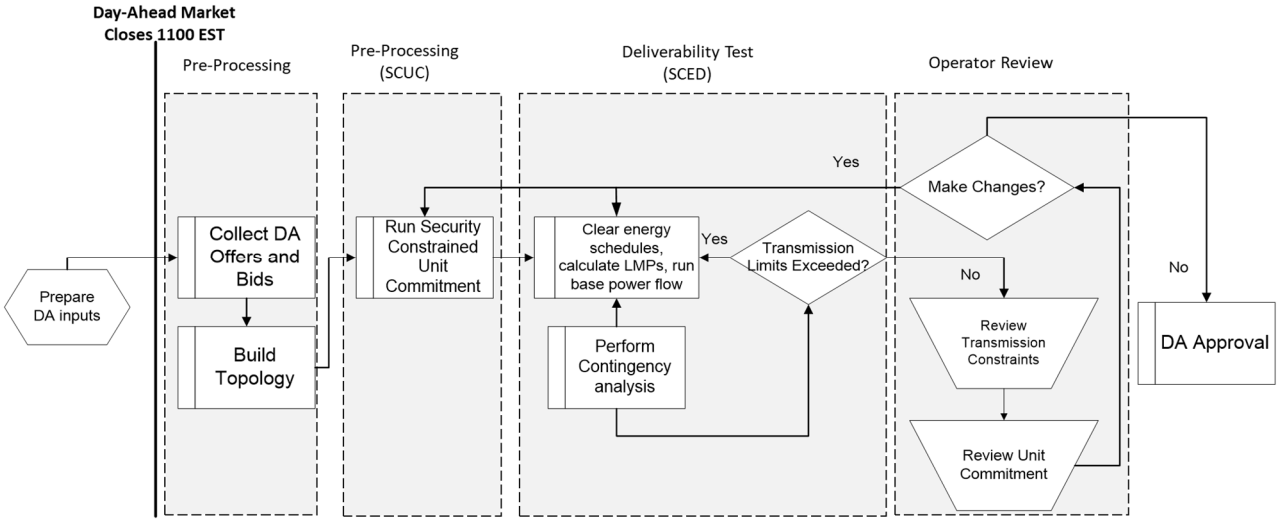

Fig. 3.2. Day-ahead market process in the MISO

3.2 Congestion management and constraint relaxation

Transmission congestion is a common and critical challenge facing majority of the system/market operators in North American power grid. Transmission congestion occurs due to the insufficient capability of transmission circuits to deliver power from the generator (sources) to load serving entities (LSEs, sinks). The resources resulting in transmission congestion include:

- Imbalance distribution of source and demand: Production cost is significantly reduced when low-price fuel is procured via economic dispatch. Thus, more generation is committed in the low-priced fuel region, less in the high-priced fuel region, and energy is transferred through transmission circuits from the low-priced fuel region to the high-priced fuel regions. This has the potential to fully load up the interfaces (or tie-lines) between low-priced fuel regions and high-priced fuel regions.
- Outage of transmission facilities: The occurrence of a single circuit-outage (or cascading outage of multiple circuits) shifts flow from the outage circuit(s) to circuits constructing

the parallel power transfer paths; this can incur overloading circuits located at the parallel power transfer paths.

- Allocation of generation and demand: Load concentration and generation resource location can also be a resource for transmission congestion. For example, in the NYISO, almost 50% of LSEs is located in the southeastern region of the state (including New York City and Long Island), typically has a relatively high local energy price provided by oil-fueled units and GTs in the local region. In the remaining territory of the state, relatively low-priced energy is available from, for example, hydroelectric resources (either internal Niagara Falls or external Hydro Quebec power). Thus, the congestion pattern, which has been observed for decades, is that significant congestion exists along the interface between central and eastern New York State. Such phenomenon results from the fact that less expensive power transfers from the western/central area to the southeastern part of the state via those interfaces.
- Other common reasons: Other typical reasons have been observed or have the potential to result in congested transmission facilities are reported as outage of generation fleet and increasing demand requirements form LSEs.

Transmission congestion has severe impact on system reliability and market efficiency. Thus, actions to avoid or relieve congestion are required and necessary. Those actions are referred to as congestion management. Classified by the economic categories, common congestion management approaches include 1) investment on power system planning to increase transfer capability, including constructing new transmission lines, upgrading existing transmission facilities, installing phase-shifters and/or flexible AC transmission system (FACTS) devices, which can result in costs and the expenses are allocated by transmission owners; and 2) operational

processes in response to transmission congestion, which involves actions taken by generating companies (GenCos) and LSEs [19], for the purpose of redistributing network flows.

Transmission congestion can be conceived as falling within two categories, depending on whether the currently enforced flow limit (also called original flow limit) associated with the congestion can be satisfied or not. If it can be satisfied, then a feasible SCED solution is achieved such that the flow equals to the original flow limit. If it cannot be satisfied, a feasible SCED solution can only be obtained if the circuit flow is allowed to exceed the flow limit; this second category requires constraint relaxation and is considered a special kind of congestion management approach. The infeasibilities SCED involved in this dissertation are associated with the second category. However, both categories of congestion are typically identified in public postings from ISOs as binding constraints.

Significant benefits can be obtained through the application of CR:

- Eliminating infeasibilities. The generation dispatch/scheduling with appropriate LMPs are required for power system operations and market settlement. It is necessary that slack variables are added to relieve the overloading network constraints and to allow a limited and temporary violation. Thus, the feasible operating solution is obtained, as well as the corresponding market settlement.
- Significant economic benefits. The constraints in SCED are approximated by the best applicable knowledge about the network and modelling capabilities in operation and market software; however, imposing them strictly and consider them as 'hard constraints', independent of their economic impact, can result in significant increases in operation costs. Thus, softening these limits with careful consideration on the impact of reliability can reduce production costs significantly.

- Price management are available with employment of CR action. Penalty prices associated with slack variables can cause LMPs to increase significantly when CR is implemented. Those LMP increases are direct reflections of system congestion and capacity scarcity, and they can serve as a price signal to the market participants to make prompt actions, such as modify their bids and offers accordingly and other actions which invariably result in decreasing the corresponding violated flow.

3.3 State of art of constraint relaxation practice in ISOs

Based on literature review and personal contact with several ISO market experts, the CR practice can be summarized in the high-level perspective is that it introduces slack variables in the transmission circuit constraints for both normal conditions and contingency conditions. The slack variables are included in the objective function with a pre-defined penalty price. Thus, the determination of penalty price is a critical issue in the CR practice of ISOs. This subsection investigates and summarizes the CR practice among various ISOs.

3.3.1 Constraint relaxation practice in the MISO

CR occurrences in the real-time market are relatively frequent; it can occur for both normal condition and contingency conditions [20]. The constraint relaxation practice in the MISO's market operations starts with a two-step solving mechanism. The first step is to assign a relatively high penalty (on the scale of several thousand dollars) to reduce the constraint violations; the shadow price for the corresponding constraint is set at the penalty price once violations are required to achieve a feasible solution. However, the above step cannot reflect the true cost of managing the transmission circuit congestion; at some point, the violations are not able to be mitigated no matter how high a penalty price is enforced. The second step determines the incremental re-dispatch costs of relieving congested circuits, in which transmission thermal limits are updated by

adding slack variables, produced in the first step, and correspondingly, the reliability margin is added on top of the original limit.

The disadvantage of this two-step CR approach is that it may not identify the best relaxation and pricing values for the violated constraints, and it has the potential to result in over-relaxation or under-relaxation. Specifically, over-relaxation (and underpriced) for transmission violations has been frequently observed. Furthermore, the shadow price is set to zero when there are no available resources for re-dispatch actions. Thus, the independent market monitor suggested to discontinue the second step for Non-Market-to-Market constraints (effective February 1, 2012), and it specified that appropriate penalty price mechanisms should be developed to reflect the transmission congestion and resource scarcity. Then, flat default marginal value limits (MVLs) were proposed by voltage level, followed by the two-step transmission constraint demand curve (TCDC), which is deployed to achieve the trade-off between violation frequency/quantity and the magnitude of shadow price [21]. MVLs with TCDC are currently utilized as CR mechanisms in the MISO markets.

3.3.2 Constraint relaxation practice in the NYISO

In the economic logic of the NYISO BMS, the transmission circuit limit is associated with the constraint reliability margin (CRM). CRM is introduced for critical transmission facilities, to guarantee system reliability and operational security. Normally, the NYISO sets a CRM of 20 MW on its transmission facilities. Transmission facilities have a different CRM value as indicated in [22]. The procedure of 'feasibility screening' is implemented to determine whether a transmission constraint is re-dispatched feasible or not. If the constraint is re-dispatched feasible with non-zero CRM, then the graduated transmission demand curve (GTDC, also known as Transmission Shortage Prices), as shown in Fig. 3.3, is imposed on the violated constraints, which is classified

by violations levels. If the constraint is re-dispatched infeasible or CRM is zero, the penalty cap is set to $4000/MWh in the market software.

Recently, an inconsistency between the GTDC approach and the NYISO tariff has been observed[3]. This inconsistency may result in inflation of the real-time shadow prices and increased market risk [23]. Starting in the June 2017 EMS/BMS deployment, the process of 'feasibility screening' is eliminated and the second step of the graduated Transmission Shortage Price is modified to $1,175/MWh, as shown in Fig. 3.3[24].

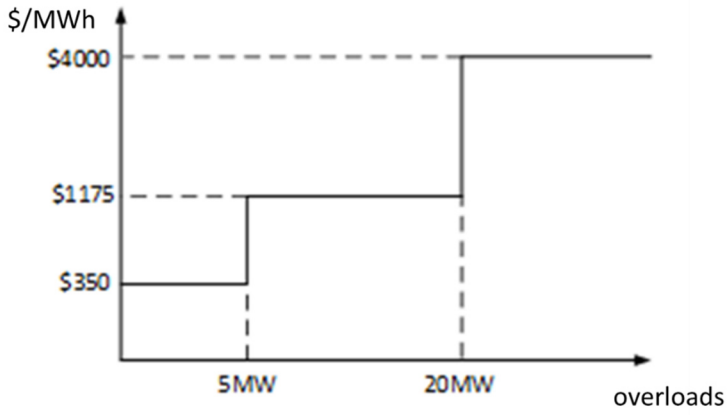

Fig. 3.3. GTDC in the NYISO market

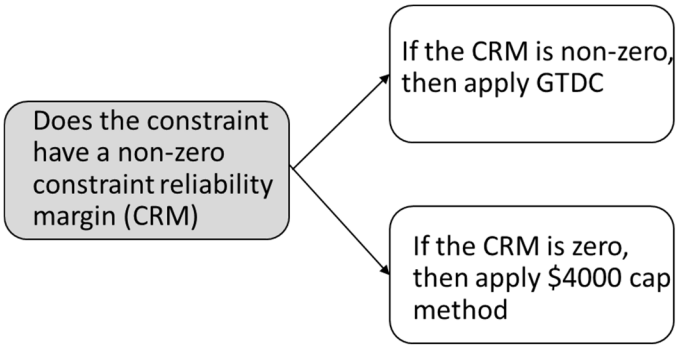

Fig. 3.4. Updated Process for CR methodology in the NYISO

[3] Some observed high shadow price outcomes seem to conflict with the provision in the NYISO market system tariff that: "[The GTDC] is the maximum shadow price that will be used in calculating LBMPs under various levels of relaxation."

3.3.3 Constraint relaxation in California ISO

The market optimization activities attempt to balance supply and demand, however, there are cases when the transmission limits cannot be satisfied in the market engine with implementation of current market rules. Accordingly, economic bids alone cannot yield feasible solution, i.e., there exists some flow violations in transmission constraints. Therefore, the policy of uneconomic adjustment is deployed by the market software to allow constraint relaxations in transmission constraints [25].

'Uneconomic adjustment' refers to constraint relaxation in overloading transmission lines, in which slack variables representing the level of necessary relaxation, with penalty price set according to the required priority hierarchy[4]. Uneconomic adjustment is irrelevant to costs and only intended as an optimization tool in the California ISO(CAISO). The value of penalty price is artificially extreme, and it is completely beyond the range of bid floor and bid cap, in order to guarantee that economic bids are relied on to reach the market solution at the first place. Furthermore, the penalty prices of different constraint category are significantly far apart from each other; this is to guarantee that adjustment of higher priority is in effect before that of the lower priority. As investigated in the previous sections, the extreme value of penalty price tend to result in LMP spike, thus it is not appropriate to determine LMP. Currently, two market runs are applied in market structure of the CAISO to achieve operationally sound and economically reasonable solutions. A scheduling run includes extreme penalty price to remove overloads-related infeasibilities and determine dispatch decision for generating units; a pricing run is set to output reasonable signals of market pricings. Specifically, the implemented penalty price is huge in the scheduling run to ensure the CR action is activated in hierarchical priority order. However, the

[4] Priority hierarchy represents the priority of constraint relaxation among soft constraints, i.e., the relaxation order of constraints categories.

penalty price in the pricing run is set according to multiple bid caps or bid floors, and it can reflect the costs of violating flow limits, as well as the management costs. For example, a penalty price is set as 3 times the bid cap. For those constraints without overloads and CR actions, the LMP prices calculated from the scheduling run and pricing run are the same; for those constraints require CR action, LMPs values from scheduling run and pricing run are different. The performance of CR procedures and corresponding parameters are evaluated on regular time basis and adjustments are made when it is necessary. Recently, motivated by stakeholder input, the CAISO proposed to eliminate the relaxation tier prices below the bid cap in February 2017. Furthermore, in response to the increased energy bid cap required by FERC, CR for small violations at the lower voltage levels will be discontinued in the CAISO.

3.3.4 Constraint relaxation in ERCOT

Constraint relaxation in Electric Reliability Council of Texas (ERCOT) is concentrated on transmission constraints and power balance constraints, and shadow price caps are established by ERCOT Board [26]~[27]. Those shadow price caps can be interpreted as: 1) the cap of transmission-related constraints is to limit the cost evaluated by the SCED algorithm to resolve an additional MW of congestion on transmission circuit to the pre-defined maximum shadow price for that transmission-related constraint; 2) The cap of the power balance constraint is to restrict the cost evaluated by the SCED algorithm when power balance constraint is violated. The SCED optimization model based on constraint relaxation is shown as Fig. 3.5.

Objective function	Minimize {Cost of dispatching generation + Penalty for violating power balance constraint + Penalty for violating transmission constraints} **OR**
	Minimize {sum of (offer price * MW dispatched) + sum (Penalty * power balance violation MW amount) + sum (Penalty *Transmission constraint violation MW amount)}
Constraints	Power balance:
	Sum (Base Point) + under gen slack – over gen slack = generation to be dispatched
	Transmission Constraints
	Sum(Shift Factor * Base Point) – violation slack ≤ limit
	Dispatch Limits
	Lower Dispatch Limits ≤ Base Point ≤ Higher Dispatch Limits

Fig. 3.5. The SCED optimization model in ERCOT

The LMP at each electrical bus is determined by:

$$LMP_{bus,t} = SP_{demand,t} - \sum_{c} GSF_{bus,c,t} \cdot SP_{c,t}$$

where, $SP_{demand,t}$= Power Balance Penalty (if a power balance violation exists) at time interval t; $GSF_{bus,c,t}$= Generation Shift Factor impact of the bus 'bus' on constraint 'c' at time interval t; $SP_{c,t}$= Shadow price of constraint 'c' at time interval 't' (capped at maximum shadow price for this constraint).

During the situation of resources scarcity, if a transmission constraint is violated, then transmission constraint and power balance constraint will cooperate with each other to make decisions. Cost of moving up the resource is equal to (Shift Factor * Transmission Constraint Penalty + Offer cost); cost of moving down the resource = power balance penalty. If cost of moving up the resource is greater than cost of moving down the resource, the resource will be moved down for resolving constraints; otherwise, the resource will be moved up to satisfy power balance requirements.

3.3.5 Constraint relaxation practices in other ISOs

1. Reserve constraint penalty factors (RCPF) in ISO-NE [28]

Due to network topology, resources allocation and sufficient power transfer capability, the transmission congestion does not occur frequently in ISO-NE. However, when overloads exist along transmission circuits, reserve requirements should be addressed to relax those constraints to provide a feasible solution. The concept of RCPF is established in the real-time market of the ISO-NE for limiting the cost that the optimization problem may incur to procure reserve products and market behavior with tight operating conditions. When system operator reports the resource scarcity issues on reserve products, those generator units, with marginal cost lower than RCPF, will be backed down to offer the reserve products rather than the energy output. Correspondingly, opportunity costs are generated for those units. The parameter settings of local RCPF starts with $50/MWh. However, this value is not high enough to be able to schedule all the available resources based on the operating experiences, so the value is changed to $250/MWh, beginning in January 1, 2010. This updated value can satisfy the reserve requirements for real-time market operation.

2. Reserve penalty factors in PJM [29]

When energy and reserve prices are undergoing specific emergency actions (such as voltage reduction and manual load dumping actions), some wrong price signals, which require commitment of additional resources, tend to be generated for market participants. The PJM deploys reserve penalty factors to solve such a problem. Similar to those applied in the NYISO and the ISO-NE, price caps for both synchronized and non-synchronized reserves are implemented. If there is a shortage of primary reserve, the reserve penalty price would be $850/MWh. Furthermore, if the shortage is within the synchronized reserves, the penalty price is $1700/MWh. The PJM states that the reserve penalty price should be set high enough to fully utilize all available

resources. The price for regulation service is set based on five-minute time intervals, and emergency resources can set the price as well.

3. Violation relaxation limits (VRLs) in Southwest Power Pool (SPP)

VRLs are activated when the shadow price to satisfy a constraint exceeds the corresponding VRLs, which includes spinning reserve requirement, operating constraints, resource ramping constraints, global power balance constraints, and resource capacity constraints. Based on the historical data and consistent sensitivity analysis on market performance, the most recent update is that SPP recommends no changes to the value selection of VRLs, expect for setting the first VRL block of operating constrain as $750/MWh, which achieves a relatively satisfactory trade-off between production costs and operational reliability [30].

3.4 Statistics of constraint relaxation practices in industry

Motivated by the thought to provide more insights of constraint relaxation practices in industry, publicly available CR-related data from a representative ISO, the NYISO, are investigated and assessed in this subsection. With the implementation of the updated Graduated Transmission Demand Curve (GTDC) starting in June 1, 2017, it is possible to map shadow price of binding constraints to flow violation values. The detailed mapping criteria is prescribed by the GTDC as:

- If the constraint cost (also known as shadow price of a constraint) = $350/MWh, the flow violation of the corresponding transmission line is <= 5MW;
- If the constraint cost = $1175/MWh, the violation is between 5MW~20MW;
- If the constraint cost is between $1175~$4000/MWh, the violation is above 20MW (here, the CRM is assumed to be 20MW for all lines).

The NYISO publishes limiting constraints for both the day-ahead market and the real-time market. Considering that the updated GTDC methodology is integrated into the business management system and deployed as of June 2017, the extracted file is named as "OASIS_Real_Time_Dispatch_Limiting_Constraints.csv", and it is from NYISO market and operations data at the NYISO public website [31]. This dataset covers data within the time range from 20170601 to 20170721. Within this specific time duration, the total number of CR occurrences is 1643, where each occurrence is based on a five-minute interval, including 203 occurrences observed under normal condition and the remaining 1440 occurrences observed under contingency conditions. Thus, the average frequency of CR action is 32.2 per day. Fig. 3.6 summaries the occurrences by the amount of flow violations. It can be observed that the low-violation event is the dominant category for CR action, followed by around 25% occurred in medium-violation events and 12.5% with high-violation events. Transmission constraints for the normal conditions and for 28 pre-defined contingency conditions are involved in this investigation, as summarized in Table 3.1. Fig. 3.7 plots the distribution of shadow prices for the events among the top 12 conditions (including both normal and contingency conditions) with high-occurrences of CR actions.

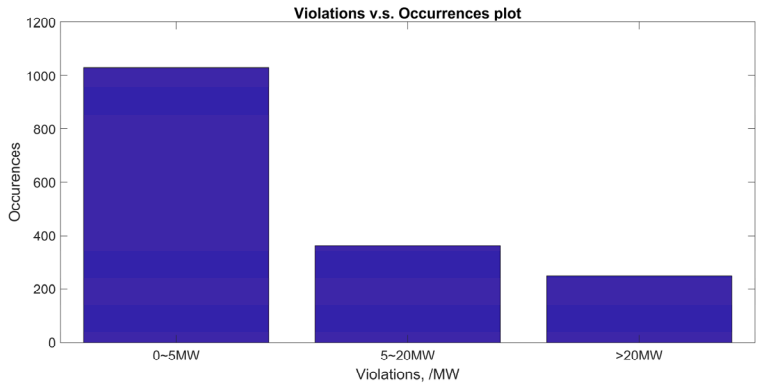

Fig. 3.6. Plot of CR occurrences for each violation category

Table 3.1. Contingency list and CR occurrences

Contingency List	Total occurrences of CR	Contingency List	Total occurrences of CR
TWR:GOETHALS 22 & 21	432	FOXHLLS-WILLWBRK_138_29212&BK1	12
BUS:PACKARD BK3 & 61 & 78	254	TSA:CE80 91&301	10
NORMAL CONDITION	203	SIN:MSU1&7040& HQ GN&LD PROXY	8
SHORE_RD-LAKSUCSS_138_368	169	SCB:GOWANUS(22):42231&G27&BEC	7
ALCOA_PA-ALCOA____115_R8105	116	NIAGARA_-ROBNSNRD_230_64	4
SHORE_RD-LAKSUCSS_138_367	112	SCB:SPBK(RNS2):Y49&M29&Y49_ST	3
PACKARD_-SAWYER___230_77	69	TWR:NIAGARA 61 & 64	3
FOXHLLS-WILLWBRK_138_29211&BK2	67	TSA:CE41 F30& 31&W79&80&81&93	2
BUS:BARRETT 292&459&G2&IC9-12	53	TWR:UCC2-41&EF24-40	1
SCB:GOWANUS(2):41&42231&R4	25	ATHENS__-PLSNTVLY_345_91	1
TWR:HOLTSVLLE 881& 882	24	TSA_E:CE80 91&301	1
TWR:PACKARD 62 & BP76	19	BUCHAN_S-MILLWOOD_345_W97	1
SCB:NEWBRDG 1380 461&BK6+4	18	NEPTUNE HVDC TIE LINE	1
SCB:GOWANUS(14):42&42232&R14	14	TSA:CE09 F38&F39&Y86&Y87&W75	1
SCRIBA__-VOLNEY___345_21	13	/	/

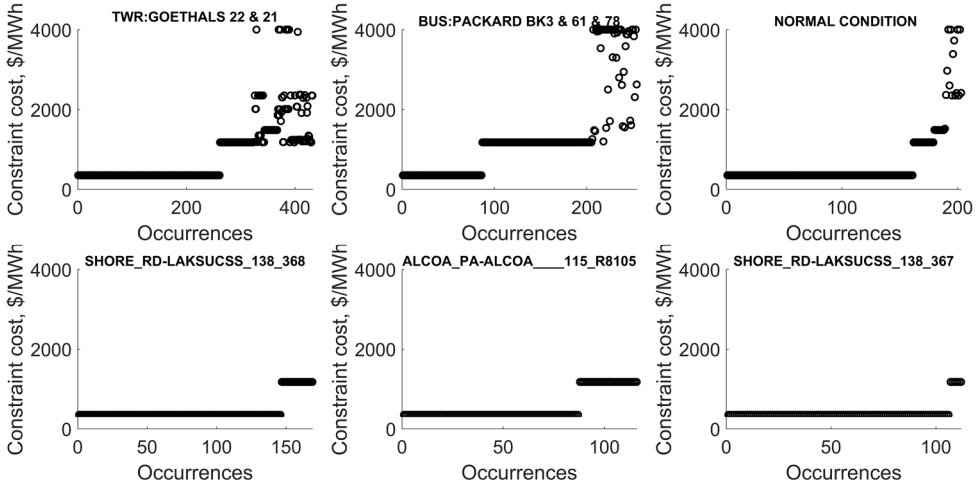

(a) Contingency (or normal condition) with top 1~6 occurrences

Fig. 3.7. Distribution of shadow price for contingency cases with high CR occurrences

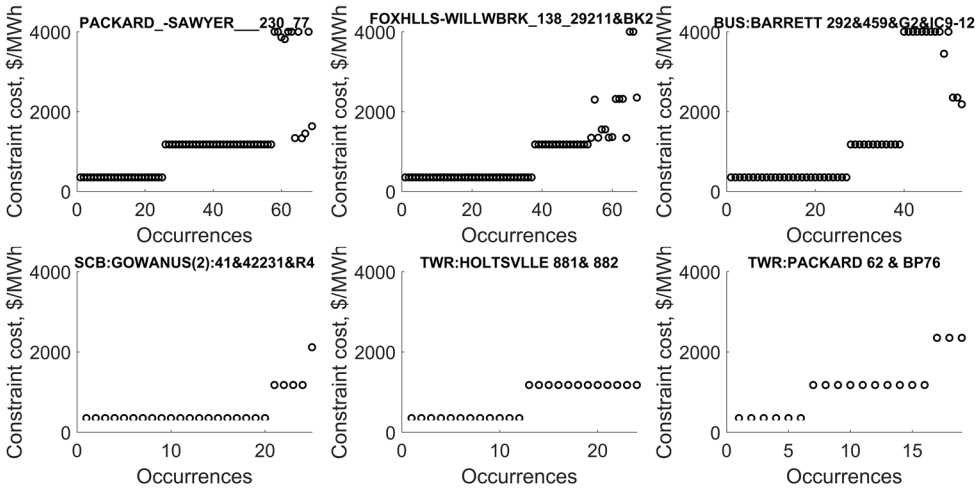

(b) Contingency with top 7~12 occurrences

Fig. 3.7. (continued)

The contingency event "*TWR: GOETHALS 22& 21*" contributes the most to the overloads violating transmission line limits, followed by contingency "*BUS: PACKARD BK3 & 61 & 78*" and the normal condition. Among those cases, 33 transmission facilities participated in CR actions, as summarized in Table 3.2. Fig. 3.8 plots the distribution of shadow price for the overloading transmission lines among the top 12 in terms of total number of occurrences.

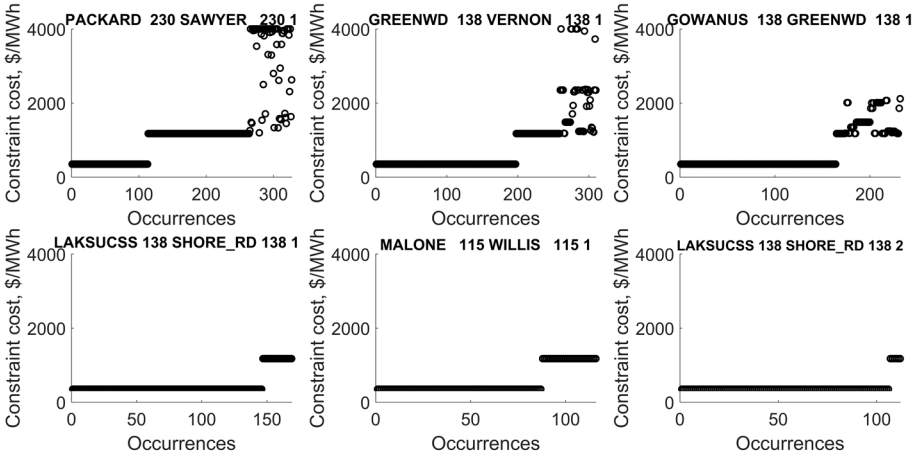

(a) Overloading circuits with top 1~6 occurrences

Fig. 3.8. Distribution of shadow price for transmission lines with high occurrences

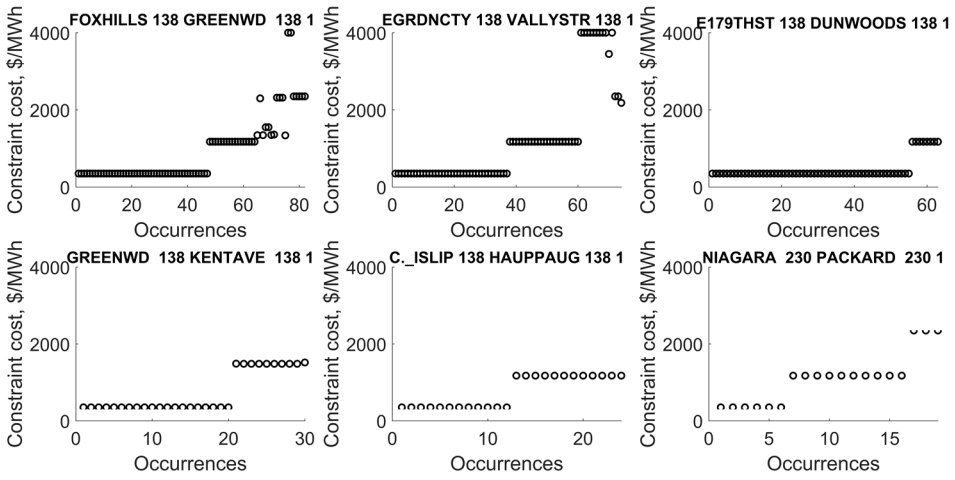

(b) Overloading circuits with top 7~12 occurrences

Fig. 3.8. (continued)

Table 3.2. Congested line list and CR occurrences

Circuit List	Total occurrences of CR	Line List	Total occurrences of CR
PACKARD 230 SAWYER 230 1	327	KENTAVE 138 VERNON 138 1	6
GREENWD 138 VERNON 138 1	310	ADIRNDCK 230 MOSES 230 1	5
GOWANUS 138 GREENWD 138 1	232	FARRAGUT 138 HUDS_AVE 138 1	5
LAKSUCSS 138 SHORE_RD 138 1	169	ADIRNDCK 230 MOSES 230 2	3
MALONE 115 WILLIS 115 1	116	NIAGARA 230 PACKARD 230 2	3
LAKSUCSS 138 SHORE_RD 138 2	112	BUCHAN_S 345 LADENTWN 345 1	2
FOXHILLS 138 GREENWD 138 1	82	FRESHKLS 138 WILLWBRK 138 1	2
EGRDNCTY 138 VALLYSTR 138 1	74	E179THST 138 HELLGATE 138 1	2
E179THST 138 DUNWOODS 138 1	63	MOTTHAVN 345 DUNWODIE 345 1	2
GREENWD 138 KENTAVE 138 1	30	RAINEY 138 VERNON 138 1	2
C._ISLIP 138 HAUPPAUG 138 1	24	GOWANUS 138 GOWANUS 138 1	1
NIAGARA 230 PACKARD 230 1	19	LAFAYTTE 345 CLRKSCRN 345 1	1
SCRIBA 345 VOLNEY 345 1	13	FARRAGUT 345 GOWANUS 345 1	1
PLSNTVLY 345 LEEDS 345 1	12	BUCHAN_S 345 MILLWOOD 345 2	1
GOETHALS 345 GOWANUS 345 1	8	EGRDNCTY 345 EGRDNCTY 138 1	1
GOETHALS 345 GOWANUS 345 2	8	CARLPLCE 138 EGRDNCTY 138 1	1
DUNWODIE 345 SHORE_RD 345 1	6	/	/

As indicated in Fig. 3.8 and Table 3.2, line "*PACKARD 230 SAWYER 230 1*" has the highest occurrences in transmission congestion, followed by line "*GREENWD 138 VERNON 138 1*" and "*GOWANUS 138 GREENWD 138 1*". Either transmission upgrades can improve the transfer capability for those lines or congestion patterns can be alleviated by applying efficient congestion management to the NYISO network.

To illustrate the relationship between high LMP price and transmission congestion, a situation selected from publicly available data is analyzed in this subsection, which sources from the NYISO website. This situation occurred at '*3:35pm, August 11, 2016*[5]*'*. At 3:35pm, the shadow price reaches $546.5/MWh along transmission line "*DUNWODIE 345 SHORE_RD 345 1*", which is the tie-line connecting Dunwoodie loading zone and Long Island loading zone in the New York Control Area [32]. Correspondingly, high LMP is observed at Long Island loading zone, which is the receiving area, of $1222.38/MWh (the congestion component is $546.5/MWh, contributing to this LMP spike). The data sources for this representative example is shown in Fig. 3.9. Considering that the actual load for that specific time interval in Zone K is 5228.5 MW, the cost induced by the CR-related congestion (implemented with high penalty price) is approximately $3 million. This is the cost associated with a single realization of CR action. According to the investigation results from the previous sub-section, the average CR occurrence rate is 32.2/per day. Thus roughly $100 million is imposed on consumer settlement, and it is procured in recovering the cost for constraint relaxation and congestion management.

It can be concluded that CR is a critical challenge imposed on ISO/RTS system operation, which occurs frequently and is associated with relatively large costs on congestion management.

[5] August 11, 2016 is the recorded summer peak of the NYISO in calendar year of 2016. The network is more congested than most if not all other days of the year. Thus, this network screenshot is representative for a congested network.

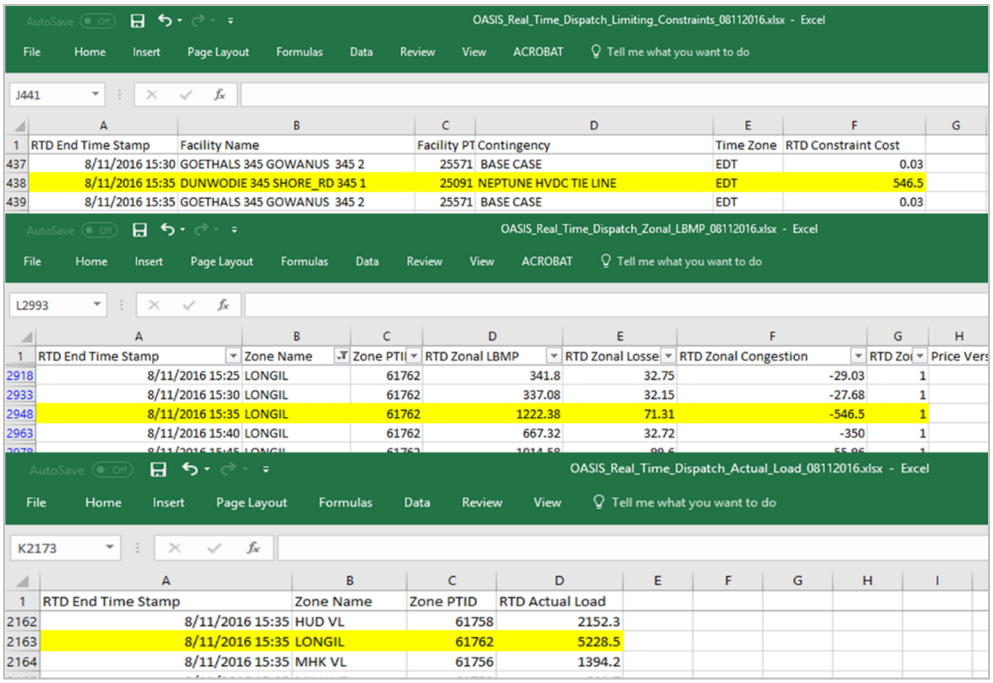

Fig. 3.9. Example for investigating relationship between LMPs and transmission congestion

3.5 Summary

This chapter summarizes the state of art for CR practice in ISO/RTOs, indicating that CR is applicable to handling SCED with infeasibilities caused by overloads along transmission circuits. The industry has made significant effort over the past decades in CR practice. From the analysis of industrial data performed in this chapter, the insight on CR practice is obtained that it occurs quite frequently in real-time operations, and they can induce huge amount of costs. That is the motivation to propose a systematic methodology for implementing CR action, which should be penalty-free and can make better utilization of the potential capacity on transmission circuits. Those risk-based methodology are the major contribution of this research and will be detailed in the following chapters.

CHAPTER 4. DETERMINISTIC RISK-BASED CONSTRAINT RELAXATION[6]

4.1 Introduction

To address the issue of constraint relaxation in solving infeasible SCED problem, related research is conducted, and valuable practice is carried out in industry, especially among ISOs/RTOs. These research and practice are summarized further in this chapter. Based on this, the detailed formulation is developed for risk-based constraint relaxation for SCED within single time-interval, as well as the corresponding solving algorithm is formulated.

4.2 Literature review

4.2.1 Constraint relaxation of SCED in academic area

CR is a general application in optimization literature; it refers to omitting specific constraint(s) or changing the constraints bounds (upper bound, lower bound or both), in order to expand the feasible region. The ultimate purpose is to produce the feasible solutions for the corresponding optimization problem. The literature implementing CR for optimization problems, especially in economic dispatch, are limited [33~37]. The methodologies deployed in the literature include hierarchical dual revised simplex method, an analytical algorithm, and a minimum violation method — referred in the dissertation as the industry-based constraint relaxation model. Those approaches are summarized as follows.

1. Direct method

Stott and Hobson present a method for constraint relaxation, where the major step is to increase all branch limits by a certain level and resolve the LP problem [33]. This procedure is

[6] Part of the material in this chapter is reprinted, with permission, from Xian Guo and James McCalley, "Risk-based constraint relaxation for security constrained economic dispatch", *Proc. 2015 North American Power Symposium (NAPS), Charlotte, NC, Sep.2015*, pp. 1-6. ©2015 IEEE.

repeated until a feasible solution is attained. This method is quite straightforward, but it tends to result in issues of over-relaxation, i.e., it relaxes more constraints than that are necessary. Nevertheless, it does not account for the effects on system security by allowing overloads along transmission circuits.

2. The hierarchical dual revised simplex method

Based on the sparse dual revised simplex method, which is tailored to benefit from sparsity properties in economic dispatch formulations [34], Irving and Sterling [35] present a hierarchical method for CR in economic dispatch. In an infeasible case, the 'softest' branch constraint is selected to be relaxed for each iteration; the degree of 'softest' is evaluated as the sensitivity to relieve the violation condition. This approach assures that the violation only affects the relevant and sensitive constraints, since for each iteration, only the soft constraints with sensitivity sufficient to alleviate violations among the overloaded line (called eligible soft constraints), are chosen to be relaxed; however, the iterations for solving linear programming problem increase significantly to eliminate the infeasibilities.

3. Analytical algorithm [36]

This method is an extension of the hierarchical dual revised simplex method; it implements a 'sensitivity-weighted sharing' strategy for situations that the sensitivity value of eligible soft constraints is not equal. A specific weighting function is designed for each soft constraint, and the constraint with higher sensitivity degree is relaxed with higher relaxation value. This relaxation procedure does not require additional iterations or machine memory. However, the deficiencies of method 2 and method 3 are similar to method 1, that is to say, they do not control the stress imposed on system security by conducting CR.

4. A minimum-violation method

This method is proposed in [37], and the objective function is to minimize total deviations, which can achieve a feasible solution with consideration on production costs. In this methodology, candidate constraints refer to those transmission lines with capacity headroom for relaxation; then a slack variable is imposed in each candidate constraint, and the penalty cost for each violation (a function of the corresponding slack variable) is imposed the objective function, correspondingly. For this methodology, the introduction of slack variables increases the computational burden, although not significantly so. This method has been widely applied in the industry, as described in Section 4.3.

In summary, in the framework of method 1, method 2 and method 3, there is no consideration of effects on system security with allowing overloads, and there are no explicit criteria to determine the relaxation margin. Method 4 does have considerations on system security impacts, at least indirectly, in that it minimizes the summation of production costs and amount of violation costs. However, in method 4, the selection of penalty price is subjective; if too low, the circuit may be over-relaxed, but if too high, the constraint relaxation may result in LMP spikes.

4.2.2 Constraint relaxation of SCED in industry

As presented in Chapter 3, the ISOs in the U.S., responsible for operating their electricity markets, have explored the CR issues and made significant efforts in addressing infeasible SCEDs. According to [38][39] and the descriptions in Section 3.3, the industry has accumulated experiences in CR actions, including both the real-time market based on SCED and the day-ahead market based on SCUC. Specifically, overloads on transmission constraints contribute the most to CR practice. In this research, the focus is on infeasible SCEDs resulting from transmission overloads.

Overall, the idea of industrial CR methodology is to introduce slack variable to those violated constraints. Then add the pre-determined penalty costs associated with the slack variable to the objective function. Thus, the infeasible SCED is secured to be solvable. The industry-based approach is formulated in great details in Section 4.3. It is noted that the great challenge is that how to select the penalty price reasonably and whether the reserve resources are sufficient for resources reallocation.

The motivation of this research work is that two distinct weaknesses are perceived in the existing industry-based methodology for performing CR action for infeasible SCEDs. The first is that it requires a penalty price for power flow violations, exogenously selected, which has significant influence on the resulting LMPs (as proved in Appendix A). The second is that constraint relaxation necessarily results in increased exposure to adverse consequences of contingencies, characterized as system risk, yet this increased exposure is not quantified and therefore not utilized in deciding which constraint to relax and how much to relax (i.e., the location and quantities of relaxation). Those are the motivations for developing the risk-based CR methodology. To this end, the benefits of implementing a risk metric is investigated for constraint relaxation in this research.

4.3 Formulation of industry-based constraint relaxation (A-CR)

As mentioned in Section 4.2, the methodology of constraint relaxation with penalty price is implemented in solving infeasible SCED in industry practices. This subsection summarizes and formulates the industry-based CR method, also refers as A-CR in this dissertation. In particular, current criteria and methodology for selection and determination of penalty price is also investigated in this section.

4.3.1 Formulation

A slack variable $\propto_l^k$ is added into a designated soft constraint (usually a constraint for restricting the transmission thermal limit), and the penalty cost associated with the slack variable is imposed on the objective function. The formulation is as follows, denoted as A-CR.

$$Min \sum_{i=1}^{NG} c_{G,i} \times P_i + \sum_{k=1}^{NC} \sum_{l \in CR}^{NL} Penalty_l^k \times \alpha_l^k \tag{4-1}$$

Subject to:

$$\sum_{m=1}^{N} \left(\sum_{i \in m} P_i \right) - \sum_{m=1}^{N} D_m - Loss = 0 \tag{4-2}$$

$$P_{i,\min} \le P_i \le P_{i,\max}, \ for \ i \in \{1,...,NG\} \tag{4-3}$$

$$\sum_{m=1}^{N} PTDF_{l,m}^0 (P_m - D_m) \le Limit_l^0, \quad for \ l \in \{all \ \ lines\} \tag{4-4}$$

$$\begin{cases} h_l^k = \sum_{m=1}^{N} PTDF_{l,m}^k (P_m - D_m), \\ for \ l \in \{all \ \ lines\} \ k \in \{contingency \ set\} \end{cases} \tag{4-5}$$

$$\begin{cases} h_l^k - \alpha_l^k \le Limit_l^k, \ (\alpha_l^k \ge 0) \\ for \ l \in CR, k \in \{contingency \ \ set\} \end{cases} \tag{4-6}$$

$$\begin{cases} h_l^k \le Limit_l^k, \\ for \ l \in NCR, k \in \{contingency \ set\} \end{cases} \tag{4-7}$$

where (4-1) is the objective function, including generation costs and penalty costs for overloading lines, (4-2) is the power balance constraint, which is represented from the level of entire network. (4-3) is the constraints for generation output, including both lower bounds and upper bounds for output. (4-4) are the transmission thermal constraints under the normal (no contingency) state, (4-5) are the post-contingency circuit flows (the pre-defined contingency set only covers the category of 'N-1' contingency), and (4-6)~(4-7) are the corresponding post-contingency thermal constraints. In particular, (4-6) represents the soft constraints for the optimization problem, i.e., those constraints

are available for relaxation under the allowable relaxation margin on limited time basis. (4-7) applies to those hard constraints, which are identified as unrelaxable. The possible reason that those constraints cannot be relaxed is that high loadings tend to incur severe effects on system security, such as cascading consequences.

As discussed in the Section 4.2, the industrial model does not monitor or control impacts on system security by allowing CR activity, and the selection of the penalty price value is heuristic, which performs as a significant challenge.

4.3.2 Determination of penalty price

Overall, ISOs set penalty prices as constants, with respect to voltage level, violation severity and reserve availability. The criteria for setting values vary according to the market rules in various ISOs. As the representative examples, the subsection describes mechanisms of selecting penalty price in the CAISO, the MISO and the ERCOT.

1. Penalty price in CAISO

Based on the ongoing testing, the CAISO proposes recommended values for Integrated Forward Market (IFM, residual unit commitment and real-time market. Specifically, the critical and representative parameters in real-time market are customized according to products category [25]. The sign convention is that penalty price is negatively valued for supply reduction and positively valued for demand reduction. For transmission constraints–branch, corridor, nomogram (for both normal condition and contingency condition), the penalty price for scheduling (or pricing) run is $5000/MW (or $500/MW). In the scheduling run, the guideline applied to transmission constraints is that an Economic Bid should be accepted if it is priced at the bid cap and it is at least 10% effective in relieving the transmission constraint. In the pricing run, a single penalty price segment is modeled at the Energy Bid cap.

2. Penalty price in MISO [38][39]

Beginning February 1, 2012, considering that insufficient shadow price is generated using constraint relaxation algorithm with available resources, as well as the reliability costs of violating the constraints is understated, the MISO adopts MVL for the shadow price when a constraint exceeds its binding limit, as recommended by IMM. Since MVL is the maximum amount that the market is willing to spend for constraint management, the price transparency is increased, and it can inspire the market participants to reduce transmission circuit flow. Currently, the MISO applies default MVL based on transmission line voltage, shown as Table 4.1. Group 1 is applied in the regular operating states; while Group 2 is implemented for transmission constraints that cannot be managed by the established MVL for the voltage categories in Group 1.

Table 4.1. MVL values of the MISO

Group 1	Group 2
• $3,000 for Interconnection Reliability Operating Limit (IROL) constraints • $2,000 for System Operating Limit (SOL) constraints with voltage ≥ 161kV • $1,000 for SOL constraints with voltage 100kV~161kV • $500 for SOL constraints with voltage $<$ 100kV	• Constraints ≤ 138kV are determined to be significantly impacted by regional flows, and these constraints use a $2,000 default MVL

Applying MVL has observable advantages, but significant price spikes occurred in the operation practice, which is caused by insufficient ramping capability over a five-minute dispatch period. However, these exceedances usually have no detrimental reliability impact. To solve such a problem, TCDC is proposed to add a second, lower MVL value for overloaded flow between 100% and 102% of transmission ratings for the binding transmission constraint. If the overloaded flows are between 100% and 102% of transmission ratings, TCDC is applicable, while the original MVL value is still maintained, when the overloads exceed 102% of transmission ratings. Table 4.2 indicates the demand curve for Group 1 and Group 2, correspondingly.

Table 4.2. Demand curve for transmission constraints (unit: $/MWh)

Voltage level	≤ 100kV	100~161kV	≥ 161kV
Group 1	400	700	1000
Group 2	700	1000	2000

3. Penalty price in ERCOT [26][27]

ERCOT has developed the mechanisms to determine penalty price (or called shadow price caps) for transmission line constraint, detailed as follows.

The penalty price for transmission lines are affected by the maximal LMP congestion component ΔLMP_{max}^{cong} $(\$y/MWh)$ that transmission circuits can handle. Given the shift factor efficiency threshold $SF_{thershold}^{efficiency}$ $(x\%)$, the maximum shadow price for transmission thermal limits constraints can be calculated as

$$SP_{\max} = \Delta LMP_{\max}^{cong} / SF_{threshold}^{efficiency} \quad (4\text{-}8)$$

Based on this method, the transmission constraint shadow price caps in the SCED algorithm is set as:

- Normal condition/Voltage violation: $5000/MW;
- 'N-1' contingency case: $4500/MW, $3500/MW, $2800/MW for 345/138/69 kV voltage categories, correspondingly.

4.4 Methodology of deterministic risk-based constraint relaxation

4.4.1 Definition and calculation of risk metric

Risk is a probabilistic metric to quantify the likelihood and severity of an event, which are the factors reflecting system security [40]. The severity of a post-contingency condition, can be assessed in terms of overload severity, cascading overload severity, low voltage severity and voltage instability severity [41]. In this research, the overload severity is the only factor being

considered in risk-based CR methodology; however, previous studies indicate that overload severity is representative, and the systematic control of overload severity benefits other categories of severity as well.

The risk metric is defined for a contingency C resulting in post-contingency loading on circuit l as the probability of occurrence for that specific contingency multiply by the thermal overload severity on circuit l resulting from that contingency, i.e., $Risk = Pr_C sev_l^C$.

1. Probabilities of contingency

(1) 'N-1' contingency

Based on a specific system network topology and operating condition characterized by load requirement and generation dispatch, the probability associated with the pre-defined 'N-1' contingencies can be calculated.

The probabilities can be rigorously quantified based on historical data and real-time information [42]. The probability of occurrence of a contingency is defined with respect to a time interval consistent with the targeted dispatch period. In most cases nowadays, the real-time dispatch time-interval is five minutes. Normalize the selected time-interval to one unit. Then, assume that the occurrence of contingency C follows the Poisson distribution. Thus, the probability of a specific contingency C is the probability that the contingency occurs at least once in the consecutive time-interval, while all other contingencies do not occur; this probability is:

$$\Pr_C = (1 - e^{-\lambda_C} \times \exp(-\sum_{C \neq i} \lambda_j) \tag{4-9}$$

where λ_C is the occurrence rate of contingency C per time-period. References [43]~[44] propose the statistical method of computing parameter λ_C with considering historical data, weather condition, geography information, and voltage level [45].

Furthermore, market operation procedure should be considered in calculating the probabilities of contingencies, and the corresponding probability for each operating point should be associated to the specific market [46]. As shown in Fig. 4.1, the day-ahead market will clear before T_0 of midnight in Day 1; it provides unit commitment and SCED outcomes. In order to guarantee the necessary probabilities are available before operating hour H of Day 2, the calculation should be accomplished between time interval $[\mathrm{H}-1, \mathrm{H}]$; this calculation is based on the most recent real-time weather information and operation status, such as forecasted load and network condition.

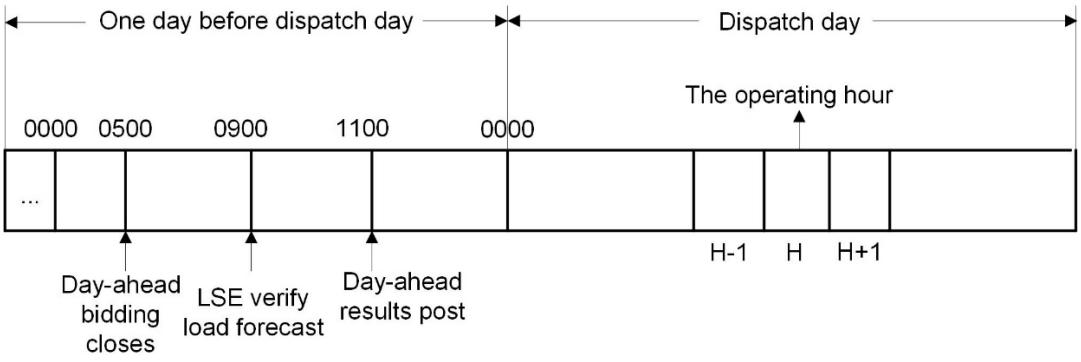

Fig. 4.1. Market operation timeline

(2) Kth-order contingency ($K \geq 2$)

The occurrence probability of a particular K successive cascading contingency is $Pr(\{i_1, i_2, \ldots, i_k\}) = \Pr(i_1) \times \Pr(i_2|i_1) \times \Pr(i_3|\{i_1, i_2\}) \ldots \times \Pr(i_k|\{i_1, \ldots i_{k-1}\})$. $\Pr(i_1)$ is defined as non-conditional probability, which has already been addressed; other probabilities are defined as conditional probability.

The conditional probabilities are achieved based on the assumption that the probability of occurrence of circuits outage $\Pr(i_2|i_1)$ can be estimated as the ratio of the increase in flow for the circuit in question following the outage to the increase in flow for the circuit in question necessary to trip it.

This probability estimation assumes that a specific value of flow can be known, beyond which the circuit in question will trip with certainty. Although for transmission circuits not protected by overcurrent relays (and most are not), this is not possible. However, it is the case that for a particular high level of flow, e.g., 130% of emergency overload rating, it is assumed that the circuit trip probability will be very high due to the heating effect on the circuit which results in sagging and potential short-circuiting to some underlying object.

As an example, in computing $Pr(i_2|i_1)$, the ratio used to estimate the probability is given by the increase in flow for circuit i_2 following outage of circuit i_1, denoted by $P_{i_2|i_1} - P_{i_2}^0$, to the increase in flow on circuit i_2 following outage of circuit that would be necessary to trip circuit i_2, denoted by $P_{i_2,trip} - P_{i_2}^0$, where $P_{i_2|i_1}$, is the flow in circuit i_2 following outage of circuit i_1, $P_{i_2}^0$ is the flow on circuit i_2 before outage of circuit i_1, and $P_{i_2,trip}$ is the circuit i_2 flow that will definitely cause it to trip. This results in:

$$\Pr(i_2 \mid i_1) = \frac{P_{i_2|i_1} - P_{i_2}^0}{P_{i_2,trip} - P_{i_2}^0} \tag{4-10}$$

As further examples, in computing $Pr(i_3|\{i_1, i_2\})$, $Pr(i_k|\{i_1, i_2, \dots, i_{k-1}\})$, the expressions are:

$$\Pr(i_3 \mid \{i_1, i_2\}) = \frac{P_{i_3|\{i_1,i_2\}} - P_{i_3|i_1}^0}{P_{i_3,trip} - P_{i_3|i_1}^0} \tag{4-11}$$

$$\Pr(i_k \mid \{i_1, \dots, i_{k-1}\}) = \frac{P_{i_k|\{i_1,\dots,i_{k-1}\}} - P_{i_k|\{i_1,\dots,i_{k-2}\}}^0}{P_{i_k,trip} - P_{i_k|\{i_1,\dots,i_{k-2}\}}^0} \tag{4-12}$$

2. Overload severity

The overload severity function should be able to quantify the consequences of the contingency and appropriately represent the circuit loading condition. Considering that severity level increases with post-contingency loading, the values of post-contingency flows in heavily-

loaded circuits dominate the corresponding severity value. The power flow is quantified as a percentage of rating to generalize the definition of overload severity function [46].

The dashed curve in Fig. 4.2 illustrates an ideal overload severity function. The solid lines approximate the ideal curve; this approximation is utilized to maintain linearity and continuous differentiability in evaluating risk.

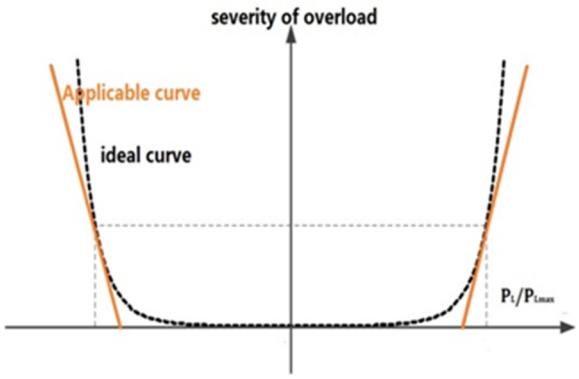

Fig. 4.2. Severity function of circuit overloading

Although the dashed line is a convex representation, computational burden is increased when computing the severity of each circuit associated with all pre-defined 'N-1' contingencies. Consequently, a piecewise-linear approximation is formed for this function [11], as shown in Fig. 4.3. The breakpoints of the approximation are chosen based on adaptive transmission ratings (ATR). ATR include 1) Long Time Emergency (LTE) rating for loadings that can be accepted for up to 4 hours; 2) Short Time Emergency (STE) rating for loadings that can be accepted for up to 15 minutes and 3) Drastic Action Limit (DAL) for loadings that cannot be tolerated and should be immediately relieved [2].

Assume that the severity for post-contingency flow under 90% LTE is zero, thus, the severity value of circuit flow between $[-0.9\text{LTE}, 0.9\text{LTE}]$ is zero. Then there are three segments: segment $1, [0.9\text{LTE}, \text{LTE}]$ *or* $[-\text{LTE}, -0.9\text{LTE}]$; segment $2, [\text{LTE}, \text{STE}]$ or $[-\text{STE}, -\text{LTE}]$ and segment $3, [\text{STE}, \text{DAL}]$ or $[-\text{DAL}, -\text{STE}]$.The severity value when the circuit flow reaches the LTE,

is c_1 . The severity value when the circuit flow equals the STE is c_2, and the maximum severity value, i.e., the value when the circuit flow equals to DAL, is 1. The value of c_1 and c_2 can be adjusted based on the perspective of the user requirements and it can be customized to specific transmission circuits.

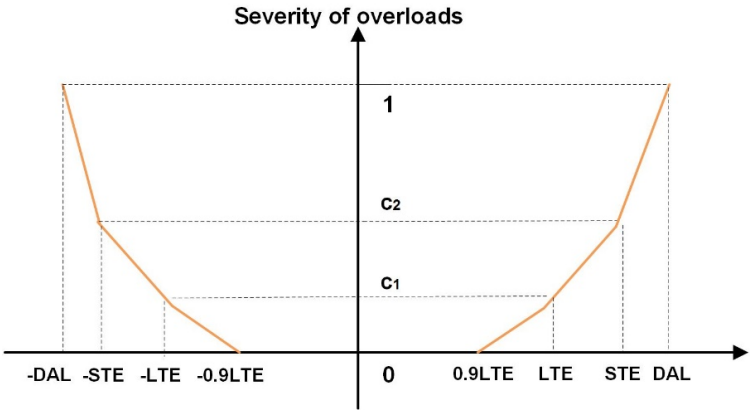

Fig. 4.3. Piecewise linear function for severity calculation

As indicated by the severity function illustrated in Fig. 4.3, heavily loaded circuits (in the framework of risk-based constraint relaxation methodology, monitoring and actions will be taken on those lines) are those having flows exceeding 90% of their LTE; this is in contrast to the industry model (and to the general industry practice), which only takes dispatch action to reduce flows exceeding LTE. However, this is not a simple down-shifting of the LTE because the re-dispatch control effort made to reduce risk within the risk-based constraint relaxation does so in proportion to the severity function. Thus, higher flows, e.g., 105% of LTE, motivates more control effort than do lower flows, e.g., 91% of LTE.

Take the right-half of the piece-wise linear severity function as an example, it is proposed that the detailed representation in modelling optimization problem (retain linearity in SCED programming) and its corresponding mathematical proof. The proof steps are also applicable to the left-half of the severity function. As mentioned above, a piece-wise linear function is utilized to identify severity value, as shown in Fig. 4.4.

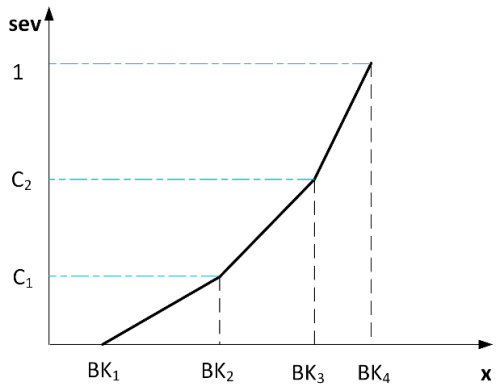

Fig. 4.4. Relationship between severity and overloading (circuit flow/conductor temperature)

The severity function $g:\mathbb{R}^+ \to \mathbb{R}^+, x \mapsto s$ is a continuous piecewise linear function defined by

$$s = g(x) = \begin{cases} 0 & 0 \le x < BK_1 \\ a_1 x + b_1 & BK_1 \le x < BK_2 \\ a_2 x + b_2 & BK_2 \le x < BK_3 \\ a_3 x + b_3 & BK_3 \le x \le BK_4 \end{cases} \tag{4-13}$$

where for each i, BK_i corresponds to the x-coordinate of an intersection of two adjacent segments as shown in Fig. 4.4; $0 < a_1 < a_2 < a_3$. The objective function has the additive structure:

$$f(\boldsymbol{s}) = \sum_i f_i(s_i) = \sum_i f_i(g_i(x_i)) \tag{4-14}$$

where $\boldsymbol{s} = (s_1, s_2, \ldots)$, and f_i is increasing for all i. With this function, the piecewise linear severity function can be formulated by a set of linear constraints:

$$\begin{cases} s \ge 0 \\ s \ge a_1 x + b_1 \\ s \ge a_2 x + b_2 \\ s \ge a_3 x + b_3 \\ 0 \le x \le BK_4 \end{cases} \tag{4-15}$$

This equivalence has been proved by two steps. First, it will be shown that (4-15) exactly gives the epigraph of g, i.e., $\{(x,s):(4-15)\} = epig$, as illustrated in Fig. 4.5.

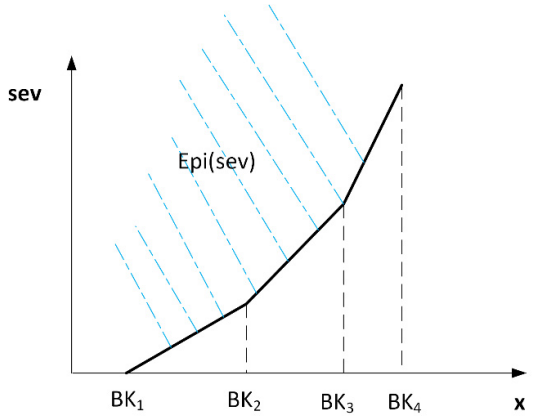

Fig. 4.5. Piece-wise linear severity function

then the optimal solution of the problem is:

$$\begin{aligned} \min_{x,s} \quad & f(\boldsymbol{s}) \\ \text{s.t.} \quad & (4-15) \\ & \text{other constraints with } \boldsymbol{s} \text{ not involved} \end{aligned} \tag{4-16}$$

satisfies $\boldsymbol{s}^* = \boldsymbol{g}(\boldsymbol{x}^*)$, where $\boldsymbol{g}(\boldsymbol{x}) = [g_1(x_1), g_2(x_2), \ldots]$, $(\boldsymbol{x}^*, \boldsymbol{s}^*)$ is an optimal solution. In other words, (4-15) is equivalent to (4-13) in for optimal solution(s), and it can be integrated to model optimization problem.

Step 1:

(1) $\{(x,s):(4-15)\} \subset epig$

This direction is trivial since epi g is exactly (4-13) with restricted domain of x for each segment constraint.

(2) $\{(x,s):(4-15)\} \supset epig$

Prove by contradiction. Suppose there exists (x',s') satisfying $(x',s') \in \text{epi}\, g$ and $(x',s') \notin \{(x,s):(4-15)\}$. The second condition implies $s' < a_i x' + b_i$ (let $a_0 = b_0 = BK_0 = 0$) for some i. Define a closed set

$$S = \{(x,s): s < a_i x + b_i, BK_i \le x \le BK_{i+1}\} \tag{4-17}$$

If $(x',s') \in S$, the contradiction follows immediately since $S \bigcap \text{epi}\, g = \varnothing$. If $(x',s') \notin S$, let (x'',s'') denote a point lies on the interior of i^{th} segment, i.e., $s'' = a_i x'' + b_i, BK_i \le x'' \le BK_{i+1}$. Since (x',s') and (x'',s'') are both in $\text{epi}\, g$, and it is trivial to show that $\text{epi}\, g$ is convex. It follows that the straight line-segment that connecting the two points is a subset of $\text{epi}\, g$. It is not difficult to show that this straight line segment should intersect the boundary of S, and since S is closed, the intersection is in S, which leads to the contradiction, given the fact that $S \bigcap \text{epi}\, g = \varnothing$.

Step 2:

Suppose $(\boldsymbol{x}', \boldsymbol{s}')$ is a feasible solution of (4-16). Then $(\boldsymbol{x}', \boldsymbol{g}(\boldsymbol{x}'))$ is also a feasible solution, because $\boldsymbol{s}$ is only involved in (4-15). Since f is increasing and $\boldsymbol{g}(\boldsymbol{x}') \le \boldsymbol{s}'$, it can be obtained that $f(\boldsymbol{g}(\boldsymbol{x}')) \le f(\boldsymbol{s}')$. Thus, no matter what $\boldsymbol{x}^*$ is, $\boldsymbol{s}^* = \boldsymbol{g}(\boldsymbol{x}^*)$.

As discussed in previous sections, the industry-based constraint relaxation approach does not monitor or control the effects on system security by constraint relaxation. The risk-based constraint relaxation is proposed to ensure the system security level when conducting constraint relaxation actions. Based on the concept that applying risk metric to evaluate system security level, the methodology of deterministic-RBCR (D-RBCR) model is detailed in this section.

4.4.2 Definition of risk indices

In designing an attractive framework of D-RBCR methodology, three critical principles are proposed as follows:

- The conditions obtained through D-RBCR should be less risky than those obtained through the A-CR.
- The particular 'N-1' contingency(s) causing the infeasibility (called critical contingency(s)) in D-RBCR should be less risky than it is (they are) with A-CR.
- The overloaded flow (which necessitates post-contingency thermal limit relaxation) from the D-RBCR should be less risky than it is with A-CR, when losing the overloaded circuit after the critical contingency (i.e., incurs 'N-1-1' contingency). The D-RBCR conditions under 'N-1-1' contingency should out-perform conditions obtained via A-CR for the same 'N-1-1' contingency; that is to say, the corresponding risk of 'N-1-1' outage should be monitored and controlled.

Correspondingly, a set of risk indices based on the basic concept of risk metric are proposed and formulated for the methodology of the D-RBCR, which are detailed as follows:

- System risk: it is a function of normalized flows for the heavier-loaded circuits, which equals to the summation over all pre-defined contingencies of each contingency probability multiplies by the corresponding contingency consequences, evaluated by severity of circuits flow.

$$Risk=\sum_{k=1}^{NC}\left(\Pr_k \sum_{l=1}^{NL} sev_l^k\right) \tag{4-18}$$

- Contingency risk: it is defined to evaluate the system security level under the contingency k, which is associated with the occurrence rate of that contingency and severity of the overloading levels induced by that contingency.

$$CtgRisk_k = \Pr_k \sum_{l=1}^{NL} sev_l^k \tag{4-19}$$

- Second contingency circuit risk: it is the contingency risk of circuit l following the outage of the contingency k, i.e., this is the second contingency occurring within an 'N-1-1' outage; it is the contingency risk under 'N-1-1' condition.

$$CctRisk_l^k = \Pr_l^k \sum_n sev_n^l \tag{4-20}$$

It is observed that Pr_l^k is a conditional probability, i.e., it is the probability of losing circuit l given a prior loss of circuit k.

4.4.3 Risk Limits and Risk Table

1. Risk limits

In the D-RBCR model, the risk indices are restricted not to exceed the predefined thresholds. Thus, the D-RBCR procedure requires contingency risk limits for each critical contingency, second contingency circuit risk limits for each overloaded circuit (which is necessary to relax limits for handling infeasibility in SCED problem), and a single system risk limit for the entire system. Upper bounds for those limits are determined by identifying the corresponding risk level under a stressed system that is considered secure under standard NERC operating criteria. Furthermore, there are some additional information should be considered when conducting risk-based CR methodology.

- **Selection of pre-defined 'N-1' contingency**

The 'N-1' contingency analysis is based on a predefined contingency set. Considering that excessive number of contingencies adds the computation burden, it can include only selected

contingencies (e.g., based on a ranking algorithm) that are known to result in high post-contingency loadings, thus they should have more observable effects on impacting system performance on security.

- **Selection of the circuits not available for constraint relaxation activity**

There may exist circuits having excessive second-contingency circuit risk, implying that a second contingency involving outage of circuit l following outage of circuit k will result in significant severity issues. Since the action of CR exposes the system to the risk for entering cascading events, it is prudent to avoid constraint relaxation for such a circuit. This consideration will be addressed in Chapter 7, according to which weak area will be identified. Those weak area are not eligible for CR actions, for the consideration on securing power system.

2. Risk table

In the D-RBCR model, the risk indices are supposed to be constrained under pre-defined thresholds. Such reference values should reflect system performance on security. The Risk Table indicates those reference values in an organized and convenient view; they are calculated off-line.

The Risk Table consists of three major subsections, as shown in Table 4.3; 1) a cell in the pink shaded area represents the reference value for 'N-1-1' risk-outage of circuit l following outage of circuit k (only critical contingencies are covered), $RiskTable(l,k) = CctRisk^{k}_{l,max}$; 2) a cell in the green shaded area represents the reference value for a particular critical contingency risk, and 3) the yellow cell indicates the reference value for system risk.

Experienced historical data is utilized to determine the cell values for the Risk Table. In this research, the system performance in A-CR model is applied to derive the margin of risk indices. Those margins are shrunken to a certain level, such as 90% of risk indices from A-CR as reference values in Risk Table. Considering that selection of penalty price has significant impacts on the

optimal solutions, several values of risk indices are calculated under multiple penalty prices, and the average of them are utilized to generate the reference values.

Table 4.3. Illustration of Risk Table

	Critical Ctgcy1	Critical Ctgcy2	…	Critical Ctgcy k
Cct 1	$RiskTable(1,1)$	$RiskTable(1,2)$	…	$RiskTable(1,k)$
Cct 2	$RiskTable(2,1)$	$RiskTable(2,2)$	…	$RiskTable(2,k)$
….	….	….	…	….
Cct l	$RiskTable(l,1)$	$RiskTable(l,2)$	…	$RiskTable(l,k)$
	$CtgRisk_{1,max}$	$CtgRisk_{2,max}$	…	$CtgRisk_{k,max}$
	$Risk_{max}$			

4.4.4 Formulation of deterministic risk-based constraint relaxation

1. Optimization model

The objective function of the deterministic risk-based CR model is to minimize the production cost, as indicated in the following formulation, denoted as D-RBCR.

$$Min \sum_{i=1}^{NG} c_{G,i} \times P_i \tag{4-21}$$

Subject to:

The same as (4-2)~(4-4).

$$h_l^k = \sum_{m=1}^{N} PTDF_{l,m}^k (P_m - D_m), \tag{4-22}$$

$$\begin{cases} h_l^k - \beta_l^k = K_{c,l} Limit_l^k, \\ for\ l \in CR,\ k \in \{contingency\ set\} \end{cases} \tag{4-23}$$

$$\begin{cases} h_l^k \le Limit_l^k, \\ for\ l \in NCR,\ k \in \{contingency\ set\} \end{cases} \tag{4-24}$$

$$sev_l^k \ge 0 \tag{4-25}$$

$$sev_l^k \ge a_{1l} h_l^k - 9 \tag{4-26}$$

$$sev_l^k \ge a_{2l} h_l^k - a_{3l} \tag{4-27}$$

$$sev_l^k \geq a_{4l} h_l^k - a_{5l} \tag{4-28}$$

(4-22) and (4-25)~(4-28) *for* $l \in \{all\ \ lines\}$ $k \in \{contingency\ set\}$

$$Risk = \sum_{k=1}^{NC} \left(\Pr_k \sum_{l=1}^{NL} sev_l^k \right) \leq Risk_{\max} \tag{4-29}$$

$$CtgRisk_k = \Pr_k \sum_{l=1}^{NL} sev_l^k \leq CtgRisk_{k,\max}\ , k \in CCS \tag{4-30}$$

$$CctRisk_l^k = \Pr_l^k \sum_n sev_n^l \leq CctRisk_{l,\max}^k\ , k \in CCS, l \in COCS \tag{4-31}$$

Constraint (4-23) introduces the relaxation level $K_{c,l}$ for each circuit l, where β_l^k is used as the violation indicator, identifying which circuits are overloaded under the current limit $K_{c,l} \times Limit_l^k$ (positive value implies that there exists additional violation, zero or negative means no violation) and needs to be relaxed. Constraints (4-25)~(4-28) model the severity evaluation, and (4-29)~(4-31) constrain the set of risk indices. The set CCS is critical contingency set, and the set COCS is critical overloaded circuits set[7].

2. Relaxation level determination

The approach to utilize risk-based OPF is to set the same relaxation level for all circuits that are candidates for constraint relaxation. However, this approach may result in occurrence of some circuit overloads even though their occurrence does not contribute to alleviating the infeasibility. For example, allowing overload on a 230kV circuit in Louisiana would not alleviate an infeasibility on a 230kV circuit in Minnesota. Thus, a preliminary problem is to determine a set $\{K_{c,i}, i = 1, \dots, NL\}$ that achieves an optimal solution under the controlled system risk.

To determine the relaxation level $K_{c,l}$, two observations are made. The first observation is that the risk-based constraint relaxation formulation constrains β_l^k, which is the violation indicator

[7] The requirements for this set is 1) needs to relax its thermal limits under contingency condition to remove infeasibility and 2) exceeds the risk limits for 'N-1-1' second contingency circuit risk.

for the infeasible SCED problem. The purpose is to identify the minimum relaxation of the candidate soft constraints, while achieving the minimization of objective function, as well as satisfying the corresponding risk constraints. The second observation is that the relaxation level should also be bounded. That is to say, the flow should be no more than what can be accommodated within the allowable time that it will take to relieve the loading. Therefore, the theory of ATR limit is imposed. In this subsection, 1.24LTE is set as the bound for maximum allowable loading level within the examined five minutes time-interval; it is slightly less than DAL value for transmission circuits, generally.

$K_{c,l}$ for circuit *l* is determined as the relaxation level necessary to solve the infeasible SCED problem; it is bounded by the maximum relaxation level —1.24LTE. This approach is described as follows.

- Determine relaxation level 1 based on violation indicator β_l^k: calculate $K_{c,l(1)}$ according to the maximum value of positive violation indicator $\max_{k=1,\ldots,\mathrm{NC}}\{\beta_l^k\}$;
- Determine relaxation level 2 based on ATR: calculate $K_{c,l(2)}$ according to the value of 1.24LTE for circuit *l*;
- Chose the smaller one between relaxation level 1 and relaxation level 2: $K_{c,l} = \min\{K_{c,l(1)}, K_{c,l(2)}\}$.

3. Solving procedure for D-RBCR

The solving procedure for D-RBCR is described as follows, and the flow chart is detailed in Fig. 4.6.

Step 1: Set $\mathrm{COCS} = \emptyset$.

Step 2: Solve the D-RBCR optimization problem. Identify the violated circuits based on the values of violation indicator β_l^k. The set of those violated circuits are denoted as **V**.

Step 3: Determine $K_{c,l}$ for each circuit flow limit, using the approach proposed in part 2 of Section 4.4.4. (For those circuit which flows within their limits, $K_{c,l}$ is set to be 1.)

Step 4: Solve the problem of D-RBCR with the updated value of $K_{c,l}$, and based on the corresponding results, update the set of violated circuits set **V**.

Step 5: Repeat Steps 3 and 4 until the set **V** is empty, then output the corresponding relaxation results.

Step 6: Test the value of $CctRisk_l^k$, if not satisfied, update COCS, and repeat Step 2~Step 6. If satisfied, output the corresponding relaxation result.

If the iteration exceeds a specific pre-determined threshold, the algorithm terminates; in that case, an infeasibility exists which cannot be removed without exceeding the DAL for one or more circuits, thus system control should be performed (such as operating control actions).

Bender's decomposition [47] method and the CPLEX solver are implemented to solve this optimization problem.

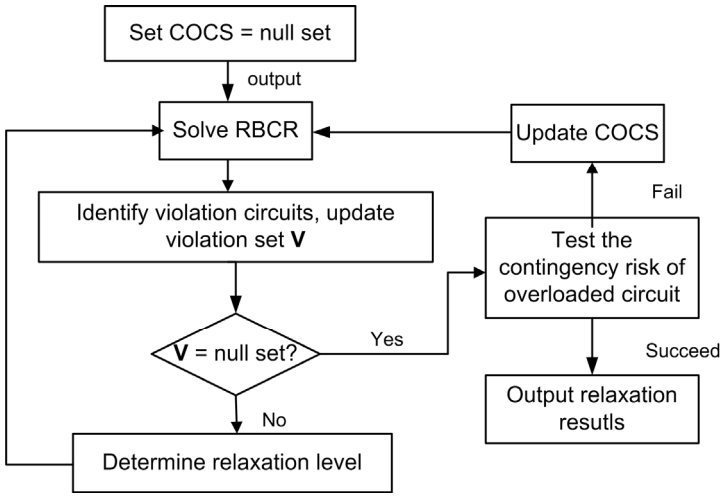

Fig. 4.6. Flowchart of deterministic risk-based constraint relaxation

4.5 Case Study—IEEE test system

4.5.1 IEEE test system and parameter determination

To examine the performance of proposed D-RBCR methodology in addressing the infeasible SCED problem, a representative IEEE test system is presented to test and illustrate the developed methodology of deterministic RBCR. A single line diagram of this system is shown in Fig. 4.7.

The corresponding circuit reactance is shown in Fig. 4.7. in per unit on a 100 MVA base. The generation costs for generators connected at buses A, B and C are

$$\mathrm{Cos}t(P_A) = 5.33\times10^{-3}P_A^2 + 11.669\times P_A + 213 \tag{4-32}$$

$$\mathrm{Cos}t(P_B) = 8.89\times10^{-3}P_B^2 + 10.333\times P_B + 200 \tag{4-33}$$

$$\mathrm{Cos}t(P_C) = 7.41\times10^{-3}P_C^2 + 10.833\times P_C + 240 \tag{4-34}$$

where P_A, $P_B$and P_C are given in MW, and $Cost$ are given in dollars/five minutes. In general, the order of marginal costs is $G_A \geq G_C \geq G_B$. The contingency probabilities of each circuit are pre-determined in Table 4.4, providing the probability that the corresponding contingency will occur during the next five minutes time-period.

Under such a network topology and setting of system operation status, the flow violation is detected in circuit B-D 'N-1' contingency condition, which makes the SCED problem infeasible. Thus, line B-D outage is the critical contingency, and the corresponding Risk Table is developed correspondingly, as shown in Table 4.5.

Table 4.4. 'N-1' contingency probability

Contingency	A-B	A-D	A-E	B-C	B-D	B-E
Probability	0.0077	0.0107	0.0115	0.0096	0.0308	0.0015
Contingency	B-F	C-E	C-F	D-E	E-F	/
Probability	0.0176	0.0001	0.0038	0.0053	0.0015	/

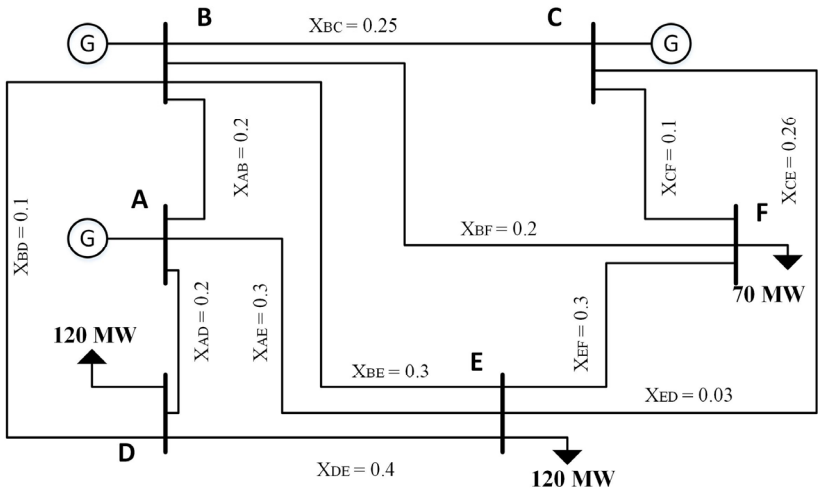

Fig. 4.7. Single-line diagram for the representative IEEE test network

Table 4.5. Risk Table for IEEE test network

Circuit	Contingency B-D	Circuit	Contingency B-D	Circuit	Contingency B-D
A-B	0.0367	B-E	0.0108	D-E	0.00001
A-D	0.2001	B-F	0.3017	E-F	0.0019
A-E	0.1687	C-E	0.0011	/	/
B-C	0.0099	C-F	0.0030	/	/
$CtgRisk_{B-D,max}$ =0.1359			$Risk_{max}$=1.14		

4.5.2 Constraint relaxation results

The results of constraint relaxation are shown in Fig. 4.8, Table 4.5 and Table 4.6.

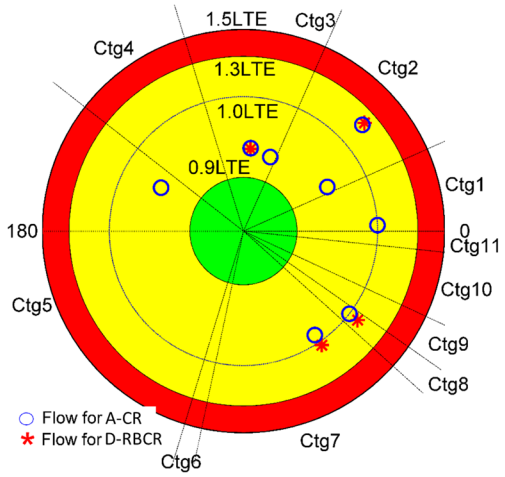

Fig. 4.8. Overflow distribution ($\geq 0.9LTE$)

Fig. 4.8 presents the security diagram under contingency situation [48], in which the sector angular spread is proportional to the contingency probability, and the radial distance from the data point to the center is proportional to the loading level. As shown in Fig. 4.8, A-CR only exerts dispatch control for the circuits having flows exceeding 1.0 LTE, and it has 5 circuit flows exceeding 0.9LTE, which are in near-violation condition. However, the action of re-dispatching in D-RBCR focuses on the system risk. It reduces the circuit flow according to its overload severity and the probability of its occurrence. Since contingency 1, 2, 3 and 5 have relatively higher probability of occurrence, D-RBCR only allows one overloaded flow exceeding 0.9LTE for contingencies 2 and 3 and no overloaded flow for contingencies 1 and 5. In particular, for contingency 2, the overloaded circuit for D-RBCR is $1.33 \times Limit_{BD}$, slightly higher than that of A-CR ($1.31 \times Limit_{BD}$), but only one overloaded flow instead of two heavily-loading flows in A-CR, and the allowable overloads in D-RBCR make less contribution to the system risk. In contrast, contingency 8 has a relatively small occurrence probability, and D-RBCR allows more heavily overloaded circuits ($1.18 \times Limit_{CF}$). That's the reason why D-RBCR has less effects on system security, quantified by the value of system risk.

According to Table 4.6, D-RBCR has better performance in economy. On one hand, it has lower production costs, since more output is dispatched from cheaper generator G_B and G_C, and less from more expensive generator G_A. For A-CR, the output from G_B has to be reduced due to the congestion line B-D. On the other hand, A-CR has larger total costs, due to the additional penalty costs. Furthermore, D-RBCR has less system risk. That is to say, it has less effects on system security to make the model feasible through conducting CR. The reason is that A-CR does not monitor on control system risk when conducting CR actions; D-RBCR adopts the risk metric to evaluate and quantify system security, and conducts constraint relaxation under the controlled

system risk and critical contingency risk. The contingency risk of the critical contingency B-D for D-RBCR is also smaller, since the optimization model has constraints to control critical contingency risk.

Table 4.6. Dispatch decision, costs and risk

Model	Gen.at bus A (MW)	Gen.at bus B (MW)	Gen.at bus C (MW)	Systm risk	Contingency risk	Prdctn costs ($/5 mins)	Total Costs ($/5 mins)
A-CR	189	42	79	1.24	0.151	4405	5230
D-RBCR	145	77	88	1.14	0.001	4315	4315

Similar to the methodology of risk-based OPF, D-RBCR introduces the risk component into the traditional LMP [11], which is called the risk-based LMP (RLMP). As indicated in Table 4.7, high LMP is observed at bus D for A-CR, due to the constraint violations and the implementation of high penalty price. This price spike comes from the congestion component in the LMP. For D-RBCR, there is no price spike observed, and the price volatility is much lower (as reflected in the LMP variance) since congestion has been significantly reduced and re-distributed over the system. Thus, risk-based constraint relaxation smooths LMP distribution at each bus.

Table 4.7. LMP at each bus (unit:$/MWh)

Model	Bus	(R)LMP	(R)LMP Energy	(R)LMP Congestion	(R)LMP Risk	(R)LMP Variance
A-CR	A	13.53	13.53	0	-	256
	B	11.24	13.53	-2.29	-	
	C	11.83	13.53	-1.70	-	
	D	52.78	13.53	39.25	-	
	E	18.28	13.53	4.75	-	
	F	15.46	13.53	1.93	-	
D-RBCR	A	13.00	13.00	0.00	0.00	6.18
	B	13.57	13.00	0.00	0.57	
	C	14.12	13.00	0.00	1.12	
	D	8.66	13.00	0.00	-4.34	
	E	11.21	13.00	0.00	-1.79	
	F	8.44	13.00	0.00	-4.56	

The infeasible SCED within single time-interval is solved successfully by the proposed method–deterministic risk-based constraint relaxation. To evaluate system security performance, it integrates the risk indices–the system risk, the critical contingency risk and the 'N-1-1' risk; the reference value is indicated by Risk Table. Furthermore, the relaxation level determination is based on the value of violation indicator and ATR constraint, which can yield an optimized decision on how much the relaxation margin is for each candidate circuit, with the controlled system security value and the critical contingency stress imposed on system operation. The LMP calculated by D-RBCR has less geographical and temporal variability throughout the network. Thus, risk-based constraint relaxation is a promising way to address the infeasible SCED problem.

4.6 Summary

Risk-based constraint relaxation has a good performance in addressing infeasible SCED problem, which allows overflowing along circuits with constrained effects on system security level. This chapter summaries and formulates the industry-based CR methodology, and based on the definition of risk indices, develops the methodology of deterministic RBCR. Furthermore, the theory and methodology have been verified by the illustration on a representative IEEE test system.

CHAPTER 5. PREDICTIVE RISK-BASED CONSTRAINT RELAXATION

5.1 Introduction

Under the circumstances of multi-interval look-ahead SCED problem, where multiple time periods are involved, the D-RBCR approach as presented in Chapter 4 are not applicable. Furthermore, the flow relaxation allowable through circuits is related to the initial condition at the beginning of the time interval (such as conductor temperature); the overloading condition is closely related to demand requirement and generation dispatch within that time interval, so that such condition frequent to be observable is that for the current time interval, there exists overloading through a particular circuit, but for the next time interval, the overloading disappears due to load change or the action of re-dispatch. Thus, it is beneficial when the RBCR methodology covers multiple time-intervals, and make significant utilization of inter-temporal effects.

It is also noted that the actual limitation determining the flow relaxation margin is conductor temperature, since heavily loading flow will incur significant increase in conductor temperature, thus sags of transmission circuits become more severe and followed by possible outage event. Shifting the research focus from traditional power flow management to conductor temperature management has observable benefits: 1) the change of temperature has time-delay characteristics, motivating those conditions that power flow violates the limits while conductor temperature is still within the limits; this indicates that such overflow is allowable and can be relaxed; 2) the flow relaxation is more precise and close to real-world consequences; 3) the pre-contingency overloading (i.e. normal condition) can be handled by constraint relaxation when conductor temperature is considered, which makes the dispatch decision less conservative.

This chapter formulates and develops the methodology of predictive risk-based constraint relaxation.

5.2 Literature review

5.2.1 Look-ahead power scheduling in power system

The essence of multi-interval look-ahead dispatch is to solve a fast look-ahead optimization problem at each time step. As shown in Fig. 5.1, in the P-RBCR model, the control decision (generation dispatch) for the entire operation horizon is determined by solving the P-RBCR optimization model, considering the predictive evolution of system state parameters. As what follows, the control decisions for the first time-interval is executed; the remaining control decisions are produced for advisory purposes, which can assist system operators to prepare for the upcoming events. This idea is similar to the framework of model predictive control, which is also called receding horizon control.

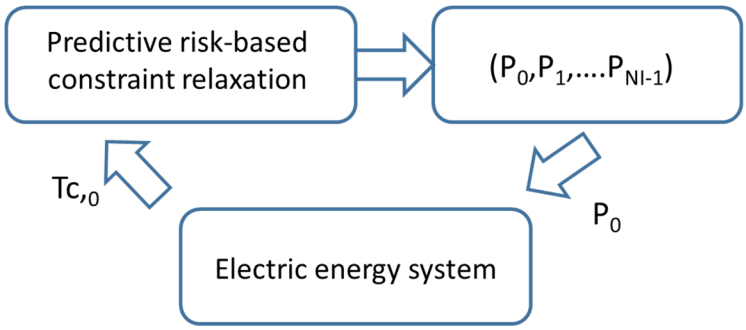

Fig. 5.1. Structure of the Predictive RBCR

5.2.2 Dynamic thermal ratings in power system

The power transfer limits of overhead transmission circuits are critical constraints for both power system planning and operation. The actual limitation of allowable loading through transmission circuits is conductor temperature, and this is related to current (flow) levels through the dynamic heat balance equation (DHBE). Static line rating (SLR) has been implemented by most transmission owners and the ISOs, and the SLR corresponds to the most severe weather

condition (for example, ambient temperature and wind velocity) and is calculated seasonally [49, 50]. Thus, computing thermal ratings by SLR tends to result in conservative operating limits. Dynamic line rating (DLR) is determined based on real-time meteorology, indicating the maximum current permissible under the current situation. The benefits of DLR have already been identified and assessed for some study cases. A recent example is that Oncor electric delivery company has installed a DLR monitoring system for eight transmission lines; these systems are active in daily operations and their effects are accounted for in the electricity market. The demonstration shows that transmission capacity has been improved 8%~14% for 90% of the monitoring time windows [51]. Application of DLR provides a cost-effective method to better utilize transmission capacity. Its utilization provides benefits for congestion management with integration of renewable energy. Reference [52] proposes a distributional-robust congestion management model, which imposes DLR on critical lines, providing the ability to control the risk of thermal overloading. References [53] and [54] develop simulation models, the implementation of which show significant economic potentials and system security enhancement of deploying DLR when integrating significant amounts of variable renewables.

DLR has been coordinated with optimal power flow for addressing issues spanning several time-scales, and they are from planning to power system scheduling. The main challenge is that DHBE adds a set of time-coupled nonlinear equality constraints to the optimization model. The studies in [55] and [56] do not involve DHBE directly; instead, they model overloading risk as a deterministic function of the level of circuit current exceeding previous thermal rating and include it as a penalty function in the objective function, and they relax the reserves rating without significant increasing computation complexity. In reference [57], DHBE is simplified by assuming that the terms unrelated to transmission line loss are constant with temperature change. In [58],

power flow and heat terms are linearized as functions of generation output and conductor temperature. Then, the iterative method of solving several linearized sub-problems generates the corresponding optimal solution. Reference [59] introduces a feasible way to integrate DHBE with AC-based security constrained unit commitment, but several assumptions are made, such as the conductor resistance is fixed at its value when at maximum temperature, and several internal relationships are linearized. Although many efforts were made to integrate DHBE in OPF, they tend to be oversimplified or non-convex, resulting in inappropriate results. The requirement of AC power flow also limits the scalability of extending the developed methodology to large-scale industry-grade power system models.

5.3 Dynamic heat balance equation

Thermal rating calculations for the conductors are performed according to the parameter relations and procedures provided in IEEE Std. 738 [49]. According to IEEE Std. 738, circuit temperature for overhead transmission conductors is a function of 1) conductor material properties, 2) conductor diameter, 3) conductor surface conditions, 4) ambient weather conditions (ambient temperature, solar radiation and wind velocity), and 5) conductor electrical current. The first two items characterize chemical and physical properties of the conductor, which can be pre-determined and remain fixed over the life span of the conductor. Thus, dynamic heat balance equation imposes that heat gain from solar radiation and conductor thermal effects equals to heat loss through natural radiation and through convection cooling effects via ambient surface wind, as indicated by the differential equation of (5-1).

$$C_P \frac{dT_c}{dt} = I^2 R(T_c) + Q_s - Q_r(T_c, T_a) - Q_c(T_c, T_a) \tag{5-1}$$

Here, T_c is conductor temperature (^oC), T_a is ambient temperature (^oC), I is conductor current (A), Q_s is heat gain from solar radiation, Q_r is heat loss by natural radiation, Q_c is

convection by wind cooling effects, and C_P is conductor heat capacity. The detailed calculation of each heat item can be referenced to [49].

The underlying concept for application of DLR in constraint relaxation is not to update the thermal rating according to real-time monitoring on ambient weather information but rather to account for the transient temperature variation using conservative weather information as currents change from one market interval to another. By using pre-determined, conservative weather data to compute transmission thermal ratings [50], the maneuverability can be increased for deploying constraint relaxation while maintaining secure conditions. Although data from real-time monitoring equipment can certainly be used, real-time monitoring equipment is not required.

DC power flow is deployed in the proposed model. It is acknowledged that DC power flow assumptions provide reasonable estimates of power flow to assess circuit overloads. This provides that the model has good performance in scalability, enabling tractable computational burden even for the large-scale ISO systems.

In what follows, the DHBE is illustrated based on an assumed conservative weather conditions. Suppose it is desired to assess the 2pm conditions of a Drake 795kcmil 26/7 ACSR conductor. From IEEE Std. 738, the value of emissivity, altitude and the azimuth of the sun can be determined. The ambient temperature is conservatively assumed to be $T_a = 40\ ^oC$ and wind speed to be 2ft/s. Then the various heat terms are described by (5-2) and (5-5) [49]:

- Radiated heat loss:

$$q_r = 0.0765 \times \left(\frac{T_c + 273}{100} \right)^4 - 7.3424 \tag{5-2}$$

- Solar heat gain:

$$q_s = 4.3082 \ \ W / ft \tag{5-3}$$

- Heat loss from current thermal effects:

$$I^2R = I^2 \times \left(8.6\times10^{-8} \times T_c + 2.005\times10^{-5}\right) \tag{5-4}$$

- Heat loss from wind convection:

$$q_c = 0.4175 \times T_c - 16.7013 \tag{5-5}$$

Then substitute each heat term into (5-1) to obtain:

$$\frac{dT_c}{dt} = \left(0.0215\times10^{-8} \times I^2\right) \times T_c - 1.9125\times10^{-4} \times \left(\frac{T_c + 273}{100}\right)^4 + \left(0.005\times10^{-5} \times I^2 + 0.0709\right) \tag{5-6}$$

The numerical experiments is conducted (under conditions of typical T_a and wind speed v_m values), deriving the relationship between $(T_{c,\Delta t} - T_{c,0})$ and $(T_{c,0}, I_{\Delta t})$ (Δt is a pre-determined time-step), as shown in Fig. 5.2. This three-dimensional figure shows that the surface is convex; indeed, it can be shown that the resulting surface is convex independent of parameters selected. This fact facilitates the idea to fit the surface with a piece-wise linear surface, resulting in a linearized relationship between current and conductor temperature change, as shown in (5-7).

$$T_{C,\Delta t} - T_{C,0} = a_i \times T_{C,0} + b_i \times I_{\Delta t} + c_i \tag{5-7}$$

where, a_i, b_i, c_i are coefficients obtained by linear regression. When there exists overloads along a specific transmission circuit, the overloads are allowed if the conductor temperature is still within satisfactory boundaries; this is as characterized by the linearized surface illustrated in Fig. 5.2.

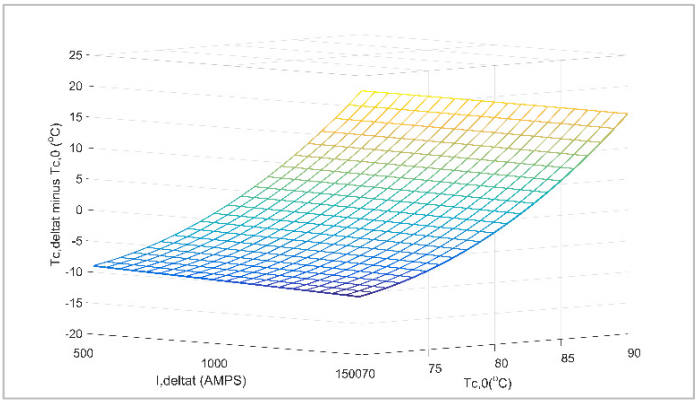

Fig. 5.2. Relationship between the circuit current and the conductor temperature

The piece-wise linear representation of the conductor temperature limitations is utilized within the predictive control model. To facilitate on-line assessment, the conductor limitation (5-7) can be developed off-line for each conductor known to be a CR candidate.

5.4 Conceptual illustration

In this subsection, to illustrate the concept and projected outcomes for risk-based constraint relaxation under the framework of multi-interval look-ahead dispatch, the dynamic thermal rating of a typical transmission facility (Drake conductor-795 Kcmil 26/7 ACSR) is modeled over a timeframe of thirty minutes (1800 seconds, with each time interval as 5 minutes). Parameters used include ambient temperature $T_a = 40\ ^oC$, wind speed is 2ft/s, maximum allowable conductor current to carry is 1150A, and maximum allowable conductor temperature $T_{c,max} = 110\ ^oC$. Assume that loading level during each five-minute time-interval remains constant. The conductor temperature variation within a specific time-interval depends on the conductor temperature at the beginning of that interval and the loading current during that interval; it is required that conductor temperature does not exceed the temperature limit for the conductor at the end of that time interval. The time constant of conductor temperature change is assumed to be 12 minutes, which is typical of ACSR conductors [49]; since the thermal time constant gives the time following a step-change in current necessary to reach 63.2% of the steady-state temperature, temperature will not reach steady state for any changes imposed during the 30-minute timeframe. The differential equation is run in MATLAB/Simulink, and the corresponding curve of loading change and conductor temperature change with time is shown in Fig. 5.3. In this figure, the green curve represents the imposed current, quantified by the right-hand axis, and the blue curve represents the resulting conductor temperature quantities, quantified by the left-hand axis. The horizontal line labeled $I_{,max}$ represents the maximum steady-state current, which is computed based on procedures and

parameters provided in the IEEE Std. 738 [49]. The horizontal line labeled $T_{c,max}$ indicates the maximum steady-state temperature allowable for this conductor. The initial current loading is 1000 A at $t=0^-$ and 1050 A at $t=0^+$, and the initial conductor temperature is 80°C.

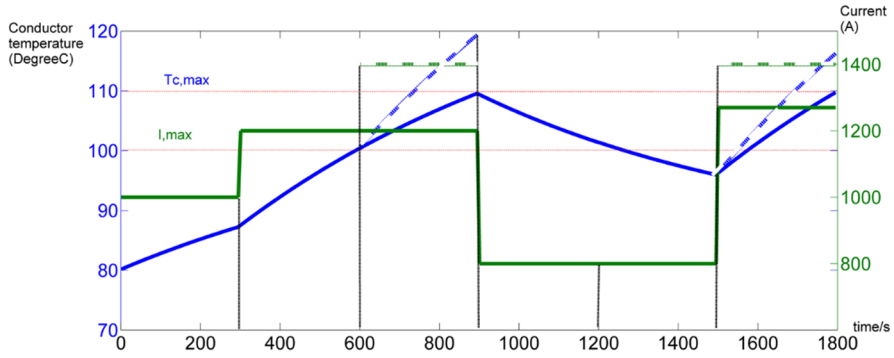

Fig. 5.3. Change of the load and conductor temperature

As shown in Fig. 5.3，

- For the second time-interval, the flow (green plot) violates the limit, but since there exists a delay in the change of conductor temperature, the conductor temperature (blue plot) remains within its limits for this time interval.
- For the third time-interval, since the initial temperature (obtained as the final conductor temperature value from the previous time-interval) is relatively high, the predicted future flow (shown as the dashed green plot) along this time interval will cause conductor temperature to exceed the limits (shown as the dashed blue plot). Therefore, such a constraint relaxation is not acceptable.
- For the third interval and sixth interval, the predicted future flows (dashed green plots) are the same; however, the resulting conductor temperatures in the two intervals (dashed blue plots) are different. This difference results from the differences on initial temperatures for the third and sixth time intervals; the sixth interval has a significantly

lower initial temperature because of the depressed flow during the fourth and fifth intervals. This observation illustrates that the utilization of conductor temperature during a constraint relaxation period increases flexibility in that conductor temperature during that time interval, since it depends not only on the flow during that time interval but also on the flow in preceding time intervals. Thus, it is the thermal dynamics that offer the possibility of using inter-temporal effects to maneuver conductor temperature during periods where constraint relaxation is needed.

- The conductor temperature violation represented by the dashed blue plots in the third and sixth time interval can be avoided by limiting the current to the green solid plots during those time intervals. This results in the blue solid plots, which maintain conductor temperature at or below the temperature limit in all time intervals and would be achieved via look-ahead dispatch.

To summarize, the conductor temperature at the end of a time interval is related to initial conductor temperature and the flow level imposed on that time-interval. A constraint relaxation is acceptable if flow violates the corresponding limits while conductor temperature is still within its limit; a constraint relaxation is considered to be unacceptable if the conductor temperature exceeds its limit. Although this approach provides additional maneuverability for CR necessitated by both normal and contingency conditions (due to the thermal dynamics), the benefit for CR necessitated by contingency conditions is generally larger than that necessitated by normal conditions because contingency conditions are always associated with a step change in flow following the contingency.

5.5 Methodology of predictive risk-based constraint relaxation

5.5.1 Risk assessment

1. Risk measurement

Risk measurement is applied to evaluate the effects on system security of thermal overloads. In comparison with system risk in D-RBCR, risk metric in P-RBCR accounts for both pre-contingency (normal condition) and post-contingency conditions. Each condition is identified as a state; thus, it ends up with the no-contingency state and a number of different contingency states. The risk metric is then computed as the summation across all states of the product of state probability and state severity (or impact). The severity of a particular state is the summation over all circuits of each circuit's severity, where the circuit severity is a function of the power flow on that circuit if not a CR circuit (belongs to NCR set), or a function of conductor temperature if a CR circuit (belongs to CR set), which are defined as sev_P and sev_C, respectively. The calculation of risk value is according to (5-8).

$$Risk = \sum_{T=1}^{NI}\left(\sum_{k=0}^{NC}\Pr^{k}\left(\sum_{l\in NCR} sev_{P,l,T}^{k} + \sum_{l\in CR} sev_{C,l,T}^{k}\right)\right) \tag{5-8}$$

where $sev_{P,l,T}^{k}$ is the severity value of the circuit l under event k in NCR set, which is evaluated by loading level; $sev_{C,l,T}^{k}$ is the severity of the circuit l under event k in CR set, which is evaluated by the level of conductor temperature. The modelling and calculation of temperature severity is similar to that of power flow severity. Thus, the descriptions about calculating temperature severity are not redundantly repeated.

5.5.2 Formulation

A three-stage solving procedure is implemented in the methodology of predictive risk-based constraint relaxation, including Stage 0, Stage 1 and Stage 2. These stages are described in what follows:

1. Stage 0 - initialization

Initialize the infeasible problem (identifies the initial set of CR circuits and NCR circuits). The starting point is the implementation of industry-based CR method. Non-negative slack variables are introduced to the transmission constraints, and the associated penalty cost is incorporated into the objective function. DC power flow is utilized in the optimization problem, and power loss is neglected. Detailed formulations are provided in (5-9)~(5-18).The major difference to the formulation of D-RBCR is that regulation reserve is involved and ramping capabilities are represented with existence of inter-temporal effects.

$$Min \sum_{T=1}^{NI}\sum_{i=1}^{NG} c_{G,i} \times P_{i,T} + \sum \text{Penalty} \times \alpha_{l,T}^{k} \tag{5-9}$$

Subject to:

$$\sum_{m=1}^{N}\left(\sum_{i\in m} P_{i,T}\right) - \sum_{m=1}^{N} D_{m,T} = 0, T \in \{1,...,NI\} \tag{5-10}$$

$$h_{l,T}^{k} = \sum_{m=1}^{N} PTDF_{l,m}^{k}\left(\sum_{i\in m} P_{i,T} - D_{m,T}\right), k \in \{0,1,...,NC\}, l \in \{1,..,NL\}, T \in \{1,..,NI\} \tag{5-11}$$

$$h_{l,T}^{k} - \alpha_{l,T}^{k} \le Limit_{l}^{k}, k \in \{0,1,...,NC\}, l \in \{1,..,NL\}, T \in \{1,..,NI\} \tag{5-12}$$

$$P_{i,T} - REG_{i,T}^{down} \ge P_{i,\min}, T \in \{1,...,NI\}\ i \in \{1,...NG\} \tag{5-13}$$

$$P_{i,T} + REG_{i,T}^{up} \le P_{i,\max}, T \in \{1,...,NI\}\ i \in \{1,...NG\} \tag{5-14}$$

$$-RMP_{i}^{up} \le \Delta T\left(P_{i,T} - P_{i,T-1}\right) \le RMP_{i}^{up}, T \in \{2,..,NI\}, i \in \{1,...NG\} \tag{5-15}$$

$$-RMP_i^{down} \le \Delta T\left(P_{i,T} - P_{i.T-1}\right) \le RMP_i^{down}, T \in \{2,..,NI\}, i \in \{1,...NG\} \quad (5\text{-}16)$$

$$\sum_{i=1}^{NG} REG_{i,T}^{up} \ge REG_{req,T}^{up}, T \in \{1,..,NI\} \quad (5\text{-}17)$$

$$\sum_{i=1}^{NG} REG_{i,T}^{down} \ge REG_{req,T}^{down}, T \in \{1,..,NI\} \quad (5\text{-}18)$$

where, (5-10) is the system power balance equation, which guarantees that the generation output satisfies load consumptions. (5-11) is the calculation of circuit flows, which are restricted by thermal limits in (5-12). (5-13)~(5-14) constrain minimum and maximum generation output with sufficient space for regulation movements. (5-15)~(5-16) are ramping constraints, which should be deployed when operating in the horizon of multiple time intervals, since distinct base points are setting up for each individual time-interval. (5-17)~(5-18) indicate the system-wide demand for regulation products. Circuits with non-zero slack variables are included in the CR set; the remaining transmission line constraints are automatically identified as NCR lines.

2. Stage 1 - feasibility

The functionality of Stage 1 is to search the infeasible SCED problem for a feasible solution. In this stage, the effects on system security imposed by allowing overloads are controlled by system risk. The objective is to identify the feasible solution, with minimization of system risk. This optimization problem is formulated as follows:

$$Min\ Risk = \sum_{T=1}^{NI}\left(\sum_{k=0}^{NC} \Pr^k\left(\sum_{l\in NCR} sev_{P,l,T}^k + \sum_{l\in CR} sev_{C,l,T}^k\right)\right) \quad (5\text{-}19)$$

Subject to:

(5-10)~(5-11)

$$T_{C,l,T}\left(h_{l,T}^k, T_{C,l,T_0}, \Delta t\right) \le T_{C,l,\max}, k \in \{0,1,..., NC\}, l \in CR, T \in \{1,..,NI\} \quad (5\text{-}20)$$

$$h_{l,T}^{k} - \alpha_{l,T}^{k} \le Limit_{l}^{k}, k \in \{0,1,...,NC\}, l \in NCR, T \in \{1,..,NI\} \tag{5-21}$$

$$\begin{cases} sev_{P,l,T}^{k} \ge 0 \\ sev_{P,l,T}^{k} \ge a_{1l} \times h_{l,T}^{k} + b_{1l} \\ sev_{P,l,T}^{k} \ge a_{2l} \times h_{l,T}^{k} + b_{2l} \\ sev_{P,l,T}^{k} \ge a_{3l} \times h_{l,T}^{k} + b_{3l} \end{cases}, k \in \{0,1,...,NC\}, l \in NCR, T \in \{1,..,NI\} \tag{5-22}$$

$$\begin{cases} sev_{C,l,T}^{k} \ge 0 \\ sev_{C,l,T}^{k} \ge a_{1l}^{c} \times h_{l,T}^{k} + b_{1l}^{c} \\ sev_{C,l,T}^{k} \ge a_{2l}^{c} \times h_{l,T}^{k} + b_{1l}^{c} \\ sev_{C,l,T}^{k} \ge a_{3l}^{c} \times h_{l,T}^{k} + b_{1l}^{c} \end{cases}, k \in \{0,1,...,NC\}, l \in CR, T \in \{1,..,NI\} \tag{5-23}$$

(5-13)~(5-18)

The overloading circuits are included in the CR set, and the dynamic heat balance equation is implemented for circuits in the CR set, which restrict conductor temperature (and not circuit flow) for the CR set, as shown in (5-20). For those circuits assigned to the NCR set, which has no observed overloads, power flow level is limited on the corresponding transmission facilities, as expressed in (5-21). (5-22)~(5-23) represent the calculation of severity value performed for the NCR circuits and CR circuits, respectively.

3. Stage 2 – optimality

Stage 2 is formulated to obtain economic dispatch decision, based on feasible region determined by Stage 1. In comparison with Stage 0, Stage 2 works with the new limits which have been relaxed, and is free of penalty price. This problem is formulated as follows:

$$Min \sum_{T=1}^{NI} \sum_{i=1}^{NG} c_{G,i} \times P_{i,T} \tag{5-24}$$

Subject to: (5-10)~(5-11)

$$h_{l,T}^{k} \le Limit\_new_{l}^{k}, k \in \{0,1,...,NC\}, l \in \{1,..,NL\}, T \in \{1,..,NI\} \tag{5-25}$$

(5-13)~(5-18)

5.5.3 Solving approach

1. Solution procedure

The P-RBCR solution procedure is illustrated in the flow chart of Fig. 5.4 , it is illustrated using simplified optimization formulations in Fig. 5.5, and it is described below.

- Stage 0, initialization: This stage initializes the infeasible problem. It identifies the locations and amounts of overloads via the slack variables that are non-zero; in addition, the CR and NCR sets of circuits are initialized in this stage.

- Stage 1, feasibility: This stage identifies the constraint relaxation decision by minimizing system risk; it iterates on the dynamic CR set until no further CR lines are found, and provides the feasible solution to stage 2. The iteration on the CR set occurs by forming linear relationships among T_0, ΔT and I to provide the conductor temperature limits; slack variables are minimized for the NCR set, and any line with positive slack becomes a new CR line, being added to the CR set. Based on the conductor temperature of CR lines, the DHBEs are applied within the optimization problem to achieve the necessary relaxation to obtain the updated new flow limits. Those overloads are allowable since the conductor temperature does not exceed the corresponding limit; the allocation of overloads by optimization algorithm degrades the system security least; it is evaluated in terms of risk value.

- Stage 2, optimality: This stage utilizes the new flow limits, and obtains the most economic dispatch decision among all feasible solutions to this predictive SCED problem, which is otherwise infeasible. As the predictive control methodology, the solution for the first time-interval is implemented; the solutions for the subsequent time intervals are considered as advisory dispatch decisions.

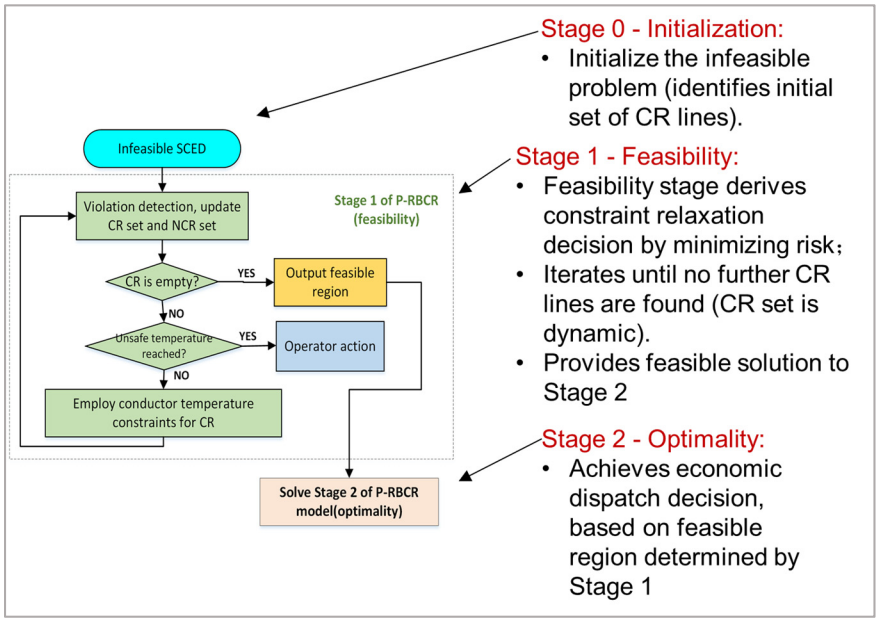

Fig. 5.4. Flow chart of the P-RBCR solution procedure

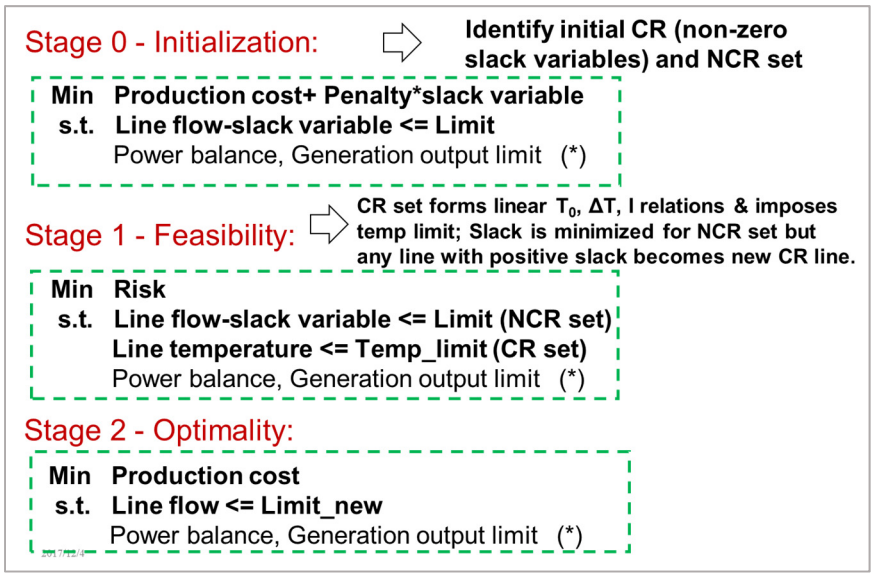

Fig. 5.5. Simplified optimization formulations for solution procedure in the P-RBCR

2. Algorithm realization: interfacing GAMS with MATLAB

As a leading modelling and mathematical tool, the General Algebraic Modeling System (GAMS) has been widely used in operations research. It has the advantages of simplicity in implementation and convenience to debug, as well as it is friendly to interface with other commonly used programming languages, such as MATLAB and Python. The GAMS software

contains advanced solving algorithms for linear programs, mixed-integer programs, and other optimization problem types. Furthermore, the GAMS software can address high-dimensional problems with large quantities of constraints and decision variables. Thus, GAMS is selected to model and solve the optimization models in P-RBCR which are linear programming problems. Nevertheless, output processing and iterative updating sets are interfaced with MATLAB, which has good flexibility in data processing. The functionality GDXMRW (GDX-MATLAB Read/Write) is utilized to exchange data between the GAMS and the MATLAB.

5.6 Case Study on a representative IEEE test system

5.6.1 Parameter and data preparation for IEEE test system

1. IEEE test system

For the purpose of verifying the proposed optimization for handling the infeasible predictive SCED problem, the methodology of P-RBCR and associated solution algorithm are tested on the modified IEEE representative system [60]. The single-line diagram for network configuration is indicated in Fig. 5.6. There are 11 transmission lines with 3 generators at buses 1, 2, and 3, respectively. System loads are located at buses 4, 5, and 6, respectively. The operating horizon for predictive control is six 5-minute time-intervals.

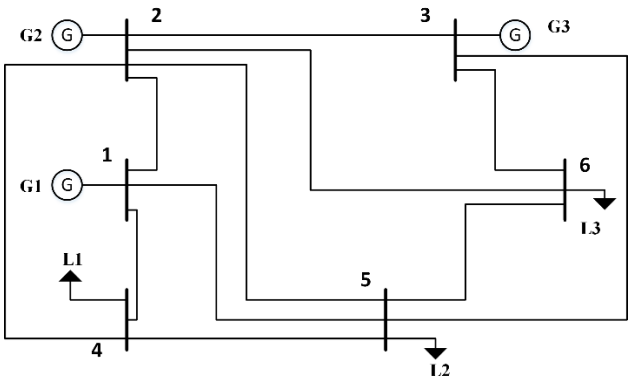

Fig. 5.6. Network topology of a representative IEEE test system

Tables 5.1~5.3 provide generator attributes, load variations and parameters for each circuit (including thermal ratings and pre-defined probabilities of 'N-1' contingency states). One state represents the normal condition and 11 states represent 'N-1' contingency conditions; the operating horizon of six time-intervals are considered in the predictive SCED. Thus, 726 inequalities are utilized to represent and model the transmission constraints. This large number of constraints indicates the complexity of the optimization problem, given the fact that this is not a very large-scale system.

Table 5.1. Generator attributes

	Pmax (MW)	Pmin (MW)	Marginal Cost ($/MW)	Ramping up rate (MW/min)	Ramping down rate (MW/min)	Regulation cost ($/MWh)
G1	200	50	30	2	2	10
G2	150	37.5	20	2	2	10
G3	180	45	40	2	2	10

Table 5.2. Load attributes (unit: MW)

	Period 1	Period 2	Period 3	Period 4	Period 5	Period 6
Load 1	78	79.3	80.6	79.3	78	79.3
Load 2	78	79.3	80.6	79.3	78	79.3
Load 3	78	79.3	80.6	79.3	78	79.3

Table 5.3. Transmission circuits parameters

From Bus	To Bus	Normal Rating (MW)	Long-term emergency rating (MW)	Short-term emergency rating (MW)	Prob. of contingency
1	2	100	110	130	0.077
1	4	100	110	130	0.077
1	5	100	110	130	0.115
2	3	60	66	78	0.096
2	4	60	66	78	0.038
2	5	60	66	78	0.115
2	6	60	66	78	0.077
3	5	60	66	78	0.100
3	6	60	66	78	0.038
4	5	60	66	78	0.153
5	6	60	66	78	0.115

2. Linear representation of dynamic heat balance equation

Suppose the initial temperature at the beginning of the time interval $T_{c,0} = 30\ ^{o}C$, and the maximum temperature that the conductor can withstand is $T_{c,max} = 100\ ^{o}C$. By conducting numerical experiments, the derived relationship between $(T_{c,\Delta t} - T_{c,0})$ and $(T_{c,0}, I_{\Delta t})$ (Δt is a specific time step), is as shown in Fig. 5.7. Furthermore, the convex surface is fitted by linear regression in MATLAB statistics toolbox; the coefficients are indicated in (5-26) with an R-square of 0.99, which verifies that the linear relationship has a satisfactory performance in approximating the complex differential formulation.

$$T_{C,\Delta t} - T_{C,0} = -0.4004 \times T_{C,0} + 0.0129 \times I_{\Delta t} + 12.97 \tag{5-26}$$

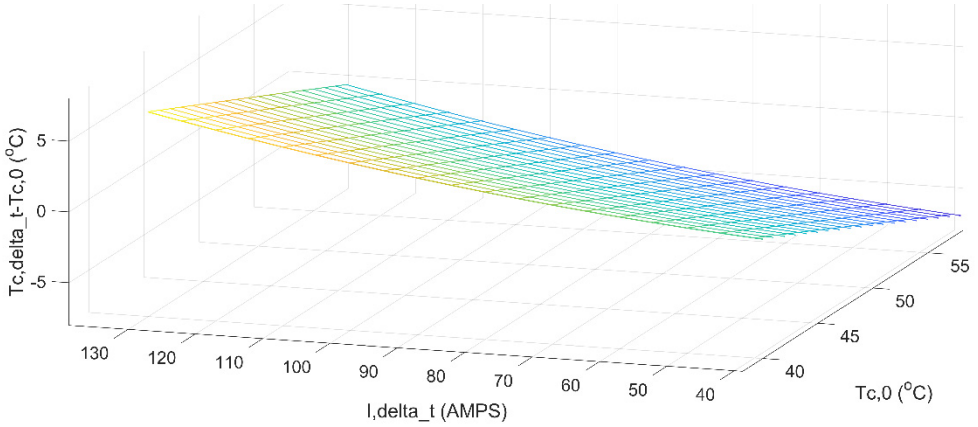

Fig. 5.7. Relationship between current flow and conductor temperature

Solve the infeasible SCED problem under A-CR, which is Stage 0 of the P-RBCR, and the violated thermal constraints (line 24, contingency 2 through the first time-interval to the sixth time-interval, denoted as P1~P6) are identified by evaluating with non-zero slack variables. Then, those violated lines are added to the CR set (restricted by conductor temperature limits), and the remaining lines stay in the NCR set (restricted by flow limits), with the objective to minimize the system risk. This process is iteratively repeated until an iteration occurs where no additional violated lines are identified; in the specific case studied here, only 2 iterations are necessary.

Finally, the new limits required to be relaxed are computed by the thermal DHBE, and the predictive SCED is re-solved. With the feasible region determined by the relaxed limits, the most economic re-dispatch decisions are identified. The results and corresponding analysis are conducted in the following sections.

5.6.2 Risk-based predictive constraint relaxation results

1. Flow/temperature change

In the feasibility stage, the thermal limits for line 24 (contingency 2, P1~P6) has been assigned to CR set. By shifting from flow limits to temperature limits, those lines are no longer violated constraints. Fig. 5.8 illustrates flow/temperature change along line 24 under contingency 2.

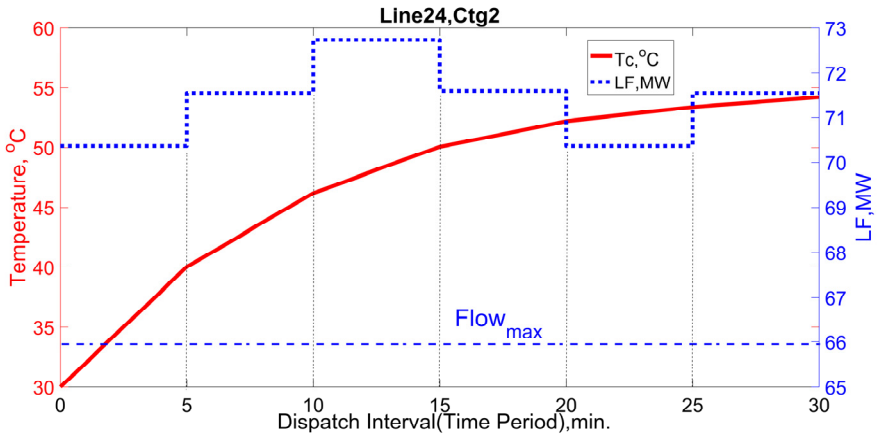

Fig. 5.8. Flow/Temperature change for line 24 under contingency 2

As shown in Fig. 5.8, for those time intervals, power flows (indicated by the blue dashed lines) exceed corresponding limits; while conductor temperature (indicated by the red solid lines) are within the temperature boundary. This effect arises from the fact that conductor temperature change is delayed relative to the power flow change. Thus, constraint relaxations, where power flow exceeds its limit, can be safe if the power flow increase is reduced before the temperature exceeds its limit.

It is observed that the slope of temperature change within each interval is decreasing as time changes; this results from the pattern of flow change, where the flow increases in the first three time-intervals and decreases in the fourth and fifth time intervals. This observation indicates that the nature of flow change can be step-wise, which follows the control signal immediately; while temperature change is a gradual and has slow dynamic process. Another observation is that the relationship between flow change and temperature change is not simply positively or negatively correlated. The behavior of temperature change is the cooperative consequences by the initial temperature at the beginning of the time interval, together with the accumulated thermal effects imposed on the conductor during the time interval. As shown in the fourth interval, flow decrease does not result in immediate temperature drop; on the contrary, temperature continues to increase but with a decreasing change rate, until the end of the operating horizon.

2. Economic performance and risk evaluation

Economy and security are the major criteria to consider when making dispatch decisions. Table 5.4 lists production cost and risk for the A-CR methodology and the P-RBCR methodology for this illustration. As provided in Table 5.4, the P-RBCR results in a solution that has superior performance at both perspectives of production economy and system security, via relatively lower production cost and lower risk. The reason for the lower production cost is that there is no penalty (which is in thousands-scale) involved in the formulation of P-RBCR and the feasible region of the optimization problem is extended. However, the P-RBCR re-dispatches available resources and reflects the true costs to alleviate congested lines. The P-RBCR sends LMP signals which reflect the system congestion status but avoids impractical price spikes; this feature will be discussed in the next subsection. The feasible solution is identified through the risk minimization of Stage 1; this provides that P-RBCR has better performance in risk evaluation.

Table 5.4. Comparisons on cost and risk

	Production cost($/30min)	Risk
A-CR	179,616	135.6
P-RBCR	51,168	130.8

3. LMP comparison between A-CR and P-RBCR

Based on the LMP calculation presented in Appendix A, LMP under A-CR and P-RBCR is calculated, as shown in Table 5.5 and Fig. 5.9. The detailed calculation procedures of those prices are presented in Appendix A, and the loss component of LMP is neglected.

Table 5.5. Breakdown of LMP for A-CR and P-RBCR (unit: $/MWh)

		A-CR			P-RBCR		
Bus	**Period**	**LMP_ Energy**	**LMP_ congestion**	**LMP**	**LMP_ Energy**	**LMP_ congestion**	**LMP**
1	P1	30	0.00	30.00	30	0.00	30.00
2		30	-287.44	-257.44	30	-70.04	-40.04
3		30	10.00	40.00	30	10.00	40.00
4		30	3057.24	3087.24	30	757.65	787.65
5		30	433.24	463.24	30	105.06	135.06
6		30	107.51	137.51	30	5.45	35.45
1	P2	30	0.00	30.00	30	0.00	30.00
2		30	-287.44	-257.44	30	-70.04	-40.04
3		30	10.00	40.00	30	10.00	40.00
4		30	3057.24	3087.24	30	757.65	787.65
5		30	433.24	463.24	30	105.06	135.06
6		30	107.51	137.51	30	5.45	35.45
1	P3	30	0.00	30.00	30	0.00	30.00
2		30	-287.44	-257.44	30	-70.04	-40.04
3		30	10.00	40.00	30	10.00	40.00
4		30	3057.24	3087.24	30	757.65	787.65
5		30	433.24	463.24	30	105.06	135.06
6		30	107.51	137.51	30	5.45	35.45
1	P4	30	0.00	30.00	30	0.00	30.00
2		30	-287.44	-257.44	30	-70.04	-40.04
3		30	10.00	40.00	30	10.00	40.00
4		30	3057.24	3087.24	30	757.65	787.65
5		30	433.24	463.24	30	105.06	135.06
6		30	107.51	137.51	30	5.45	35.45

Table 5.5. (continued)

Bus	Period	A-CR			P-RBCR		
		LMP_ Energy	LMP_ congestion	LMP	LMP_ Energy	LMP_ congestion	LMP
1	P5	30	0.00	30.00	30	0.00	30.00
2		30	-287.44	-257.44	30	-70.04	-40.04
3		30	10.00	40.00	30	10.00	40.00
4		30	3057.24	3087.24	30	757.65	787.65
5		30	433.24	463.24	30	105.06	135.06
6		30	107.51	137.51	30	5.45	35.45
1	P6	30	0.00	30.00	30	0.00	30.00
2		30	-287.44	-257.44	30	-70.04	-40.04
3		30	10.00	40.00	30	10.00	40.00
4		30	3057.24	3087.24	30	757.65	787.65
5		30	433.24	463.24	30	105.06	135.06
6		30	107.51	137.51	30	5.45	35.45

Congestion on line 24 results in relatively high LMP at buses 4 and 5. The reason for bus 2 has a negative congestion component is that one additional MW withdrawal at bus 2 reduces the congestion along line 24, thus decreasing the total cost.

The LMP components are plotted in Fig. 5.9 (some of the price values exceeding $3000 have been cut off at the top in order to ensure that the resolution of relatively lower price values is acceptable); from this, it can be observed that the A-CR and the P-RBCR share the unique energy component, since the generator data, load attributes and system topology for those two models are the same. Another observation is that the P-RBCR decreases the congestion component, which avoids the artificially high LMP spike, yet still retains the congestion pattern of A-CR unmasked.

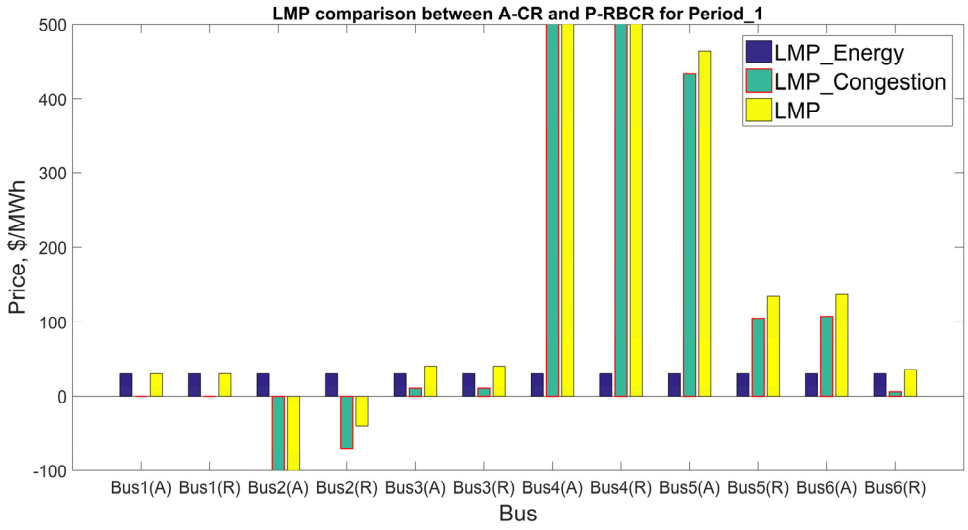

Fig. 5.9. Breakdown and comparisons of LMP between the A-CR and the P-RBCR

5.7 Case Study on contrived NYISO system

The methodology of P-RBCR can be applied to real-world ISO system. Based on the public available data, a mini-NYISO system is contrived, with details shown in Appendix B. As what follows, the methodology of P-RBCR is tested on the mini-NYISO system in this subsection.

5.7.1 Evaluation of the mini-NYISO system

The day of June 13th, 2017 is the recorded peak day in the operation report for the month of June 2017. Thus, the time stamp from 20:00 to 20:25 is picked up as the examined operating horizon, since the LMP spike is observed to occur frequently during this time horizon, which indicates a relatively highly-congested network and stressful operating condition. By manipulating the interface limit, the congestion pattern was successfully repeated, which is similar to what is observed in the NYISO production system**.** Overloads have been observed in the initial condition, as shown in Table 5.6. The corresponding LMPs are listed in Table 5.7; only those LMPs for Period 1 are presented since the remaining periods are observed as similar patterns. A high congestion price is shown for Zones Millwood, Dunwoodie, NYC and Long Island. Furthermore,

the LMPs in the western and central zones tend to be lower than those in the southeastern zones. This is caused by the imbalanced distribution of resources and loads in the NYISO. Overall, Zone NYC and Long Island contribute to 50% of the total load; expensive gas-turbines contribute the most as the energy output resources in those zones and cheap generation is concentrated in western and central zones, including the Niagara hydro units. Congestion on the Central-East interface has been historically challenging for the NYISO system. Thus, LMPs in those zones tend to be higher. This verifies that the contrived mini-NYISO system is a reasonable and realistic approximation to the operation and market performance of the NYISO system.

Table 5.6. Limiting facilities

Periods	**Limiting facility**
P1	Hudson valley →Millwood ; Millwood → Dunwoodie ; Dunwoodie → NYC ; NYC → Long Island
P2	Hudson valley → Millwood ; Millwood → Dunwoodie ; Dunwoodie → NYC; NYC → Long Island
P3	Dunwoodie → NYC; NYC → Long Island
P4	Dunwoodie → NYC; NYC → Long Island
P5	Dunwoodie → NYC; NYC → Long Island
P6	Millwood → Dunwoodie; Dunwoodie → NYC ; NYC → Long Island

Table 5.7. Breakdown of LMP in A-CR (unit:$/MWh)

Bus	**Period No.**	**LMP_Energy**	**LMP_Congestion**	**LMP**
West	P1	33.24	0	33.24
Genessee	P1	33.24	4.02	37.26
Central	P1	33.24	0	33.24
North	P1	33.24	0	33.24
Mohawk Valley	P1	33.24	0	33.24
Capital	P1	33.24	0	33.24
Hudson valley	P1	33.24	11.76	45
Millwood	**P1**	**33.24**	**4011.76**	**4045**
Dunwoodie	**P1**	**33.24**	**8011.76**	**8045**
NYC	**P1**	**33.24**	**12011.76**	**12045**
Long Island	**P1**	**33.24**	**8011.76**	**8045**

5.7.2 Constraint relaxation results

Apply the methodology of P-RBCR on the mini-NYISO system. The results are presented and analyzed in the following subsections.

1. Flow/ temperature change

In the feasibility stage, transmission constraints for the limiting transmission facilities in the initial condition are assigned to the CR set. For those circuits, temperature limits are deployed instead of flow limits, and no further violations are observed. For example, the Dunwoodie -NYC line exhibits interesting temperature/flow dynamics, as indicated in Fig. 5.10.

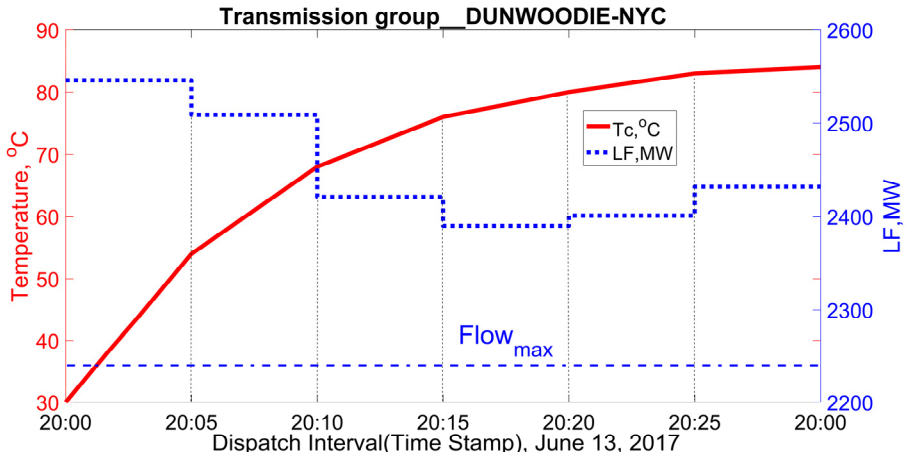

Fig. 5.10. Flow/temperature change for the Dunwoodie-NYC line[8]

As shown in Fig. 5.10, the flow significantly exceeds its limit, but the temperature does not, so such a constraint relaxation is acceptable.

2. Production cost and risk evaluation

Table 5.8 provides comparisons on production cost and risk for the A-CR and the P-RBCR constraint relaxation methodology. Inspection of these data result in observations that are similar to those made for the representative IEEE test system, i.e., the decisions obtained by the P-RBCR

[8] The conductor temperature limit is 100 ^{o}C.

approach results in more economic and more secure operating conditions for handling infeasible SCED by actions of constraint relaxation.

Table 5.8. Comparisons on production cost and risk

	Production cost ($/30min)	**Risk**
A-CR	14,517,679	115
P-RBCR	4,086,710	5

3. LMP comparisons between A-CR and P-RBCR

Fig. 5.11 plots the breakdown of LMP for A-CR and P-RBCR. Since other periods have the same conclusion and patterns, only the plots for periods 1 and 2 are provided. The observations based on those plots are consistent with those made from results analysis on the representative IEEE test system, that is to say, the methodology of P-RBCR reduces price spikes while retaining price signals to mitigate system congestion.

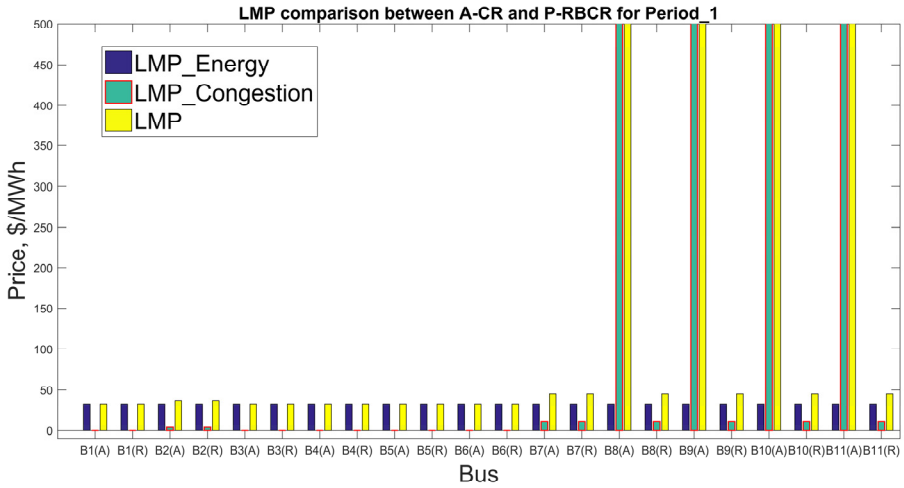

(a) Period 1

Fig. 5.11. LMP plots for the A-CR v.s. the P-RBCR

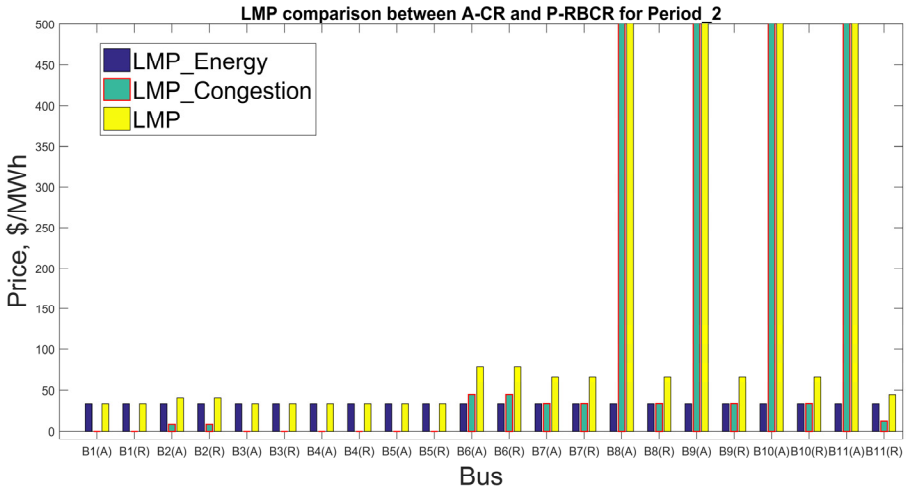

(b) Period 2

Fig. 5.11. (continued)

5.8 Summary

This chapter illustrates and verifies the methodology of P-RBCR using both a representative IEEE test system and contrived real-world ISO system by utilizing a combined MATLAB/GAMS framework. The temperature/flow curve verifies that overloads are allowable when the incurred conductor temperatures do not hit the corresponding boundaries; cost and risk analysis show that the P-RBCR identifies relatively better re-dispatch solutions to remove constraint violations, in terms of obtaining system security and production economics. Furthermore, the P-RBCR reduces occurrence of the LMP spike, while the price signals necessary to provide congestion management are remained.

CHAPTER 6. STOCHASTIC RISK-BASED CONSTRAINT RELAXATION[9]

6.1 Introduction

With significant integration of renewable energy resources, system operation and dispatch are facing with stochastic factors. Different from deterministic and predictive constraint relaxations, there exist randomness and uncertainties in the optimization problem. Thus, the methodology of stochastic risk-based constraint relaxation is proposed and developed in this chapter. The objective has observable and significant meanings in terms of two aspects: 1) solve the infeasibility problem with minimized effects on system security; 2) make use of the headroom in the conventional emergency thermal limits which is conservative.

6.2 Literature review

Significant study has been conducted on integration of variable renewable energy to power scheduling model. Reference [61] applies Benders decomposition to handle the randomness from wind generation output in the day-ahead unit commitment model. Reference [62] proposes and verifies the idea that the combination of reserve method and stochastic programming has a good performance in addressing uncertainty factors in unit commitment problem. Reference [63] conducts sub-hourly stochastic economic dispatch, including the controllability of fast response units on a sub-hourly basis. Reference [64] introduces analytical criteria to determine the

[9] Part of the material in this chapter is reprinted, with permission, from Xian Guo and James McCalley, "Risk-based constraint relaxation with high penetration of wind resources", *Proc. 2017 19th International Conference on Intelligent System Application to Power Systems (ISAP), San Antonio, TX, Sep. 2017,* pp. 1-6. ©2017 IEEE.

application of stochastic programming and leverages the progressive hedging algorithm and the L-shaped method to efficiently solve the stochastic problem.

Based on the best knowledge from literature review, there is no related literature addressing the topic of constraint relaxation for stochastic power scheduling problem. Reference to the idea and thoughts from the D-RBCR and the P-RBCR methodology, and with involvement of stochastic factors, significant changes should be made to adapt to the stochastic problems. Such methodology is defined as stochastic risk-based constraint relaxation, S-RBCR.

6.3 Methodology of stochastic risk-based constraint relaxation

6.3.1 Relaxation margin determination

The DHBE can be applied in the methodology of S-RBCR. Here, to fit customized requirements from application occasions, the alternative approach to determine relaxation margin is proposed in this subsection.

Relaxation margin is proposed to determine how much overloads along the transmission circuits are allowable for a specific time duration (duration of a time interval), which satisfies reliability requirements. That is to say, the circuit flow in the S-RBCR cannot exceed the corresponding relaxation margin. The selection of relaxation margin is determined by the ATR, which represents the thermal rating of the transmission line accounting for the lag between the time of a change in current (or power flow) and the time of the corresponding change in conductor temperature. This lag depends on conductor thermal dynamics, as dictated by the physical characteristics of the transmission circuit. Fig. 6.1 illustrates the dependence of thermal rating as a function of loading duration [2].

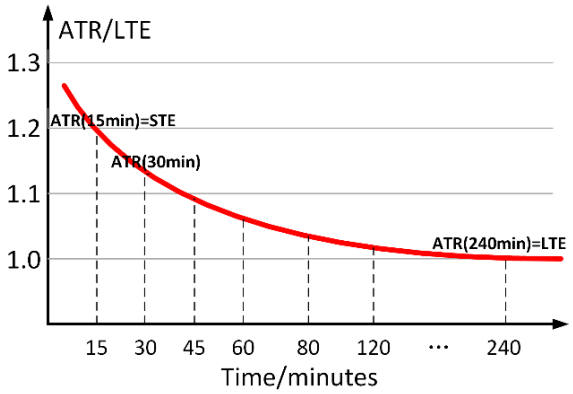

Fig. 6.1. The thermal rating characteristic as a function of loading duration

The ATR is calculated as the current I which satisfies the dynamic heat balance equation, as shown in (6-1), which depends on Joule heating, solar heating, Q_s, radiative cooling, Q_r, and convection cooling, Q_C [65]. This DHBE has been addressed in chapter 5, however, the formulation is repeated here for convenience.

$$C_p \frac{\partial T_c}{\partial t} = I^2 R(T_c) + Q_s - Q_r(T_c, T_a) - Q_c(T_c, T_a, w) \tag{6-1}$$

The rating calculation, as illustrated in Fig. 6.1, is set up to guarantee that under a specific loading condition, I, and a specific time duration, T, the increasing conductor temperature will not exceed the maximum designated temperature, $T_{c,MDT}$, as shown in (6-2),

$$T_{c,0} + \int_0^T \frac{\partial T_c(e, I)}{\partial t} dt \le T_{c,MDT} \tag{6-2}$$

where, $T_{c,0}$ is the conductor temperature prior to the short-time overloading. Since ambient parameter vector $\mathbf{e} = [\boldsymbol{T_a}, \boldsymbol{w}]$ is random, the conductor temperature, T_c, is also random. Assume that ambient parameter $\mathbf{e}$ follows a specific distribution (such as normal distribution), the ATR can be determined corresponding to a specific time duration, T, denoted as I_T, which satisfies

$$P\left(T_{c,0} + \int_0^T \frac{\partial T_c(e, I)}{\partial t} dt \le T_{c,MDT} \right) \ge 1 - \varepsilon \tag{6-3}$$

where Ɛ quantifies the maximum allowable probability of thermal overload; it is a predefined threshold.

In a specific look-ahead horizon, it should be guaranteed that the relaxed limits will not exceed the allowable relaxation margin. To illustrate, a six 5-mininute look-ahead horizon is considered; it is required the satisfaction of a Type 1 -ATR (5mins), Type 2-ATR (10mins), Type 3-ATR (15mins), Type 4-ATR (20mins), Type 5-ATR (25mins), Type 6-ATR (30mins), Type 7-continuous thermal limit. Here, the STE/LTE metrics are generalized by using the types 1-7 values, where Type 3 is STE and Type7 is LTE. The acceptable relaxation margin for each time interval can be one from Type1- Type7, and simultaneously satisfy the following two criteria: 1)At most *n* consecutive time periods can apply Type *n* thermal limits (e.g, Suppose interval 3, 4 and 5 adopt Type 3-ATR, if interval 6 still adopt Type 3-ATR, then Type 3-ATR will exist for 20 minutes, while the corresponding circuit flow (Type3-ATR) can only be withstood no more than 15 minutes); and 2) The total number of Type *n* thermal limits realization should not exceed *n* within the specific look-ahead horizon (e,g, Type 1-ATR can only be applied to one time-interval in the entire operating horizon; while maximum two time-intervals (for intervals that are not consecutive) for Type 2-ATR).

Relaxation margin determination is applied when the thermal limits should be relaxed and updated, in preparation for the next iteration, as what will be presented in the thereafter sections.

6.3.2 Risk assessment–Conditional value at risk

With the penetration of variable renewable resources, circuit flow, h_l^k, is increasingly uncertain; therefore it is represented as a random variable determined by $h_l^k = f(P_G, P_W, D)$, which expresses that circuit flow is a function of generation output from conventional units G, variable units W and demand D. Assume that the circuit flow over the next 5 minutes, given the

current dispatch, is subject to a specific distribution, as illustrated by the probability density function indicated in Fig. 6.2. The probability density function is conditional on the flow at current dispatch decision, expressing the density of the flow over the 5-minute time-interval.

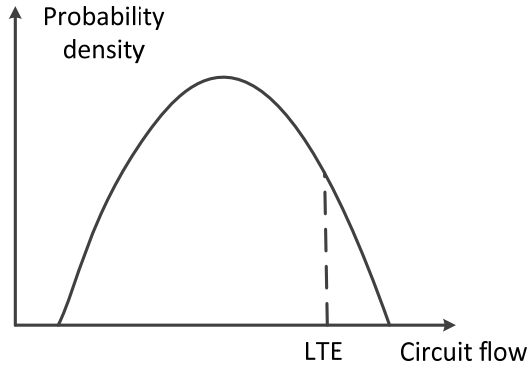

Fig. 6.2. Probability density function of the circuit flow

To avoid significant overloads, compute the conditional value at risk (CVaR) to evaluate severity of heavy loadings [66], i.e., the stress imposed on system security due to the temporary overloads. There are three types of CVaR, including:

- *Circuit CVaR*, denoted as $CVaR_l^k$: Conditional value at risk for a specific circuit l under event k ($k = 0$, corresponding to normal condition); it is calculated as the expected power flow exceeding LTE, expressed as continuous form (6-4). Since several deterministic variable output scenarios are utilized to represent stochastic output from variable units, (6-4) can be substituted by the corresponding discrete form, as indicated by (6-5).

$$CVaR_l^k = \int_{h_l^k \geq LTE} h_l^k \, d\mathbb{P}\left(h_l^k\right) = \int \mathbb{I}_{h_l^k \geq LTE}\left(h_l^k\right) \cdot h_l^k \, d\mathbb{P}\left(h_l^k\right) \tag{6-4}$$

$$CVaR_l^k = \sum_{s=1}^{NS} \rho_s \cdot \mathbb{I}_{h_l^k \geq LTE}\left(h_l^k\right) \cdot h_l^k \tag{6-5}$$

where, $\mathbb{I}_{[.]}(.)$ is an indicator function; $\mathbb{P}\left(h_l^k\right)$ is the probability density function of power flow h_l^k; $\mathbb{I}_{h_l^k \geq LTE}\left(h_l^k\right) \cdot h_l^k$ can be formulated as a piecewise linear function of h_l^k.

- *Contingency CVaR*, denoted as $CVaR_{Ctg}^{k}$: Conditional value at risk for a specific event k (consider normal condition and all credible 'N-1' contingencies.); it is the summation of Circuit CVaR over all circuits under the same event k, described as (6-6).

$$CVaR_{Ctg}^{k} = \sum_{l=1,l\neq k}^{NL} CVaR_{l}^{k} \tag{6-6}$$

- *System CVaR*, denoted as $CVaR_{system}$: Conditional value at risk for the entire system, evaluating the effects on system security level imposed by overloads. The expression of $CVaR_{system}$ is expressed in (6-7).

$$CVaR_{system} = \sum_{k=0}^{NC} CVaR_{Ctg}^{k} = \sum_{k=0}^{NC} \sum_{l=1,l\neq k}^{NL} CVaR_{l}^{k} \tag{6-7}$$

In particular, the stochastic property of variable output is represented by the selected discrete scenarios, each characterized by its probability, so system CVaR can further be described as (6-8), in which (6-5) is substituted into (6-7).

$$CVaR_{system} = \sum_{k=0}^{NC} \sum_{l=1,l\neq k}^{NL} \sum_{s=1}^{NS} \rho_s \cdot \mathbb{I}_{h_l^k \geq LTE}\left(h_l^k\right) \cdot h_l^k \tag{6-8}$$

The objective of S-RBCR is to minimize system CVaR over the entire look-ahead horizon.

6.3.3 Scenario reduction of stochastic factors—Uncertainty set

The number of qualified scenarios increases significantly with penetration of stochastic factors. With all representative scenarios considered in the optimization problem, the computation burden increases correspondingly. Thus, the scenario reduction is a critical and commonly utilized in stochastic programming. In this dissertation, the methodology of uncertainty set is selected to conduct scenario reduction.

The stochastic output from variable generating resources can be represented by a symmetrical polyhedral set, and $\Delta d(i,t)$ is defined as variable output deviation from the

forecasted value at location i, which requires the satisfaction from (6-9).The maximum deviation $\Delta d_{max}(i)$ is determined based on the investigation and analysis of the historical data[67].

$$\left|\Delta d\left(i,t\right)\right| \le \Delta d_{\max}\left(i\right) \tag{6-9}$$

Considering that there exist correlations between stochastic resources at various locations, the variable output from units at different locations cannot obtain upper operating limits or lower operating limits, simultaneously [68]. This paradigm is indicated as (6-10).

$$\sum_{i} \frac{\left|\Delta d\left(i,t\right)\right|}{\Delta d_{\max}\left(i\right)} \le \gamma \tag{6-10}$$

where $\gamma \in [0, N_i]$, N_i is the total number of bus with uncertainties and randomness. A typical two-dimensional uncertainty set is illustrated in Fig. 6.3, and the deviations for the stochastic factors are $|\Delta W_1| \le 10; |\Delta W_2| \le 20$. As proved in [69], the vertices of the uncertainty set provide the solutions for worst scenarios. Thus, those scenarios located on the vertices of the uncertainty set are selected as the representative scenarios; they occur with corresponding probabilities. This constructs the set of reduced scenarios and realizes scenarios reduction.

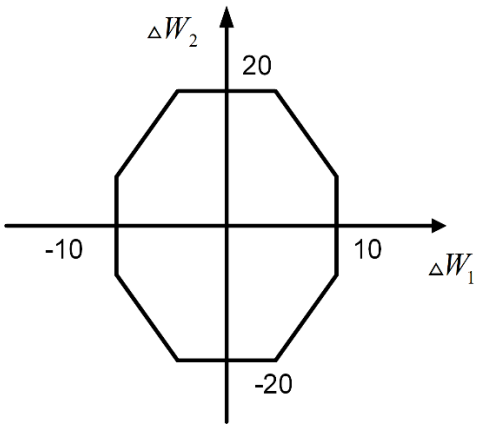

Fig. 6.3. A typical two-dimensional uncertainty set ($\gamma = 1.4$)

6.3.4 Formulation and solving algorithm

1. Formulation of stochastic SCED problem

The formulation and investigation of S-RBCR takes wind resouces as a representative type of generating units with intermittent and various output, which can be generalized to other variable resouces with output uncertainties.

The objective of stochastic SCED is to minimize total costs incurred through the entire look-ahead horizion, including production costs from conventional generator and wind curtialment costs[70]. Considering that wind output is uncertain, curtailments of various wind are applied to guarantee the system power balance is satisfied under corresponding wind output scenarios. Thus, the generation dispatch decision from conventional units is the first-stage decision variable; the necessary amount of the wind curtailment is the second-stage decision variable. Allowing wind curtailment indicates that the output from wind resources can be dispatched down, which is consistent with the ISO procedures for treating dispatchable renewable energy [70]. The model for stochastic SCED is shown as (6-11)~(6-18); it is presented in the extended form of stochastic programming.

$$Min \sum_{T=1}^{NI}\sum_{i=1}^{NG}\left(c_{G,i}\times P_{G,i,T}\right)+\sum_{T=1}^{NI}\left(\sum_{s=1}^{NS}\rho_s\times\left(\sum_{j=1}^{NW}c_{W\_C,j}\times P_{W\_C,j,s,T}\right)\right) \tag{6-11}$$

Subject to:

$$\begin{cases}\sum_{i=1}^{NG}P_{G,i,T}+\sum_{j=1}^{NW}(P_{W,j,s,T}-P_{W\_C,j,s,T})-\sum_{m=1}^{N}D_{m,T}-Loss_{T,s}=0,\\ T\in\{1,...,NI\},s\in\{1,..,NS\}\end{cases} \tag{6-12}$$

$$\begin{cases}P_{G,i,T}-REG_{G,i,T}^{down}\geq P_{G,i,\min}\\ P_{G,i,T}+REG_{G,i,T}^{up}\leq P_{G,i,\max}\end{cases},T\in\{1,...,NI\}\ i\in\{1,...NG\} \tag{6-13}$$

$$\begin{cases} 0 \le P_{W\_C,j,s,T} \le P_{W,j,s,T}, \\ T \in \{1,...,NI\}\ j \in \{1,...NW\}, s \in \{1,..,NS\} \end{cases} \tag{6-14}$$

$$\begin{cases} h_{l,s,T}^{k} = \sum_{n=1}^{N} PTDF_{l,n}^{k} \left(\sum_{i \in n, j \in n} \left(P_{G,i,T} + \left(P_{W,j,s,T} - P_{W\_C,j,s,T} \right) - D_{n,T} \right) \right), \\ k \in \{0,1,...,NC\}, l \in \{1,..,NL\}, T \in \{1,..,NI\}, s \in \{1,..,NS\} \end{cases} \tag{6-15}$$

$$\begin{cases} h_{l,s,T}^{k} \le Limit_{l}^{k} \\ k \in \{0,1,...,NC\}, l \in \{1,..,NL\}, T \in \{1,..,NI\}, s \in \{1,..,NS\} \end{cases} \tag{6-16}$$

$$\begin{cases} -RMP_{G,i}^{up} \le \Delta T \left(P_{G,i,T} - P_{G,i,T-1} \right) \le RMP_{G,i}^{up} \\ -RMP_{G,i}^{down} \le \Delta T \left(P_{G,i,T} - P_{G,i,T-1} \right) \le RMP_{G,i}^{down} \\ T \in \{2,..,NI\}, i \in \{1,...NG\} \end{cases} \tag{6-17}$$

$$\begin{cases} \sum_{i=1}^{NG} REG_{G,i,T}^{up} \ge REG_{req,T}^{up} \\ \sum_{i=1}^{NG} REG_{G,i,T}^{down} \ge REG_{req,T}^{down} \end{cases}, T \in \{1,..,NI\} \tag{6-18}$$

where, (6-12) describes the power balance equation, which guarantees that the demand is satisfied by adjusting conventional dispatch and wind curtailment amount under each scenario. (6-13) and (6-14) indicate generation related constraints on output limits. (6-15) and (6-16) represent power flow along the transmission circuits and the corresponding limits. Those limits will be updated in the S-RBCR model. (6-17) is ramping up and ramping down constraints for conventional generating units. (6-18) imposes regulation reserve requirements, including regulation up and regulation down requirements on the system-wide level.

2. *Infeasiblities of stochastic SCED model*

Electricity markets report unmanageable transmission overloads that cause the stochastic SCED model to be infeasible [71]. The widely-used methodology for addressing this situation is to

introduce slack variables to the thermal limits constraints while imposing associated penalty costs on the objective function. The formulation of A-CR with stochastic factor is shown as follows:

$$\begin{aligned} Min \sum_{T=1}^{NI}\sum_{i=1}^{NG}\left(c_{G,i}\times P_{G,i,T}\right)+\sum_{T=1}^{NI}\left(\sum_{s=1}^{NS}\rho_s\times\left(\sum_{j=1}^{NW}c_{W\_C,j}\times P_{W\_C,j,s,T}\right)\right) \\ +Penalty\times\sum_{T=1}^{NI}\left(\sum_{s=1}^{NS}\left(\rho_s\times\sum_{l=1,l\neq k}^{NL}\sum_{k=0}^{NC}\alpha_{l,s,T}^{k}\right)\right) \end{aligned} \tag{6-19}$$

Subject to: (6-12)~(6-15), (6-17)~(6-18), and the below equation (6-20).

$$\begin{cases} h_{l,s,T}^{k}-\alpha_{l,s,T}^{k}\le Limit_{l}^{k} \\ k\in\{0,1,...,NC\},l\in\{1,..,NL\},T\in\{1,..,NI\},s\in\{1,..,NS\} \end{cases} \tag{6-20}$$

As has been observed in the deterministic format, there is a significant deficiency inherent to A-CR as well: the effect of the relaxation decision on system security is not quantified, and as a result, it is not directly constrained. Thus, the utilization of A-CR results in relaxation decisions that can have very different degrees of influence on system security; some relaxation decisions may be highly conservative and safe, while others may be very risky. There are two reasons for this: 1) the stochastic A-CR does not quantify the relaxation margin; and 2) the stochastic A-CR does not quantify the likelihood of the condition, e.g., it treats the high-probability event in the same way as that it treats the relatively low-probability event.

To address this issue, the methodology of stochastic-RBCR is proposed, which identifies the relaxation decision and corresponding dispatch scheduling that minimizes the overall risk to the circuits and to the system by allowing that flows occurring with higher probability should be more tightly constrained. Similar to the methodology of P-RBCR, the methodology of S-RBCR consists of two major stages: the feasibility stage and the optimality stage:

- **Stage 1:** The feasibility stage drives the constraint relaxation decision by minimizing system CVaR, and it provides a feasible solution to the optimization problem through constraint

relaxation, which is infeasible otherwise. Then, the thermal limit is updated according to the necessary overloads and relaxation margin. This procedure repeats until there is no additional violating overloads.

- **Stage 2:** Based on the feasible region, determined by the relaxed thermal limits that have been detected in Stage 1, the economic dispatch decision is achieved in the optimality stage.

The formulation of Stage 1 for the P-RBCR is described as:

$$Min \sum_{T=1}^{NI} CVaR_{system,T} \tag{6-21}$$

Subject to: (6-8), (6-12)~(6-15), and (6-17)~(6-18), and the below equation (6-22).

$$\begin{cases} h_{l,s,T}^{k} - \alpha_{l,s,T}^{k} \le Limit\_new_{l}^{k} \\ k \in \{0,1,...,NC\}, l \in \{1,..,NL\}, T \in \{1,..,NI\}, s \in \{1,..,NS\} \end{cases} \tag{6-22}$$

The formulation of Stage 2 for S-RBCR has the same formulation as stochastic SCED problem, except for the fact that the tight thermal limits is substituted with the relaxed values, which are determined by relaxation results from Stage 1.

6.4 Case Study

The representative IEEE test system for testing P-RBCR is modified to verify the methodology of S-RBCR. The system consists of 11 circuits, 3 conventional generators (connected at Bus1,2,3), 3 loads (connected at Bus 4,5,6) and a single wind plant as injected at Bus 4. The parameters of conventional generators are provided in Table 6.1.

The operation horizon of look-ahead dispatch is six 5-minute time-intervals. The uncertainties associated with the wind output is captured by 6 representative scenarios, which are achieved by the process of scenario reduction, as shown in Table 6.2. In addition, 12 events are considered in this network, i.e., there exists one normal condition (represented as Ctg0) and 11 'N-

1' contingencies (Ctg1~Ctg11); their occurrence probabilities are assumed to be pre-defined and are provided in Table 6.3.

Table 6.1. Parameters of conventional generators

	Bus	Pmin (MW)	Pmax (MW)	VOM ($/MWh)	FOM ($/MWh)
G1	1	50	200	12.74	13.17
G2	2	37.5	150	12.12	13.17
G3	3	45	180	12.32	13.17

(Note: VOM–variable operation and maintenance cost; FOM–fixed operation and maintenance cost.)

Table 6.2. Wind output scenarios (unit: MW)

1	S1	S2	S3	S4	S5	S6
P1	11.4	9.8	11.3	10	9.5	9.7
P2	29.6	31	31.7	29.2	31.9	33.1
P3	44.3	47.9	50.3	47.6	39	42
P4	57.2	62.1	63	68	66.3	66.7
P5	58.5	50.7	52	52.1	58.6	57.6
P6	71.6	73.1	66.7	71	63.9	73.1
Prob.	0.1	0.1	0.1	0.23	0.23	0.23

(Note: P represents time interval; S represents wind output scenarios.)

Table 6.3. Event probabilities

Ctg	**0**	**1**	**2**	**3**	**4**	**5**
Prob.	1	0.08	0.03	0.001	0.03	0.03
Ctg	**6**	**7**	**8**	**9**	**10**	**11**
Prob.	0.02	0.559	0.03	0.05	0.07	0.1

For the above setting up of network parameters, the stochastic SCED problem is identified as infeasible. Thus, the methodology of A-CR and S-RBCR are applied to the test system, respectively, to eliminate the infeasibilities. The corresponding results and analysis are described in the following sections.

6.4.1 Relaxation margin determination

According to the methodology presented in Section 6.3.1, it is assumed that the ambient temperature T_a follows a normal distribution with mean of $15\ ^oC$ and standard deviation of 6.3; wind speed $\boldsymbol{w}$ also follows a normal distribution with mean of 1.1m/s and standard deviation of

1.3. The relaxation margin can be achieved for the test system, which subjects to the pre-defined thermal overloading probability, ε=0.05. The relaxation margin is shown as Table 6.4.

Table 6.4. The ATR for each circuit

	Type1	Type2	Type3	Type4	Type5	Type6	Type7
L12	143	137.5	132	126.5	121	115.5	110
L14	143	137.5	132	126.5	121	115.5	110
L15	143	137.5	132	126.5	121	115.5	110
L23	85.8	82.5	79.2	75.9	72.6	69.3	66
L24	114.4	110	105.6	101.2	96.8	92.4	88
L25	85.8	82.5	79.2	75.9	72.6	69.3	66
L26	85.8	82.5	79.2	75.9	72.6	69.3	66
L35	85.8	82.5	79.2	75.9	72.6	69.3	66
L36	85.8	82.5	79.2	75.9	72.6	69.3	66
L45	85.8	82.5	79.2	75.9	72.6	69.3	66
L56	85.8	82.5	79.2	75.9	72.6	69.3	66

6.4.2 Two-stage S-RBCR

1. Stage 1: Feasibility

The two-stage S-RBCR methodology is realized in the GAMS, interfacing with MATLAB. The thermal limits required to be relaxed and the corresponding relaxation level are illustrated in Table 6.5 (partial results), which minimizes system CVaR value. The number n represents that for this time-period, Type n thermal limit is selected for the corresponding constraint. The constraints without flow violations still stick to the original thermal limits. From Table 6.5, it can be confirmed that the two criteria for relaxation margin selection are satisfied.

Table 6.5. Constraint relaxation decisions

Constraint	P1	P2	P3	P4	P5	P6
24Ctg2S1	2	2	7	7	7	7
24Ctg2S2	2	6	7	7	7	7
24Ctg2S3	2	2	7	7	7	7
24Ctg2S4	2	6	7	7	7	7
24Ctg2S5	2	2	7	7	7	7
24Ctg2S6	2	6	7	7	7	7

(24Ctg2S1 indicates the thermal limit for circuit 2-4 under contingency 2 and scenario 1)

2. Stage 2: Optimality

Applying the relaxed thermal limit and running Stage 2 optimization problem, the corresponding dispatch decision can be achieved, as indicated in Table 6.6.

Table 6.6. Generation dispatch decisions (unit: MW)

	P1	P2	P3	P4	P5	P6
G1.Energy	168.6	158.6	148.6	138.6	128.6	118.6
G2.Energy	87.5	77.5	67.5	57.5	47.5	37.5
G3.Energy	58.4	48.4	45	45	45	45

Although units G2 and G3 have relatively lower unit production costs, their respective locations are remote from the load center, which will result in more power loss via the long-distance power transfer. Thus, more power is generated from unit G1.

6.4.3 Analysis and comparsions

Based on power flow analysis, the heavily-loading circuits are identified. These circuits are Ctg2(S1,S2,S3), Ctg2(S4,S5,S6), Ctg1(S1,S2,S3), Ctg1(S4,S5,S6), Ctg7(S1,S2,S3) and Ctg7(S4,S5,S6) with occurrence probabilities of 0.003, 0.0069, 0.008, 0.0184, 0.0559 and 0.1286. The corresponding flows are represented in Fig. 6.4; it is referred to as the security diagram. In this figure, the angle of sector indicates the relative occurrence probability of the event[10] ; the distance from the data point to the origin is proportional to the flow associated with that data point. It can be concluded that S-RBCR reduces the extent of violations for contingencies having higher occurrence probability. This implies that S-RBCR redistributes circuit loadings in a way to minimize the system CVaR.

[10] The occurrence probability is not mapped with the sector angle in a precise way. For the convenience, the higher probability is represented with relativity larger sector area, and vice versa.

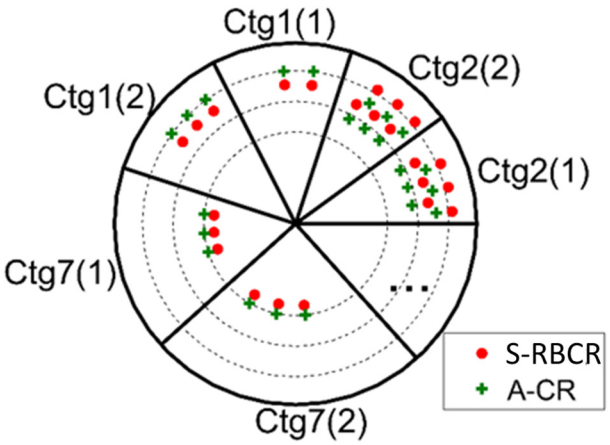

Fig. 6.4. Diagram of heavily-loading flows
(Note: (1)-S1, S2 and S3; (2)-S4, S5 and S6)

Table 6.7 lists system CVaR value and dispatch costs. It can be observed that S-RBCR has relatively lower CVaR value, since the relaxation decision is determined by minimizing CVaR and excessive efforts have been made on controlling effects on system security by allowing heavily-loading flows; however, A-CR has no direct control on system security level. Furthermore, S-RBCR achieves a more economic dispatch, which results from the fact that the constraint relaxation strategies for S-RBCR and A-CR are different, making it possible that S-RBCR produces a relatively more economic dispatch solution. Furthermore, in A-CR, the objective function is operation costs plus penalty costs; the objective function of S-RBCR is purely the minimization of operation costs. Thus, S-RBCR tends to yield more economic results.

In conclusion, the methodology of S-RBCR takes advantage of headroom in circuit capacity by using thermal dynamic balance equations to explicitly account for the effect of increased loading on each conductor while controlling effects on system security, providing the corresponding relaxation decision.

Table 6.7. CVaR and dispatch costs

	A-CR	S-RBCR Step 1	S-RBCR Step 2
System CVaR	110	98	104
Operation costs ($)	76,892	/	76,099
Total costs ($)	272,782 (penalty is included)	/	76,099

6.5 Summary

This chapter proposes the methodology of S-RBCR to handle circuit flow violations in stochastic SCED problem. The allowable relaxation margin is determined by the ATR and thermal overloading probability. The security degradation by overloads are evaluated and controlled by the stochastic risk metrics–CVaR. In conclusion, S-RBCR provides a basis for relaxing circuit flow limits to obtain market solutions with controlled effects on system security level, under the presentence of stochastic power flows. Comparing with the widely industrial CR methodology, the S-RBCR methodology tends to achieve constraint relaxation decision in a more economic and more secure way.

CHAPTER 7. RISK-BASED STRESS MONITORING FOR CASCADING CONTINGENCIES[11]

7.1 Introduction

When the operation condition is close to limits, the power system undergoes significant stress. Such stress is incurred because of several reasons, 1) an aging network facility can bring potential component outage; 2) the demand for higher supply reliability has increased operation complexity; 3) generation uncertainty and variability increase with the increasing penetration of wind and solar power; and 4) increased load demands and power transfers can expose the system to increased cascading risk. The level of stress is the complement to system security [72]; as security increases, the stress level decreases. Increased stress leads to less secure conditions in two ways: (1) outage events are more likely to occur under stressed situations due to increased risk of protective system mis-operation and of circuit expansion and sag; (2) outage events are more likely to cause other outage events, resulting in cascading contingencies. Thus, stress monitoring with quantified indicators is useful to provide signals characterizing stressed conditions and facilitate identification of operational changes that can reduce chance of extreme events.

Thus, this chapter proposes an actionable steady-state stress monitoring indicator. This work can complement the CR methodology in that it enables identification of circuits for which limits should not be relaxed.

---

[11] Part of the material in this chapter is reprinted, with permission, from Xian Guo and James McCalley, "Risk-based stress indicator for cascading contingencies", *Proc. 2016 North American Power Symposium (NAPS), Denver, CO, Oct. 2016,* pp. 1-6. ©2016 IEEE.

7.2 Literature review

In the current literature, some actionable stress monitoring and risk indices can be identified, and most of them focus on monitoring voltage stability, such as L-indicator in [73], Thevenin impedance based indicator in [74], steady-state sensitivities in [75,76], and the decision-tree based voltage security with PMU data in [77]. However, the stress exposed to steady-state system relates more to overloading condition (the consequences of low voltage and voltage instability can be revealed by the circuit overloads) and furthermore cascading events. There are also works on monitoring overloaded circuits, including Loading margin in [78,79], and 'N-1' contingency in [80]. But reference [80] considers only 'N-1' contingencies; it does not provide information on cascading contingency. In this chapter, a risk-based stress monitoring indicator is utilized to identify weak areas and high-risk cascading events[12], thus providing early warning for system operators of exposure to high-risk events.

7.3 Risk-based stress indicator

A summary of the proposed and developed risk-based stress indicators includes, together with their application, are as follows:

- *Propagation risk*: This indicator evaluates which circuit to select as the propagation node of cascading sequence. That is to say, it determines next circuit outage.
- *Cascading sequence risk*: This indicator provides the ability to evaluate system security level under a K^{th}-order cascading sequence.

[12] The cascading sequence refers to sequential circuit outage, such as 'N-1' and 'N-1-1', which means the outage of circuits occurs one by one, not simultaneously, denoted as K^{th}-order cascading contingency, and the notation is $\{i_1, i_2, \dots, i_k\}$. The cascading node refers to the circuit included in the cascading sequence. Cascading tree refers to a set of identified high-risk cascading sequence.

- *Cascading tree risk*: This indicator evaluates the security exposure to a high-risk cascading tree, i.e., a set of potential cascading sequences for an initial operating condition.
- *Circuit risk*: This indicator evaluates the level to which a circuit contributes to the cascading tree risk. The circuit risk can be applied in detecting weak area (a group of weak circuits) in current system.

The above indicators will be described in detail in the following subsections.

7.3.1 Definition and calculation of risk indicators

1. Propagation risk

Propagation risk is the tendency that a contingency will propagate to next level, i.e., the impact on the probability of another circuit trip. Fig. 7.1 illustrates the $(K-1)^{th}$ step in construction of a cascading contingency. The decision-making for whether the sequence will be extended to another circuit trip or not, and if so, which circuit will be more likely to be tripped is determined by the propagation risk for the candidate circuits.

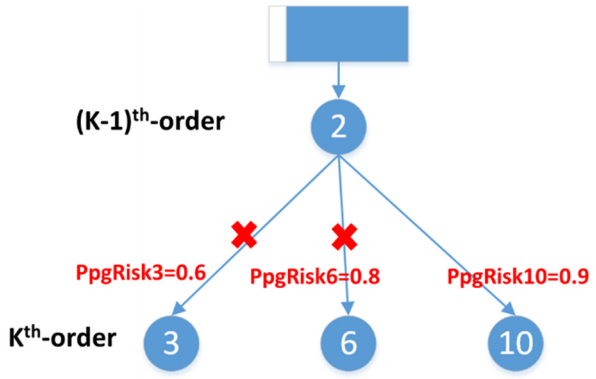

Fig. 7.1. Illustration of the application of propagation risk

The propagation risk measures the impact on the outage probability of candidate circuits from the existing $(K-1)^{th}$ cascading contingency. It is assumed that more heavily-loaded circuits

(with flow exceeds 90% LTE threshold) imposes higher probability of outage. That is to say, the outage probability of a certain circuit is a function of the power flow level on that circuit. Assuming the circuit trips immediately after the flow exceeds DAL, the probability of circuit trip under certain flow level P can be calculated as (7-1):

$$\Pr(P) = \frac{\max(P - 0.9LTE, 0)}{DAL - 0.9LTE} \tag{7-1}$$

where P is the flow level and Pr(.) is the circuit outage probability, which is the function of power flow on that circuit. Pr(.) has two segments: 0 if flow is less than 0.9LTE; linearly increase from 0 to 1 between 0.9LTE and DAL. The function is illustrated in Fig. 7.2.

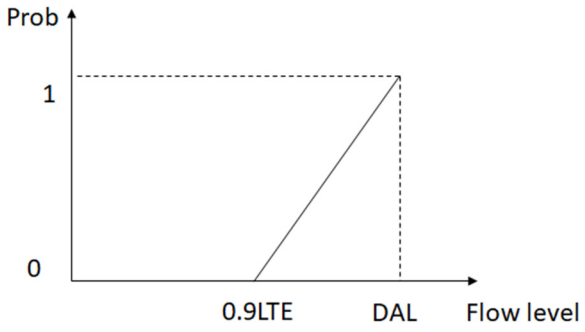

Fig. 7.2. The probability function of circuit trip

The probability change of circuit trip between pre-contingency (with flow level P_0) and post-contingency (with flow level P_1) can be expressed as:

$$\Pr(P_1) - \Pr(P_0) = \frac{\max(P_1 - 0.9LTE, 0)}{DAL - 0.9LTE} - \frac{\max(P_0 - 0.9LTE, 0)}{DAL - 0.9LTE} \tag{7-2}$$

It can be observed that the circuit trip probability function has the same expression as the severity function (7-3) as derived from chapter CHAPTER 4. In other words, the severity function can be considered as equivalent to circuit trip probability function. Fig. 7.3 illustrates the two-segment severity function.

$$sev(P_1) = \frac{\max\left(P_1 - 0.9LTE, 0\right)}{DAL - 0.9LTE}, \quad sev(P_0) = \frac{\max\left(P_0 - 0.9LTE, 0\right)}{DAL - 0.9LTE} \tag{7-3}$$

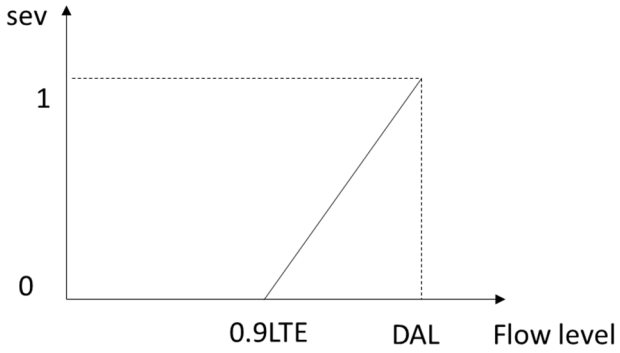

Fig. 7.3. Two-segment severity function

Therefore, the propagation risk can be calculated as:

$$PpgRisk = \Pr(P_1) - \Pr(P_0) = sev(P_1) - sev(P_0).$$

Furthermore, the two-segment circuit trip probability function can be extended into multi-segment circuit trip probability function. The multi-segment circuit trip probability function is the same as the piece-wise linear severity function used in risk calculation of Section 4.4.1 .

The impact on circuit trip probability from the preceding contingency is calculated as the probability change on circuit trip between pre-contingency and post-contingency, i.e., the change on circuit severity due to the preceding contingency, as described in (7-4). Considering the dependency of next circuit outage on preceding circuit outage is valuable. For example, operators in Southern California Edison area will not concern the overloading circuit in Canada; overloads on that circuit results from the initial outage of a circuit located in Southern California Edison area. The concept of 'delta severity' covers the criteria of both absolute power flow value and flow change, which is a realistic approximation to the development of real-world cascading event.

$$PpgRisk_{i_k}^{i_{k-1}} = \Delta sev_{i_k}^{i_{k-1}} = sev_{i_k}^{\{i_1,\ldots,i_{k-1}\}} - sev_{i_k}^{\{i_1,\ldots,i_{k-2}\}} \tag{7-4}$$

Here, $\Delta sev_{i_k}^{i_{k-1}}$ is the change in severity level of circuit i_k due to the outage of circuit i_{k-1}. Circuits with propagation risk exceeding a selected threshold are chosen to propagate the cascading sequence; and, thus extend the cascading tree. As illustrated in Fig. 7.1, the threshold of propagation risk is set as 0.85. Then circuit 10 selected as the candidate node to propagate to higher-order cascading node.

2. Cascading sequence risk

Cascading sequence risk is developed to evaluate system security level with respect to a cascading contingency path. Such an identified cascading contingency path may be a second-order contingency ('N-1-1' outage), third-order ('N-1-1-1' outage) or even K[th]-order contingency[13].

(1) First-order cascading sequence risk

The first-order cascading sequence risk is computed as the total 'delta severity' for all remaining intact circuit. $\Delta sev(i_2|i_1)$ is denoted as the severity level change for a specific circuit i_2 following outage of circuit i_1. Assume that cascading nodes are mutually exclusive, the cascading sequence risk function is expressed as:

$$CctRisk_{i_1} = \sum_{i_2 \neq i_1}^{NL} \Delta sev\left(i_2 \mid i_1\right) \tag{7-5}$$

where NL is the total number of circuits in pre-contingency condition. (7-5) is called the first-order cascading sequence risk function, which captures the system risk of encountering a single contingency; the risk of successive contingencies is represented through the higher-order cascading sequence risk.

[13] Kth-order contingency event indicates K lines outage in a sequence.

(2) Second-order cascading sequence risk

The model can be improved by extending $\Delta sev(i_2|i_1)$ into a 'N-1-1' contingency $\Delta sev(i_3|\{i_1,i_2\})$. $\Delta sev(i_3|\{i_1,i_2\})$ captures the severity impact of circuit i_3 following outage of circuits i_1 and i_2. All remaining intact circuits $i_3 = 1,2,\dots NL$, $i_3 \neq i_1 \; or \; i_2$ are screened. Therefore, the second-order cascading sequence risk can be computed as follows:

$$CctRisk_{\{i_1,i_2\}} = \sum_{i_3 \neq i_1,i_2}^{NL} \Delta sev\left(i_3 \,|\, \{i_1,i_2\}\right) \tag{7-6}$$

The second-order cascading sequence risk function explicitly captures the risk of encountering two consecutive contingencies, i.e., a second-order cascading sequence.

(3) Kth-order cascading sequence risk

Similarly, the Kth-order cascading sequence risk function can be computed as

$$CtgRisk_{\{i_1,\dots,i_k\}} = \sum_{i_j \neq i_1,\dots,i_k}^{NL} \Delta sev\left(i_j \,|\, \{i_1,i_2,\dots,i_k\}\right) \tag{7-7}$$

The Kth-order cascading sequence risk function captures the risk of encountering a specific K^{th} successive cascading sequence. Fig. 7.4 illustrates one second-order cascading sequence—C1{2,3}; four third-order cascading sequence —C2{2,6,3}, C3{2,6,10}, C4{2,10,3}, C5{2,10,6}; and one fourth-order cascading sequence —C6{2,6,8,29}. They correspond to the second-order, third-order and fourth-order cascading sequence risk, respectively.

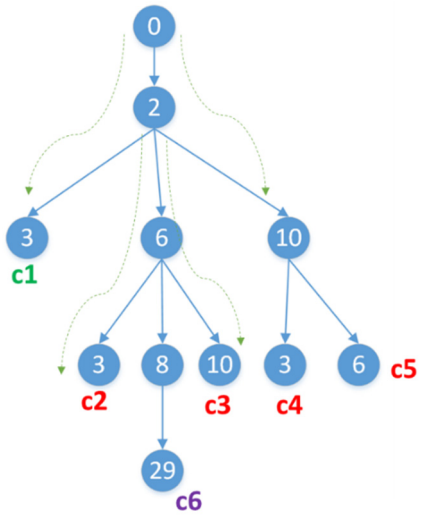

Fig. 7.4. Identified high-risk cascading tree

3. Cascading tree risk

Cascading tree risk evaluates the propensity of cascading risk, i.e., the risk of a set of cascading sequence under a specific initial operating point. Based on the risk-based tree search, the selected cascading sequence is identified as $C_1, C_2, \ldots, C_m$. Assume that the identified cascading sequences are mutually exclusive, summation of each cascading sequence risk is the cascading tree risk exposed to the specific operating condition, as indicated in (7-8).

$$CcdRisk = \sum_{i=1}^{m} CtgRisk_{C_i} \tag{7-8}$$

The circuit risk for circuit 10 is the summation of the cascading sequence C_3, C_4 and C_5 on cascading sequence risk. The cascading tree risk evaluates the exposure of an operating condition to cascading contingencies. The application of cascading tree risk in power system can be the short-term operation and long-term planning.

4. Circuit risk

The determination of weak circuits (circuit with higher circuit risk) is based on the contribution of the circuit to the cascading tree or a set of cascading sequences it can be calculated.

It is the summation of cascading sequence risk of all cascading sequences, which involve the circuit i_k, as indicated in (7-9),

$$CctRisk_{i_k} = \sum_{c} CtgRisk_{c_i}, \{j \in cascade\ c\} \tag{7-9}$$

Nevertheless, the concept of circuit risk can also be extended so that it is related to the specific contribution of the investigated circuit to a high-risk cascading sequence. The basic concept is that the circuit outage occurs earlier, the greater contribution of that circuit is to that cascading sequence.

7.3.2 Power flow calculation based on successive line outage distribution factor (SLODF)

The calculation of severity function depends only on real power flows on the circuits. To efficiently compute these power flows, the use of successive Line Outage Distribution Factors (SLODFs) is introduced in this subsection. In this section, the terminology line and circuit are used interchangeably.

1. Power flow calculation

The SLODF for circuits i_2 conditional on i_1 represents the change of the power flowing in circuit i_2 due to the removal of the circuit i_1 from the network, denoted as $d_{i_2|i_1}$. The SLODFs can be applied to compute cascading power flows as follows:

$$P_{i_2|i_1} = d_{i_2|i_1} \times P_{i_1}^0 + P_{i_2}^0 \tag{7-10}$$

where $P_{i_1}^0$ and $P_{i_2}^0$ are pre-contingency flows on circuits i_1 and i_2, respectively, and, $d_{i_2|i_1}$ is the first-order SLODF, corresponding to the flow change on circuit i_2 due to circuit i_1 outage. The flows computed by (7-10) is referred to as first-order flows.

According to this theory, second-order flows can be obtained, which are flows following outage of circuit i_2 following outage of circuit i_1. For example, the circuit i_3 flow is denoted as $P_{i_3|\{i_1,i_2\}}$ and computed as

$$P_{i_3|\{i_1,i_2\}} = d_{i_3|\{i_1;i_2\}} \times P^0_{i_2|i_1} + P^0_{i_3|i_1} \tag{7-11}$$

where $d_{i_3|\{i_1;i_2\}}$ is the second-order SLODF corresponding to the flow change on circuit i_3 due to outages on i_2 following outage of circuits i_1,$P^0_{i_2|i_1}$ is the flow on circuit i_2 following outage of circuit i_1 and $P^0_{i_3|i_1}$ is the flow on circuit i_3 following outage of circuit i_1 but before outage of circuit i_2.

Thus, the K[th]-order flows can be achieved, as shown in (7-12).

$$P_{i_{k+1}|\{i_1,\ldots,i_k\}} = d_{i_{k+1}|\{i_1,\ldots;i_k\}} \times P^0_{i_k|\{i_1,\ldots,i_{k-1}\}} + P^0_{i_{k+1}|\{i_1,\ldots,i_{k-1}\}} \tag{7-12}$$

2. Calculation of Successive-LODF

The first-order SLODF for a circuit i_2 connecting buses m and n after the outage of the circuit i_1 between nodes p and q can be obtained by [81]:

$$d_{i_2|i_1} = -b^0_{mn} \frac{(g^{pq}_m - g^{pq}_n)}{1 + b_{pq}(g^{pq}_p - g^{pq}_q)} \tag{7-13}$$

where $b^0_{mn}$is the susceptance between m and n, corresponding to the original network topology with no circuit outage, which is a negative number for any standard circuit. The numerator of (7-13) can be computed from

$$g^{pq}_p - g^{pq}_q = e^T_{pq} g^{pq} \tag{7-14}$$

where $e^T_{pq} = [0,0,\ldots,1(p),\ldots,-1(q),0\ldots]$, and $B' g^{pq} = e_{pq}$, B' is the conventional 'B-prime' matrix obtained from the Y-bus, corresponding to the network topology which includes circuit i_1. Performing LU decomposition obtains the value of g^{pg}, so there is no need to invert the B' matrix [81][p31,82].

The second-order SLODF for a circuit i_3 connecting buses r and s after the first outage of circuit i_1 followed by the second outage of circuit i_2 between nodes m and n can be obtained by:

$$d_{i_3|\{i_1;i_2\}} = -b_{rs}^{(|i_1)} \frac{(g_r^{mn} - g_s^{mn})}{1 + b_{mn}(g_m^{mn} - g_n^{mn})} \tag{7-15}$$

where, $b_{rs}^{(|i_1)}$ is the susceptance between r and s, corresponding to the network topology with circuit i_1 out of service, and the other terms in (7-15) are computed as in (7-13) except with circuit i_1 out of service.

The K[th]-order SLODF is:

$$d_{i_{k+1}|\{i_1,\ldots;i_k\}} = -b_{ij}^{(|\{i_1,\ldots,i_{k-1}\})} \frac{(g_i^{xy} - g_j^{xy})}{1 + b_{xy}(g_x^{xy} - g_y^{xy})} \tag{7-16}$$

where, $b_{ij}^{(|\{i_1\ldots,i_{k-1}\})}$ is the susceptance between i and j, corresponding to the network topology with circuit $i_1, \ldots, i_{k-1}$ out of service, and the other terms in (7-16) are computed as in (7-13) except with circuit $i_1, \ldots, i_{k-1}$ out of service.

7.4 Development of risk-based stress indicator for cascading contingencies

7.4.1 Contingency selection

When calculating the K[th]-order risk indicators, it is noted that some contingency scenarios may result in isolated system (IS). As shown in Fig. 7.5, there exists three types of isolated system:

- Type I: Only a single bus is included in IS;
- Type II: Multiple buses are included in IS, and the generation output can satisfy the demand;
- Type III: Multiple buses are included in IS, but the generation cannot satisfy the demand.

When selecting the contingency scenario for each level, the graph-theory is applied with the breadth first search method [83] to detect the possible ISs. If an IS belongs to Type I or Type III system, the corresponding contingency will not be included in the set of candidate contingency scenarios; while IS belongs to Type II with a certain number of buses, which can be included in the candidate contingency set.

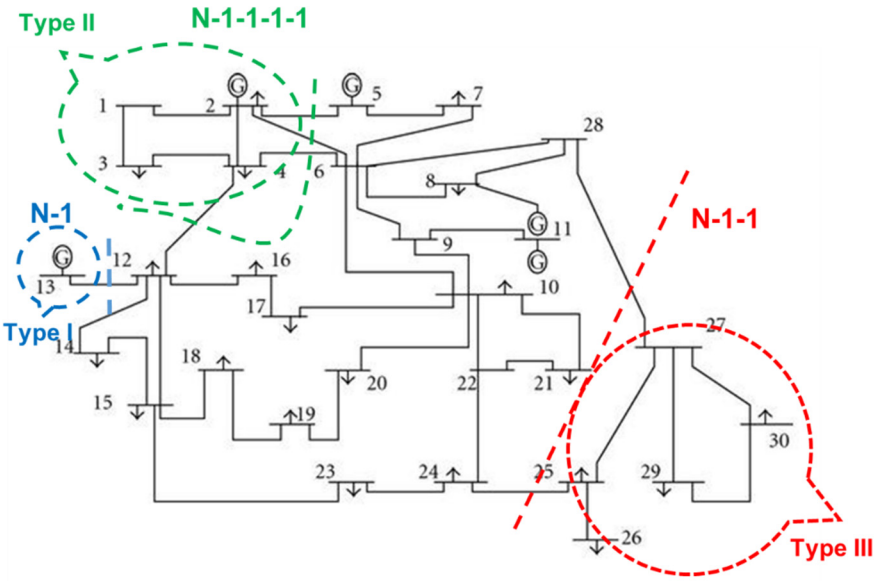

Fig. 7.5. Detection of isolated system

7.4.2 Procedure of developing cascading tree

To utilize the propagation risk in developing high-risk cascading trees for steady-state power system analysis (under an operating point), there are several steps to follow:

- *Step1:* Set m=1;
- *Step2:* Develop the m^{th}-order candidate contingency set, and calculate the propagation risk $PpgRisk_{i_k}$ for candidate circuits;
- *Step3:* Rank $PpgRisk_{i_k}$ from higher value to lower value, then choose the highest n (a pre-defined value, such as 2) and satisfy the pre-defined threshold, to be included in the initial events of $(m+1)^{th}$-order cascading contingency, then set m=m+1;
- *Step4:* Repeat Step2~Step 3 until a level is reached where no additional circuits satisfy the propagation criteria (and so the cascade stops), or a pre-defined maximum propagation level is reached;
- *Step5:* Calculate cascading sequence risk for each identified high-risk cascading contingency; determine the corresponding cascading tree risk for this specific operating point

and circuit risk for each circuit.

Within the framework of constraint relaxation, much 'safer' overloads tend to be allowed. That is to say, it tends to relax those circuits which will not expose the current power system to severe consequences, such as cascading contingency. Thus, cascading assessment can be integrated with the decision making for constraint relaxation–use lower level risk to achieve the dispatch decision; after that, conduct cascading assessment.

7.5 Numerical example–a representative IEEE test system

The IEEE RTS-96 system is selected for illustrating the risk-based stress monitoring methodology. There are 108 circuits (shown in Table 7.1) and three areas. The DC power flow is used for calculation. The load, generator data and circuit impedance are referenced to data from the Power Systems Test Case Archive from Washington State University [84].

Table 7.1. Circuit data in RTS-96 test system

No.	FromBus.	BusName	ToBus	BusName	No.	FromBus	BusName	ToBus	BusName
1	101	ABEL	102	ADAMS	**20**	111	ANNA	114	ARNOLD
2	101	ABEL	103	ADLER	**21**	112	ARCHER	113	ARNE
3	101	ABEL	105	ALKEN	**22**	112	ARCHER	123	AUSTEN
4	102	ADAMS	104	AGRICOLA	**23**	113	ARNE	123	AUSTEN
5	102	ADAMS	106	ALBER	**24**	113	ARNE	215	BARTON
`6	103	ADLER	109	ALI	**25**	114	ARNOLD	116	ASSER
7	103	ADLER	124	AVERY	**26**	115	ARTHUR	116	ASSER
8	104	AGRICOLA	109	ALI	**27**	115	ARTHUR	121	ATTLEE
9	105	ALKEN	110	ALLEN	**28**	115	ARTHUR	124	AVERY
10	106	ALBER	110	ALLEN	**29**	116	ASSER	117	ASTON
11	107	ALDER	108	ALGER	**30**	116	ASSER	119	ATTAR
12	107	ALDER	203	BAFFIN	**31**	117	ASTON	118	ASTOR
13	108	ALGER	109	ALI	**32**	117	ASTON	122	AUBREY
14	108	ALGER	110	ALLEN	**33**	118	ASTOR	121	ATTLEE
15	109	ALI	111	ANNA	**34**	119	ATTAR	120	ATTILA
16	109	ALI	112	ARCHER	**35**	120	ATTILA	123	AUSTEN
17	110	ALLEN	111	ANNA	**36**	121	ATTLEE	122	AUBREY
18	110	ALLEN	112	ARCHER	**37**	121	ATTLEE	325	CURTISS
19	111	ANNA	113	ARNE	**38**	123	AUSTEN	217	BATES

Table 7.1. (continued)

No.	FromBus.	BusName	ToBus	BusName	No.	FromBus	BusName	ToBus	BusName
39	201	BACH	202	BACON	**74**	301	CABELL	302	CABOT
40	201	BACH	203	BAFFIN	**75**	301	CABELL	303	CAESAR
41	201	BACH	205	BALN	**76**	301	CABELL	305	CALVIN
42	202	BACON	204	BAILEY	**77**	302	CABOT	304	CAINE
43	202	BACON	206	BAJER	**78**	302	CABOT	306	CAMUS
44	203	BAFFIN	209	BALZAC	**79**	303	CAESAR	309	CARTER
45	203	BAFFIN	224	BORDET	**80**	303	CAESAR	324	CURIE
46	204	BAILEY	209	BALZAC	**81**	304	CAINE	309	CARTER
47	205	BALN	210	BANKS	**82**	305	CALVIN	310	CARUSO
48	206	BAJER	210	BANKS	**83**	306	CAMUS	310	CARUSO
49	207	BAKER	208	BALCH	**84**	307	CAREW	308	CARREL
50	208	BALCH	209	BALZAC	**85**	308	CARREL	309	CARTER
51	208	BALCH	210	BANKS	**86**	308	CARREL	310	CARUSO
52	209	BALZAC	211	BARDEEN	**87**	309	CARTER	311	CARY
53	209	BALZAC	212	BARKLA	**88**	309	CARTER	312	CAXTON
54	210	BANKS	211	BARDEEN	**89**	310	CARUSO	311	CARY
55	210	BANKS	212	BARKLA	**90**	310	CARUSO	312	CAXTON
56	211	BARDEEN	213	BARLOW	**91**	311	CARY	313	CECIL
57	211	BARDEEN	214	BARRY	**92**	311	CARY	314	CHAIN
58	212	BARKLA	213	BARLOW	**93**	312	CAXTON	313	CECIL
59	212	BARKLA	223	BLOCH	**94**	312	CAXTON	323	COMTE
60	213	BARLOW	223	BLOCH	**95**	313	CECIL	323	COMTE
61	214	BARRY	216	BASOV	**96**	314	CHAIN	316	CHIFA
62	215	BARTON	216	BASOV	**97**	315	CHASE	316	CHIFA
63	215	BARTON	221	BEHRING	**98**	315	CHASE	321	COBB
64	215	BARTON	224	BORDET	**99**	315	CHASE	324	CURIE
65	216	BASOV	217	BATES	**100**	316	CHIFA	317	CHUHSI
66	216	BASOV	219	BEDE	**101**	316	CHIFA	319	CLAY
67	217	BATES	218	BAYLE	**102**	317	CHUHSI	318	CLARK
68	217	BATES	222	BELL	**103**	317	CHUHSI	322	COLE
69	218	BAYLE	221	BEHRING	**104**	318	CLARK	321	COBB
70	219	BEDE	220	BEETHOVEN	**105**	319	CLAY	320	CLIVE
71	220	BEETHOVEN	223	BLOCH	**106**	320	CLIVE	323	COMTE
72	221	BEHRING	222	BELL	**107**	321	COBB	322	COLE
73	223	BLOCH	318	CLARK	**108**	323	COMTE	325	CURTISS

The high-level representation of the network topology is shown in Fig. 7.6.

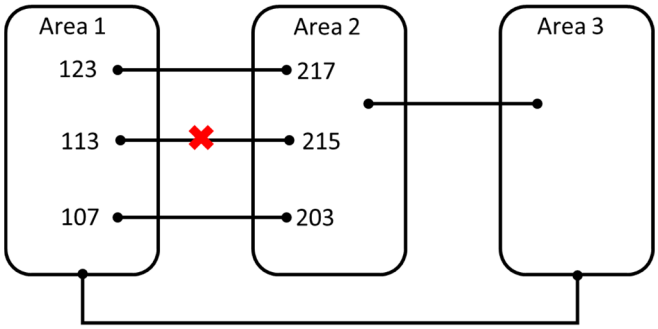

Fig. 7.6. High-level representation of network topology for RTS-96 system

The K^{th}-order risk calculation is realized by programming in MATLAB. The initial contingency is an 'N-1' contingency consisting of 113-215 outage. For the RTS-96 system, the maximum propagation level is set as 6, i.e., the development of cascading contingency stops when six circuits outage. To verify the power flow results achieved from SLODF, they are compared with those results from MATPOWER 5.1, and it has been confirmed that the results are consistent.

7.5.1 Cascading tree development

The corresponding cascading tree is shown in Table 7.2. Here, 16 high-risk cascading sequences are identified, which constructs the high-risk cascading tree with the cascading tree risk as 256.03. The corresponding cascading sequence risk is summarized in Table 7.2. As shown in the table, each cell is the cascading node (represented by circuit number) involved in the specific cascading sequence. As observed in the figure, following tie-line 113-215 (circuit 24) outage, the parallel tie-lines 123-217 (circuit 38) and line 107-203 (circuit 12) are also identified in the high-risk cascading tree. This observation is consistent with the intuition that outage of one of the parallel tie-lines will transfer power flows to the parallel tie-lines and increase their loading, and thus increase the tendency of those parallel tie-lines to cascade. Furthermore, Fig. 7.7 summarizes the flow change rate between normal condition and 'N-1' contingency (circuit 24 outage) condition.

As indicated in the figure, the parallel path (circuit 38 and circuit 12) increase the most, in comparison with other transmission paths.

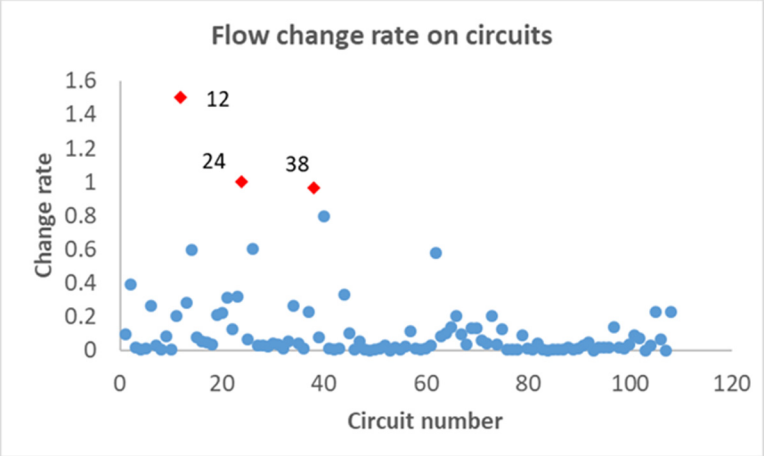

Fig. 7.7. Flow change rate between normal and 'N-1' contingency

Table 7.2. Cascading tree development

Cascades No.	N-1	N-1-1	N-1-1-1	N-1-1-1-1	N-1-1-1-1-1	N-1-1-1-1-1-1	Ctg Risk
1	24	38	40	44	45	13	37.32
2	24	38	57	45	47	48	29.21
3	24	38	57	45	51	/	28.88
4	24	38	97	102	103	13	27.61
5	24	12	2	6	20	30	20.12
6	24	38	97	102	44	34	17.04
7	24	38	14	2	6	20	16.00
8	24	38	57	44	39	/	15.15
9	24	38	40	44	14	2	14.76
10	24	38	75	/	/	/	14.42
11	24	12	6	34	23	20	10.91
12	24	12	6	1	/	/	6.09
13	24	12	40	/	/	/	5.63
14	24	12	44	39	/	/	5.62
15	24	2	6	/	/	/	4.09
16	24	26	2	6	/	/	3.19

The total number of circuits identified by the risk-based cascading tree is 24. Table 7.3 describes the circuits with top 10 circuit risk; those circuit are also color coded in Table 7.2, correspondingly. As observed in the tables, high circuit risk is motivated by relatively higher cascading sequence risk and the quantity of cascading sequences involves the circuit is relatively larger.

Table 7.3. Circuits with top 10 circuit risk

Circuit	38	45	44	57	13	6	2	40	12	20
Circuit Risk	200.38	95.41	89.88	73.24	64.93	60.40	58.15	57.71	48.37	47.03

Fig. 7.8 is the visualization graph of circuit risk. Those circuits with higher circuit risk are closer to red and have wider line width, indicating such circuits have greater contribution to the cascading tree development under the current operating condition. In addition, black color implies that the corresponding circuit risk is zero.

It is shown in that Circuit 38 (bus 123-bus 217) is marked with red to indicate that this circuit has relatively more contributions to the development of high-risk cascading tree. With such circuit outage, the system is exposed to a severe overloading situation. Thus, the system operator should be concerned if any of such circuits outage. Nevertheless, no temporary overloading is allowed across these circuits. Circuits with color closer to blue contribute less stress to the system; a temporary overloading condition is of less concern.

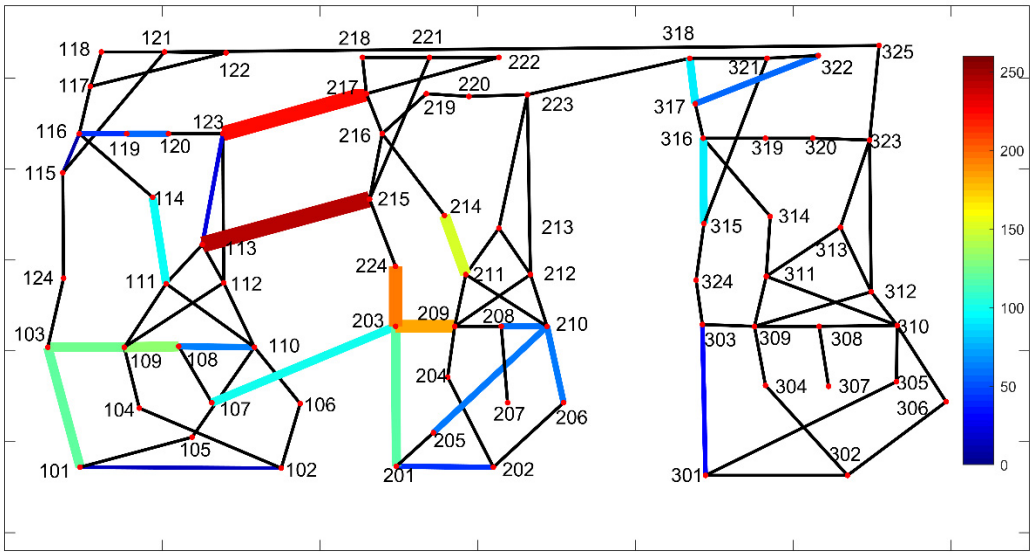

Fig. 7.8. Visualization of circuit risk

7.5.2 Risk mitigation

The identified circuits with high circuit risk can provide early warnings to system operator, helping them identify high-risk cascading sequence, thus motivate immediate actions to relieve the cascading tree risk. An intuitive action of risk mitigation is illustrated in this subsection. As observed in the previous section, circuit 38 presents the highest circuit risk. The action of re-dispatch is to decrease the initial flow on circuit 38. Under the updated operating condition, the procedure of risk-based tree search was rerun, and the developed cascading tree is shown in Table 7.4~Table 7.5. The cascading tree risk has been decreased from 256.03 to 49.73; only 7 high-risk cascading sequences are identified. As shown in the table, circuit 38 has not been picked up by the cascading tree. This example verifies that by alleviating the flow along weak circuits (which have relatively high circuit risk), the cascading tree risk imposed on the system can be significantly reduced.

Table 7.4. Cascading tree after risk mitigation

Cascades No.	N-1	N-1-1	N-1-1-1	N-1-1-1-1	N-1-1-1-1-1	N-1-1-1-1-1-1	**Ctg Risk**
1	24	12	2	6	20	30	20.12
2	24	12	6	34	23	20	9.99
3	24	12	6	1	/	/	5.09
4	24	12	40	/	/	/	4.63
5	24	12	44	39	/	/	4.62
6	24	2	6	/	/	/	3.09
7	24	26	2	6	/	/	2.19

Table 7.5. Circuits with top 10 circuit risk

Circuit	12	6	20	2	30	23	34	1	40	39
Circuit risk	44.45	40.48	30.11	25.40	20.12	9.99	9.99	5.09	4.63	4.62

Fig. 7.9 is the visualization graph of circuit risk after risk mitigation. Circuit 38 does not present cascading risk. The previously heavy-stressed circuits have been relieved and are not exposed to high-risk cascading contingency under the updated operating point. The visualization of circuit risk verifies that reducing load on "weak circuits" by re-dispatch is beneficial in alleviating cascading risk; it is an effective approach to mitigate the cascading tree risk.

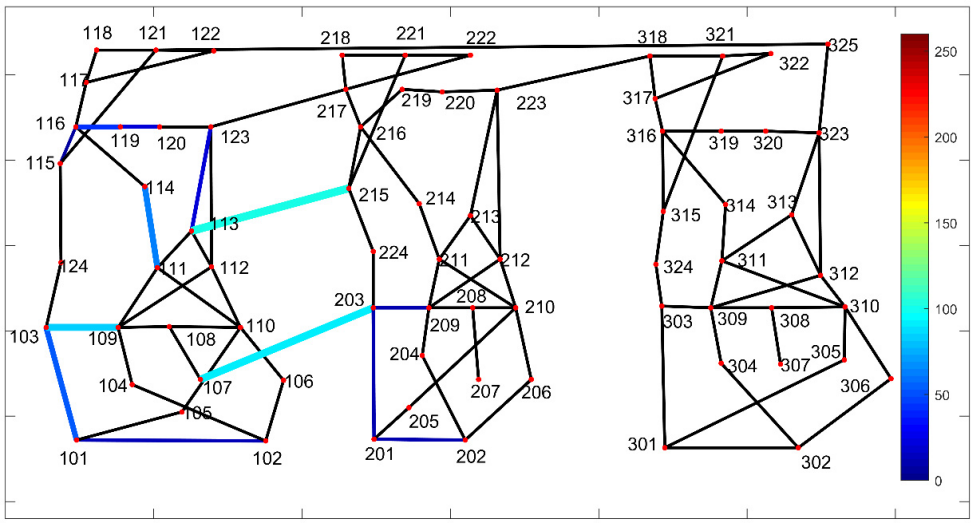

Fig. 7.9. Visualization of circuit risk (after risk mitigation)

7.6 Summary

To monitor system stress in handling cascading events, the risk-based indicator is proposed for steady-state power system, as actionable stress indicator, which measures the ability in assessing overloading consequences brought by cascading events.

- Develop a systematic procedure to calculate risk indicators, and utilize the propagation risk to determine the propagation of cascading sequence, thus constructing the cascading tree. The cascading tree risk to evaluate the propensity of cascading events under a specific operating point. The circuit risk is applied to identify weak area in current power system.
- K^{th}-order power flow is calculated using Successive-LODF, which can realize the calculation efficiency when successive cascading events are involved. Thus, the risk-based stress monitor indicator is expected to have a promising application in practice.

CHAPTER 8. SUMMARY

8.1 Summary of contributions and work

Motivated by the challenge of solving the infeasible SCED problem, a risk metric is developed to evaluate the system security level. Based on this, a method of risk-based constraint relaxation is formulated for the SCED with a single time-interval approach and with a multiple time-interval approach, where the multiple time-interval formulation utilizes the theory of look-ahead dispatch, as well as the RBCR model is built with integration of stochastic factors. Furthermore, the framework of cascading assessment is proposed by implementing a risk-based stress indicator for cascading contingencies, which identifies a weak circuit or group of circuits within power systems. Exposure to high cascading risk can be mitigated by reducing the loading on such circuits that are certainly not good candidates for performing constraint relaxation. In brief, this research has two aspects of major contributions, which are summarized as follows:

1. Developed the methodology of constraint relaxation decision-making within the framework of SCED, for both single time-interval and multiple time-interval approaches.

The specific achievements related to this contribution are as follows:

(1) Developed the methodology of deterministic risk-based constraint relaxation.

The family of risk metrics includes the system risk, the critical contingency risk and the second contingency circuit risk. These metrics are used to evaluate the system security level under all pre-defined contingencies, which can include an N-k (k>=1) event, ranging from loss of a single element ('N-1') to loss of an entire substation (in which event k can be as high as 10 or even 20). The risk-based constraint relaxation model for solving infeasible SCED within a single time-interval was formulated. This model allows overloading in specific circuits while controlling the

system security level. This is realized by restricting the risk metric to within the pre-determined limits. The proposed methodology is verified in a representative IEEE test system, indicating that D-RBCR is effective in redistributing flows to increase loading on low-risk circuits and decrease loading on high-risk circuits, which is an approach that decreases the overall stress on the network. In addition, the D-RBCR methodology does not require a penalty price, which is an attribute that mitigates LMP spikes.

(2) Developed the methodology of predictive risk-based constraint relaxation.

The traditional conductor power flow management is shifted to conductor temperature management, which results in identifying actual temperature limitation for conductors that comprise the current-carrying circuits. The application of the dynamic heat balance equation relates the power flow along transmission circuits to the conductor temperature. The relaxation level achieved in this way is more precise. This methodology is developed to handle constraint relaxations that result from pre-contingency constraints as well as those that result from post-contingency constraints. The application of the predictive RBCR makes use of inter-temporal effects and prepares the power system at a time-interval for subsequent system change in the next time-intervals; this multi-interval dispatch achieves economic benefits beyond that obtained from a single-interval dispatch. The proposed methodology is tested and investigated on both an IEEE test system and the contrived network of an actual ISO system.

(3) Develop the methodology of stochastic risk-based constraint relaxation.

To evaluate stochastic factors associated with the SCED problem, the concept of CVaR is adopted in the development of stochastic risk metric for conducting constraint relaxation within stochastic power scheduling problems. The set of risk metric includes the circuit CVaR, the

contingency CVaR and the system CVaR. Furthermore, two-step optimization framework of S-RBCR is tested and verified on the representative IEEE test system.

2. **Develop the methodology of risk-based cascading assessment**

   This is realized by proposing and implementing actionable stress monitor indicator for steady-state power system analysis, i.e., risk-based stress indicator for successive cascading contingencies.

   The specific achievements related to this contribution are as follows:

   Develop a set of risk indicators–the propagation risk (to develop the high-risk cascading sequence), the cascading sequence risk (to evaluate the system security level under a particular cascading sequence), the circuit risk (to identify weak area), the cascading tree risk (to assess the propensity of cascading events under a particular operating point). Nevertheless, the detailed flowchart is constructed to develop the high-risk cascading tree; it covers the approach to detect and to deal with the isolated system, which is incurred by a contingency event. The development of cascading tree is illustrated on a representative IEEE test system.

8.2 Future work

Based on the achievements on the methodology of risk-based decision making and risk-based cascading assessment, some promising future research directions are suggested as follows:

(1) Extend this risk-based methodology to address congestion management in the forward market (SCUC). With the introduction of integer variables, the model complexity is increased significantly; the definition of risk indices should be adjusted and improved to adapt to the corresponding market procedures and the operating criteria in DAM.

(2) Apply this risk-based methodology to the research market behavior of market participants. Utilize the risk-based decision-making theory to assist market participant to achieve

competitive bidding strategies when they participant in the electricity market. The involvement of risk attitude is also of great interest, since the acceptance level to risk has significant impacts on market participants behaviors.

(3) Utilize the risk-based methodology for other popular market products, such as the ancillary service market and the transmission congestion contracts market. Risk issues are also frequently observed on the secondary energy market, besides the primary energy market. Thus, the risk-based methodology can also be extended to such markets, to help develop more optimized market design, from the perspective of risk.

(4) Integrate dynamic factors in risk-based stress monitoring for cascading contingencies. Dynamic factors, such as voltage performance, can also be utilized as additional criteria to generate high-risk cascading contingencies. The relationship between steady-state factors and dynamic factors can be either the cooperative category or 'master-slave' category.

REFERENCES

[1] MISO Market Subcommittee Presentation, "Constraint Relaxation Status Updates". https://www.misoenergy.org/Library/Repository/Meeting%20Material/Stakeholder/MSC/2011/20110628/20110628.

[2] S. Maslennikov and E. Litvinov, "Adaptive Emergency Transmission Rates in Power System and Market Operation," IEEE Transactions on Power Systems, vol.24, no.2, pp.923-929, May 2009.

[3] V. Miranda and L. Proenca, "Why Risk Analysis Outperforms Probabilistic Choice as the Effective Decision Support Paradigm for Power System Planning", IEEE Transactions on Power Systems, vol.13, no.2, pp. 643-648, May 1998.

[4] P. Linares, "Multiple Criteria Decision Making and Risk Analysis as Risk Management Tools for Power System Planning", IEEE Transactions on Power Systems, vol.17, no.3, pp. 895-900, Aug. 2002.

[5] W. Li, P. Choudhury, D. Gillespie, and J. Jue, "A Risk Evaluation Based Approach to Replacement Strategy of Aged HVDC Components and its Application at BCTC", IEEE Transactions on Power Delivery, vol.22, no.3, pp. 1834-1840, 2007.

[6] A. Janjic and D. Popovic, "Selective Maintenance Schedule of Distribution Networks Based on Risk Management Approach", IEEE Transactions on Power Systems, vol.22, no.2, pp. 597-604, 2007.

[7] G. Strbac, R. Moreno, D. Pudjianto, and M. Castro, "Towards a Risk-Based Network Operation and Design Standards", IEEE Power and Energy Society General Meeting. Detroit, MI, July 2011.

[8] T. Zheng and E. Litvinov, "Operational Risk Management in the Future Grid Operation", IEEE Power and Energy Society General Meeting. Detroit, MI, July 2011.

[9] P. Varaiya, F. Wu and J. Bialek, "Smart Operation of Smart Grid: Risk-Limiting Dispatch", Proceedings of IEEE, vol.99, no.1, pp. 40-57, Jan. 2011.

[10] Q. Wang, J. McCalley, T. Zheng and E. Litvinov, "A Computational Strategy to Solve Preventive Risk-Based Security-Constrained OPF," IEEE Transactions on Power Systems, vol.28, no.2, pp.1666-1675, May 2013.

[11] Q. Wang, G. Zhang, J. McCalley, T. Zheng and E. Litvinov, "Risk-Based Locational Marginal Pricing and Congestion Management," IEEE Transactions on Power Systems, vol.29, no.5, pp.2518-2528, Sept. 2014.

[12] Shaun Johnson. NYISO Day-Ahead Market Overview. https://www.ferc.gov/CalendarFiles/20110628072825-Jun28-SesA1-Johnson-NYISO.pdf

[13] New York Independent System Operator. NYISO Market Participant User Guide. http://www.nyiso.com/public/webdocs/markets_operations/documents/Manuals_and_Guides/Guides/User_Guides/mpug.pdf

[14] California Independent System Operator. Market process and products in CAISO. https://www.caiso.com/market/Pages/MarketProcesses.aspx

[15] Mid-continent Independent System Operator. MISO overview training. https://www.misoenergy.org/Library/Repository/Meeting%20Material/Stakeholder/Training%20Materials/100%20Level%20Training/Level%20100%20-%20MISO%20Overview.pdf

[16] New York Independent System Operator. NYISO Day-Ahead Scheduling Manual. http://www.nyiso.com/public/webdocs/markets_operations/documents/Manuals_and_Guides/Manuals/Operations/dayahd_schd_mnl.pdf

[17] California Independent System Operator. Price Inconsistency Market Enhancements-Issue Paper &Straw Proposal. https://www.caiso.com/Documents/IssuePaper_StrawProposal-PriceInconsistencyMarketEnhancements.pdf

[18] Y. Al-Abdullah, "Energy Market Transparency: Analyzing the impacts of constraint relaxation and out-of-market correction practices in electric energy markets," Ph.D. Dissertation, Arizona State University, May 2016.

[19] A. Pillay, S. Karthikeyan, and D. Kothari, "Congestion management in power systems – a review," International Journal of Electrical Power and Energy Systems," 70 (2015): 83-90.

[20] Personal Communication with market expert, Dr. Yonghong Chen, Principal Advisor at MISO, conducted by Dr. J. McCalley. School of Electrical and Computer Engineering, Iowa State University, 2017.

[21] Mid-continent Independent System Operator. Transmission Constraint Demand Curve Proposal. Materials for November MSC, 2012.

[22] New York Independent System Operator. Transmission congestion pricing. MIWG materials. http://www.nyiso.com/public/webdocs/markets_operations/committees/bic_miwg/meeting_materials/2016-12-21/Constraint%20Reliability%20Margin%20CRM.pdf

[23] New York Independent System Operator. MMU Assessment of the Graduated Transmission Demand Curve Implementation. MIWG meetings. http://www.nyiso.com/public/webdocs/markets_operations/committees/bic_miwg/meeting_materials/2016-11-03/Evaluation%20of%20Potential%20Market%20Problem%20by%20MMU_11-02-2016_final.pdf

[24] New York Independent System Operator. Transmission constraint pricing. BIC meeting.

[25] California Independent System Operator, "Parameter Tuning for Uneconomic Adjustments in the MRTU Market Optimizations". May 2008. https://www.caiso.com/Documents/DraftFinalProposal-Parameter Tuning Uneconomic AdjustmentsinMRTUMarketOptimization09-Jun-2008.pdf

[26] Electric Reliability Council of Texas, "Setting the Shadow Price Caps and Power Balance Penalties in Security Constrained Economic Dispatch", Wholesale Market Operations, Oct.2010.

[27]Electric Reliability Council of Texas, "SCED Power Balance Penalty Curve". ERCOT Business Practice.

[28] ISO New England, "2009 Assessment of the Electricity Markets in New England", External Market Monitor, June 2010.

[29] Pennsylvania-Jersey-Maryland (PJM), "Order On Compliance Filing," issued April 2012.

[30] South Power Pool. 2016 Annual VRL Analysis for SPP market. https://www.spp.org/documents/40439/2015_2016%20vrl%20analysis.pdf

[31] New York Independent System Operator. Markets & Operations Data. http://www.nyiso.com/public/markets_operations/market_data/power_grid_data/index.jsp

[32] New York Independent System Operator. Sub-zone boundaries. http://www.nyiso.com/public/webdocs/markets_operations/documents/Manuals_and_Guides/Manuals/Additional_Manuals/tablea1_subzone_boundaries.pdf

[33] B. Stott and E. Hobson, "Power System Security Control Calculations Using Linear Programming, Part II," IEEE Transactions on Power Apparatus and Systems, vol.PAS-97, no.5, pp.1721-1731, Sept. 1978.

[34] B. Stott and J. Marinho, "Linear Programming for Power-System Network Security Applications," IEEE Transactions on Power Apparatus and Systems, vol.PAS-98, no.3, pp.837-848, May 1979.

[35] M. Irving and M. Sterling, "Economic Dispatch of Active Power with Constraint Relaxation," IEE Proceedings C on Generation, Transmission and Distribution, vol.130, no.4, pp.172-177, July 1983.

[36] S. Zhang and M. Irving, "Analytical Algorithm for Constraint Relaxation in LP-based Optimal Power Flow," IEE Proceedings C on Generation, Transmission and Distribution, vol.140, no.4, pp.326-330, July 1993.

[37] O. Alsac, J. Bright, M. Prais, and B. Stott, "Further Developments in LP-Based Optimal Power Flow," IEEE Transactions on Power Systems, vol.5, no.3, pp.697-711, Aug. 1990.

[38] Mid-continent ISO, "Filing of the Midcontinent Independent System Operator, Inc., to Revise Its Tariff to Add a Transmission Constraint Demand Curve", FERC Docket No. ER13-2295-000.

[39] Mid-continent ISO, "Constraint Relaxation Update", Market Subcommittee, May 1, 2012. https://www.misoenergy.org/Library/Repository/Meeting%20Material/Stakeholder/MSC/2012/20120605/20120605%20MSC%20Item%2003a%20Constraint%20Relaxation.pdf

[40] M. Ni, J. McCalley, V. Vittal, etc. "Software implementation of online risk-based security assessment," IEEE Transactions on power systems, vol.18, no.3, pp.1165- 1172, Aug. 2003.

[41] J. McCalley, V. Vittal, and N. Abi-Samra, "An overview of risk based security assessment," IEEE Power Engineering Society Summer Meeting, 1999., vol.1, no., pp.173-178, Jul 1999.

[42] D. Niebur and A.J. Germond, "Power System Static Security Assessment Using the Kohonen Neural Network Classifier", IEEE Transaction on Power Systems, vol.7, no.2, pp.865-872, May 1992.

[43] F. Xiao, J. McCalley, Y. Ou, et al., "Contingency Probability Estimation Using Weather and Geographical Data for On-Line Security Assessment," Int. Conf. on Prob. Methods Applied to Power Syst., Stockholm, June 2006.

[44] J. McCalley, F. Xiao, Y. Jiang, et al., "Computation of Contingency Probabilities for Electric Transmission Decision Problems," Proc. of the 13th Int. Conf. on Intelligent Syst. Appl. to Power Syst., Arlington, Nov. 2005.

[45] G. Grimmett and D. Stirzaker, Probability and Random Process, 3rd ed., Oxford University Press, 2001.

[46]Qin Wang, "Risk-Based Security-Constrained Optimal Power Flow: Mathematical Fundamentals, Computational Strategies, Validation and Use Within Electricity Markets," Ph.D. dissertation, Dept. of ECpE, Iowa State Univ., Ames, IA, 2013.

[47] A. Geoffrion, "Generalized Benders decomposition", Optimization Theory Application., vol. 10, no. 4, pp. 237–260, 1972.

[48] F. Xiao and J. McCalley, "Risk-Based Security and Economy Tradeoff Analysis for Real-Time Operation," IEEE Transactions on Power Systems, vol.22, no.4, pp.2287-2288, Nov. 2007.

[49] Transmission and Distribution Committee. "IEEE Standard for Calculating the Current-Temperature Relationship of Bare Overhead Conductors". IEEE Std 738™-2012.

[50] ISO New England. "Procedures for determining and implementing transmission facility ratings in New England". ISO New England planning procedure No.7.

[51] Oncor's pioneering transmission dynamic line rating demonstration lays foundation for follow-up developments. Oncor, May 2014.

[52] F. Qiu and J. Wang, "Distributionally Robust Congestion Management with Dynamic Line Ratings," in IEEE Transactions on Power Systems, vol. 30, no. 4, pp. 2198-2199, July 2015.

[53] C. J. Wallnerström, Y. Huang and L. Söder, "Impact from Dynamic Line Rating on Wind Power Integration," in IEEE Transactions on Smart Grid, vol. 6, no. 1, pp. 343-350, Jan. 2015.

[54] Bolun Xu, A. Ulbig and G. Andersson, "Impacts of dynamic line rating on power dispatch performance and grid integration of renewable energy sources," Innovative Smart Grid Technologies Europe (ISGT EUROPE), 2013 4th IEEE/PES, Lyngby, 2013, pp. 1-5.

[55] B. Banerjee, D. Jayaweera, and S. M. Islam, "Alleviating PostContingency Congestion Risk of Wind Integrated Systems with Dynamic Line Ratings," in Universities Power Engineering Conference (AUPEC), 2014 24th Australasian, 2014.

[56] B. Banerjee, D. Jayaweera, and S. M. Islam, "Optimal scheduling with dynamic line ratings and intermittent wind power," in PES General Meeting | Conference & Exposition, 2014 IEEE, 2014, pp. 1-5

[57] M. Wang and X. Han, "Study on Electro-thermal Coupling Optimal Power Flow Model and Its Simplification," in IEEE Power & Energy Soc. General Meeting, Minneapolis, 2010.

[58] N. Alguacil, M. Banakar and F. Galiana, "Electrothermal Coordination Part II: Case Studies," IEEE Trans. Power Syst., vol. 20, no. 4, pp. 1738-1745, 2005.

[59] M. Nick; O. Alizadeh-Mousavi; R. Cherkaoui; M. Paolone, "Security Constrained Unit Commitment With Dynamic Thermal Line Rating," in IEEE Transactions on Power Systems, vol.PP, no.99, pp.1-12

[60] A. Wood and B. Wollenberg, Power Generation, Operation and Control, 2nd. New York, NY, USA: Wiley, 1996.

[61] J. Wang, M. Shahidehpour, and Z. Li, "Security-constrained unit commitment with volatile wind power generation," IEEE Trans. Power Syst., vol. 23, no. 3, pp. 1319–1327, Aug. 2008.

[62] P. Ruiz, C. Philbrick, E. Zak, K. Cheung, and P. Sauer, "Uncertainty management in the unit commitment problem," IEEE Trans. Power Syst., vol. 24, no. 2, pp. 642–651, May 2009.

[63] H. Gangammanavar, S. Sen and V. M. Zavala, "Stochastic Optimization of Sub-Hourly Economic Dispatch with Wind Energy," in IEEE Transactions on Power Systems, vol. 31, no. 2, pp. 949-959, March 2016.

[64] Y. Gu, L. Xie, "Stochastic Look-Ahead Economic Dispatch with Variable Generation Resources," in IEEE Transactions on Power Systems, no.99, pp.1-13.

[65] J. Zhang, J. Pu, J. D. McCalley, H. Stern and W. A. Gallus, "A Bayesian approach for short-term transmission line thermal overload risk assessment," in IEEE Transactions on Power Delivery, vol. 17, no. 3, pp. 770-778, Jul 2002.

[66] Conditional value at risk–CVaR.
http://www.investopedia.com/terms/c/conditional_value_at_risk.asp.

[67] G. Zhang and J. McCalley, "Stochastic look-ahead economic dispatch with flexible ramping product," 2015 IEEE Power & Energy Society General Meeting, Denver, CO, 2015, pp. 1-5.

[68] B. Wang; Hobbs, B.F., "Flexiramp market design for real-time operations: Can it approach the stochastic optimization ideal," 2013 IEEE Power and Energy Society General Meeting (PES), pp. 21-25, July 2013.

[69] Morales. J. M., Conejo. A. J., Madsen. H. and Pinson. P.; Zugno. M., Integrating Renewables in Electricity Markets, Operational Problems. New York: Springer, 2014.

[70] Wind Resource Integration–the NYISO Approach. http://www.nedo.go.jp/english/ired2014/program/pdf/s4/s4_1_2_emilie_nelson.pdf.

[71] Mid-continent ISO. 2011 state of the market report for the MISO electricity markets. https://www.misoenergy.org/Library/Repository/Report/IMM/2011%20State%20of%20the%20Market%20Report.pdf.

[72] M. Glavic, D.Novosel, E. Heredia, etc., "Real-time voltage control under stressed conditions-See it fast to keep calm," IEEE Power& Energy Magazine, July/August 2012.

[73] P. Kessel and H. Glavitsch, "Estimating the voltage stability of a power system," IEEE Trans. Power Del., vol. 1, no. 3, pp. 346–354, Jul. 1986.

[74] M. Glavic and T. Van Cutsem, "A Short Survey of Methods for Voltage Instability Detection," Proc. 2011 IEEE PES General Meeting, San Diego (USA), Jul. 2011.

[75] J. Van Hecke (convenor), N.D. Hatziargyriou and T. Van Cutsem (editors), "Indices predicting voltage collapse including dynamic phenomena," Report of CIGRE working group, CIGRE Publication, 1994.

[76] IEEE/PES, Power System Stability Subcommittee, Voltage stability assessment: Concepts, practices and tools, 2002.

[77] R. Diao, K. Sun, V. Vittal, R. J. O'Keefe, etc., "Decision tree-based online voltage security assessment using PMU measurements," IEEE Trans. Power Syst., vol. 24, no. 2, pp. 832–839, May 2009.

[78] Dobson and L. Lu, "New methods for computing a closest saddle node bifurcation and worst case load power margin for voltage collapse," IEEE Trans. Power Syst., vol. 8, no. 3, pp. 905-913, Aug. 1993.

[79] S. Greene, I. Dobson, and F. Alvarado, "Sensitivity of the loading margin to voltage collapse with respect to arbitrary parameters," IEEE Trans. Power Syst., vol. 12, no. 1, pp. 262-272, Feb. 1997.

[80] Q. Wang, J. McCalley, T. Zheng, and E. Litvinov, "A Computational Strategy to Solve Preventive Risk-based Security-Constrained Optimal Power Flow", IEEE Transactions on Power Systems, 2012.

[81] A. Debs, "Modern Power System Control and Operation", Kluwer, 1988.

[82] Class notes for EE 553, Iowa State University, J. McCalley, accessed November 5, 2017 http://home.eng.iastate.edu/~jdm/ee553/SensitivitiesGSF.pdf.

[83] Breadth-first search.
https://en.wikipedia.org/wiki/Breadth-first_search.

[84] RTS-96 system.
https://www2.ee.washington.edu/research/pstca/rts/pg_tcarts.htm

APPENDIX A. LMP CALCULATION

LMPs varies among geographical locations, providing economic signals for wholesale electricity markets. LMPs are defined for each bus, as the incremental production cost to satisfy the next MW of withdrawal at that bus. As indicated in Chapter 2, the LMP spike is perceived in this work as undesirable, as it stresses the market in a way that is arguably arbitrary (owing to the lack of rigor behind choice of the penalty price) and thus motivates changes to the A-CR methodology. This section derives the LMP calculation for Stage 0 (A-CR with multiple time-intervals) and Stage 2 (Optimality stage of the P-RBCR methodology).

A.1. LMP calculation in A-CR

The formulation of A-CR is repeated here with corresponding Lagrange multipliers in the parentheses, as follows. Here, system loss is neglected.

$$Min \sum_{T=1}^{NI}\left(\sum_{i=1}^{NG} c_{G,i}\times P_{i,T} + \sum_{k=0}^{NC}\sum_{l=1}^{NL} \text{Penalty}\times \alpha_{l,T}^{k}\right)$$

Subject to:

$$\sum_{m=1}^{N}\left(\sum_{i\in m} P_{i,T}\right) - \sum_{m=1}^{N} D_{m,T} = 0, T\in\{1,...,NI\} \quad (\lambda_{1,T}\geq 0)$$

$$\begin{cases} \sum_{m=1}^{N} PTDF_{l,m}^{k}\left(\sum_{i\in m} P_{i,T} - D_{m,T}\right) - \alpha_{l,T}^{k} \leq Limit_{l}^{k}, \\ k\in\{0,1,...,NC\}, l\in\{1,..,NL\}, T\in\{1,..,NI\} \end{cases} \quad (\beta_{1,l,T}^{k}\geq 0)$$

$$P_{i,T} - REG_{i,T}^{down} \geq P_{i,\min}, T\in\{1,...,NI\}\ i\in\{1,...NG\} \quad (\mu_{1,i,T}^{min}\geq 0)$$

$$P_{i,T} + REG_{i,T}^{up} \leq P_{i,\max}, T\in\{1,...,NI\}\ i\in\{1,...NG\} \quad (\mu_{1,i,T}^{max}\geq 0)$$

$$-RMP_{i}^{up} \leq \Delta T\left(P_{i,T} - P_{i,T-1}\right) \leq RMP_{i}^{up}, T\in\{2,..,NI\}, i\in\{1,...NG\} \quad (\delta_{1l,i,T}^{up}, \delta_{1u,i,T}^{up}\geq 0)$$

$$-RMP_{i}^{down} \leq \Delta T\left(P_{i,T} - P_{i.T-1}\right) \leq RMP_{i}^{down}, T\in\{2,..,NI\}, i\in\{1,...NG\} \quad (\delta_{1l,i,T}^{down}, \delta_{1l,i,T}^{down}\geq 0)$$

$$\sum_{i=1}^{NG} REG_{i,T}^{up} \geq REG_{req,T}^{up}, T\in\{1,..,NI\} \quad (\eta_{1,T}^{up}\geq 0)$$

$$\sum_{i=1}^{NG} REG_{i,T}^{down} \geq REG_{req,T}^{down}, T \in \{1,..,NI\} \quad (\eta_{1,T}^{down} \geq 0)$$

According to the LMP definition, the LMP at bus m for period T can be obtained as the partial derivative of Lagrange function. The Lagrange function across the entire operation horizon is indicated in (A.1).

$$\begin{aligned} L_1 = & \sum_{T=1}^{NI}\left(\sum_{i=1}^{NG} c_{G,i} \times P_{i,T} + \sum_{k=0}^{NC}\sum_{l=1}^{NL} \text{Penalty} \times \alpha_{l,T}^{k}\right) - \sum_{T=1}^{NI} \lambda_{1,T} \times \left(\sum_{m=1}^{N}\left(\sum_{i\in m} P_{i,T}\right) - \sum_{m=1}^{N} D_{m,T}\right) \\ & + \sum_{T=1}^{NI}\sum_{k=0}^{NC}\sum_{l=1}^{NL} \beta_{1,l,T}^{k} \times \left(\sum_{m=1}^{N} PTDF_{l,m}^{k}\left(\sum_{i\in m} P_{i,T} - D_{m,T}\right) - \alpha_{l,T}^{k} - Limit_{l}^{k}\right) \\ & + \sum_{T=1}^{NI}\sum_{i=1}^{NG} \mu_{1,i,T}^{\min} \times \left(-P_{i,T} + REG_{i,T}^{down} + P_{i,\min}\right) + \sum_{T=1}^{NI}\sum_{i=1}^{NG} \mu_{1,i,T}^{\max} \times \left(P_{i,T} + REG_{i,T}^{up} - P_{i,\max}\right) \\ & + \sum_{T=2}^{NI}\left(\delta_{1l,i,T}^{up} \times \left(-RMP_{i}^{up} - \Delta T\left(P_{i,T} - P_{i,T-1}\right)\right) + \delta_{1u,i,T}^{up} \times \left(\Delta T\left(P_{i,T} - P_{i,T-1}\right) - RMP_{i}^{up}\right)\right) \\ & + \sum_{T=2}^{NI}\left(\delta_{1l,i,T}^{down} \times \left(-RMP_{i}^{down} - \Delta T\left(P_{i,T} - P_{i,T-1}\right)\right) + \delta_{1u,i,T}^{down} \times \left(\Delta T\left(P_{i,T} - P_{i,T-1}\right) - RMP_{i}^{down}\right)\right) \\ & + \sum_{T=1}^{NI} \eta_{1,T}^{up} \times \left(-\sum_{i=1}^{NG} REG_{i,T}^{up} + REG_{req,T}^{up}\right) + \sum_{T=1}^{NI} \eta_{1,T}^{down} \times \left(-\sum_{i=1}^{NG} REG_{i,T}^{down} + REG_{req,T}^{down}\right) \end{aligned} \quad (A.1)$$

Take the partial derivative of L_1 with respect to load $D_{m,T}$, i.e., the LMP at bus i for period T is calculated as (A.2).

$$LMP_{m,T}^{1} = \frac{\partial L_1}{\partial D_{m,T}} = \lambda_{1,T} - \sum_{k=0}^{NC}\sum_{l=1}^{NL}\left(\beta_{1,l,T}^{k} \times \sum_{m=1}^{N} PTDF_{l,m}^{k}\right) \quad (A.2)$$

In reference to convex optimization theory, the Karush-Kuhn-Tucker (KKT) conditions are imposed at the optimal point. Thus,

$$\frac{\partial L_1}{\partial \alpha_{l,T}^{k}} = \text{Penalty} - \beta_{1,l,T}^{k} = 0 \quad (A.3)$$

Then, by substituting (A.3) into (A.2), the LMP can be converted into (A.4).

$$LMP_{m,T}^{1} = LMP_{m,T}^{1,energy} + LMP_{m,T}^{1,congestion} = \lambda_{1,T} - \sum_{k=0}^{NC}\sum_{l=1}^{NL}\left(Penalty \times \sum_{m=1}^{N} PTDF_{l,m}^{k}\right) \quad (A.4)$$

Since it does not consider the power loss along transmission lines, the loss component of LMP is zero[14]. Therefore, the energy component is the shadow price of the power balance equation, which is set by the bid of the marginal unit, which is the unit that would supply the next MW of load over the requirements. The energy component is the same across the entire network. On the other hand, the congestion component is the by-product of transmission constraints, which reflects the congestion status of each specific circuit. The congestion component can have various values, which reflect the corresponding congestion level.

Another observation from (A.4) is that the selection of penalty price has significant impact on the value of the congestion component in LMP. That is the source for the LMP spike if the penalty is too high, or under pricings if the penalty is too low.

A.2. LMP calculation in optimality stage of the P-RBCR

The formulation of optimality stage of the P-RBCR is repeated here with the corresponding Lagrange multipliers in parentheses, as follows:

$$Min \sum_{T=1}^{NI}\sum_{i=1}^{NG} c_{G,i} \times P_{i,T}$$

Subject to:

$$\sum_{m=1}^{N}\left(\sum_{i\in m} P_{i,T}\right) - \sum_{m=1}^{N} D_{m,T} = 0, T \in \{1,...,NI\} \qquad (\lambda_{2,T} \geq 0)$$

$$\begin{cases} \sum_{m=1}^{N} PTDF_{l,m}^{k}(\sum_{i\in m} P_{i,T} - D_{m,T}) \leq Limit\_new_{l}^{k}, \\ k \in \{0,1,...,NC\}, l \in \{1,..,NL\}, T \in \{1,..,NI\} \end{cases} \quad (\beta_{2,l,T}^{k} \geq 0)$$

$$P_{i,T} - REG_{i,T}^{down} \geq P_{i,\min}, T \in \{1,...,NI\}\ i \in \{1,...NG\} \quad (\mu_{2,i,T}^{min} \geq 0)$$

$$P_{i,T} + REG_{i,T}^{up} \leq P_{i,\max}, T \in \{1,...,NI\}\ i \in \{1,...NG\} \quad (\mu_{2,i,T}^{max} \geq 0)$$

[14] This assumption is reasonable because the loss component takes a relatively small proportion of the whole LMP value; the dominant component of the LMP is the congestion component, which can be a significant contributor to the LMP spike caused by CR.

$$-RMP_i^{up} \le \Delta T\left(P_{i,T} - P_{i,T-1}\right) \le RMP_i^{up}, T \in \{2,..,NI\}, i \in \{1,...NG\} \quad (\delta_{2l,i,T}^{up}, \delta_{2u,i,T}^{up} \ge 0)$$

$$-RMP_i^{down} \le \Delta T\left(P_{i,T} - P_{i.T-1}\right) \le RMP_i^{down}, T \in \{2,..,NI\}, i \in \{1,...NG\} \quad (\delta_{2l,i,T}^{down}, \delta_{2l,i,T}^{down} \ge 0)$$

$$\sum_{i=1}^{NG} REG_{i,T}^{up} \ge REG_{req,T}^{up}, T \in \{1,..,NI\} \quad (\eta_{2,T}^{up} \ge 0)$$

$$\sum_{i=1}^{NG} REG_{i,T}^{down} \ge REG_{req,T}^{down}, T \in \{1,..,NI\} \quad (\eta_{2,T}^{down} \ge 0)$$

Here, system loss is neglected. According to the incremental cost definition of price, the LMP at bus m for period T can be calculated by taking the partial derivative of Lagrange function. The Lagrange function across the entire operation horizon is indicated in (A.5).

$$\begin{aligned} L_2 = & \sum_{T=1}^{NI}\left(\sum_{i=1}^{NG} c_{G,i} \times P_{i,T} + \sum_{k=0}^{NC}\sum_{l=1}^{NL} \text{Penalty} \times \alpha_{l,T}^k\right) - \sum_{T=1}^{NI} \lambda_{2,T} \times \left(\sum_{m=1}^{N}\left(\sum_{i \in m} P_{i,T}\right) - \sum_{m=1}^{N} D_{m,T}\right) \\ & + \sum_{T=1}^{NI}\sum_{k=0}^{NC}\sum_{l=1}^{NL} \beta_{2,l,T}^k \times \left(\sum_{m=1}^{N} PTDF_{l,m}^k \left(\sum_{i \in m} P_{i,T} - D_{m,T}\right) - Limit\_new_l^k\right) \\ & + \sum_{T=1}^{NI}\sum_{i=1}^{NG} \mu_{2,i,T}^{\min} \times \left(-P_{i,T} + REG_{i,T}^{down} + P_{i,\min}\right) + \sum_{T=1}^{NI}\sum_{i=1}^{NG} \mu_{2,i,T}^{\max} \times \left(P_{i,T} + REG_{i,T}^{up} - P_{i,\max}\right) \\ & + \sum_{T=2}^{NI}\left(\delta_{2l,i,T}^{up} \times \left(-RMP_i^{up} - \Delta T\left(P_{i,T} - P_{i,T-1}\right)\right) + \delta_{2u,i,T}^{up} \times \left(\Delta T\left(P_{i,T} - P_{i,T-1}\right) - RMP_i^{up}\right)\right) \\ & + \sum_{T=2}^{NI}\left(\delta_{2l,i,T}^{down} \times \left(-RMP_i^{down} - \Delta T\left(P_{i,T} - P_{i,T-1}\right)\right) + \delta_{2u,i,T}^{down} \times \left(\Delta T\left(P_{i,T} - P_{i,T-1}\right) - RMP_i^{down}\right)\right) \\ & + \sum_{T=1}^{NI} \eta_{2,T}^{up} \times \left(-\sum_{i=1}^{NG} REG_{i,T}^{up} + REG_{req,T}^{up}\right) + \sum_{T=1}^{NI} \eta_{2,T}^{down} \times \left(-\sum_{i=1}^{NG} REG_{i,T}^{down} + REG_{req,T}^{down}\right) \end{aligned} \quad (A.5)$$

Take the partial derivative of L_2 with respect to load $D_{m,T}$, i.e., the LMP at bus i for period T is calculated as (A.6).

$$LMP_{m,T}^2 = \frac{\partial L_2}{\partial D_{m,T}} = \lambda_{2,T} - \sum_{k=0}^{NC}\sum_{l=1}^{NL}\left(\beta_{2,l,T}^k \times \sum_{m=1}^{N} PTDF_{l,m}^k\right) \quad (A.6)$$

The LMP in the P-RBCR is free of an influence from the penalty price, reducing the potential to cause an LMP spike. Transmission constraints in the CR set are binding under the

updated limits with relaxation, resulting in non-zero congestion component. The congestion components still have the ability to reflect price signals for a congested network.

APPENDIX B. DEVELOPMENT OF CONTRIVED NYISO SYSTEM

Appendix B describes the development of the mini-NYISO test system, based on the publicly available data and information. The intent of this effort is to provide a system having transmission configuration, generation fleet, load attributes, and reserve requirements that reasonably reflect the high-level corresponding features in the actual NYISO system.

B.1. Transmission grid

NYISO operates the competitive wholesale market across New York State, managing nearly 11,000 miles of high-voltage transmission lines and dispatching more than 500 electric generators. The footprint of the New York Control Area (NYCA) covers 11 aggregated loading zones, as shown in Fig.B.1. The identification of load zones is based on interface transfer capability and the regulatory area of Transmission Owners.

To reflect this network configuration, it is found in the Reliability Needs Requirement Assessment report [85] that the NYISO was represented by an 11-zone bubble model. In this research, each zone is aggregated to a single bus, and those buses are connected by 345kV transmission lines. In summary, the simplified network has the topology of 11-buses and 11 lines. For the exchange with neighboring areas, i.e., PJM, ISO-NE, Hydro Quebec and Ontario, the external transaction is modeled as fixed injection or withdrawal at the corresponding bus. For example, about 800MW of power is imported to Capital Zone from ISO-NE. Thus, the external injection is modeled as a blocked generator (800MW) with zero production cost, which is connected at Bus 6. Similarly, exports are modeled as either a blocked unit with negative output or a load injection at the corresponding bus. The proposed mini-NYISO system is presented Fig.B.2.

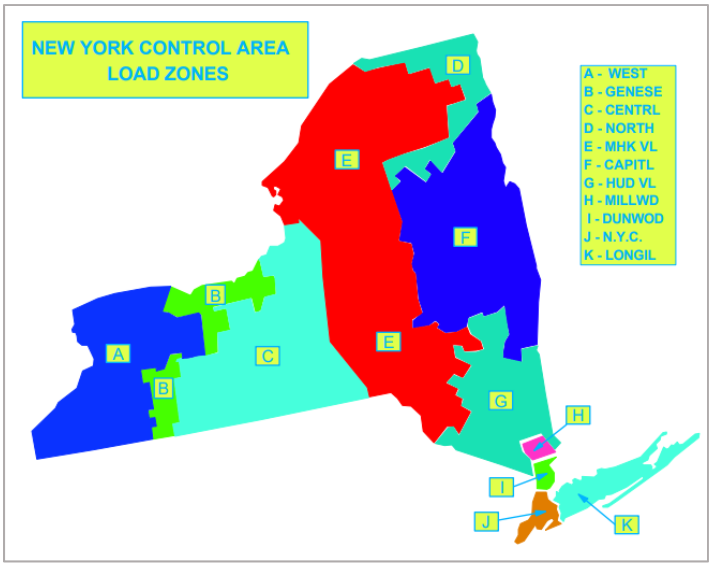

Fig.B.1. New York Control Area load zones

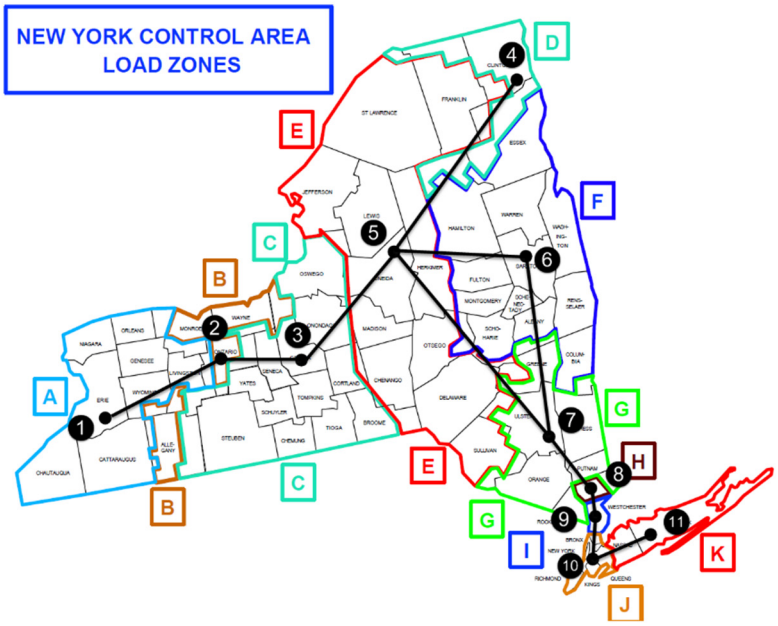

Fig.B.2. Mini-NYISO testing system

The benchmark values of resistance and reactance are approximated for those 11 lines, with consideration of physical properties of transmission lines. As mentioned above, the voltage level is 345kV. Thus, the impedance per unit (meter/mile) is determined by the conductor type, conductor bundling, conductivity of materials, and temperature. It is assumed that physical parameters of the

345kV AC transmission line are as listed in Table B.1 [86]. Thus, per unit data for impedance is derived from ACSR tables for overhead transmission lines.

Table B.1. Physical parameters of 345kV transmission line

	Conductor Type	Conductor Bundling	Constant Temperature (°C)
345kV AC lines	Dove (556 kcmil)	6-conductor bundle per phase with 2.5' diameter and 45' to separate phases	25 °C

Another attribute contributing to impedance of the entire transmission line is the total length of each modeled line. Several counties are located in the footprint of each loading zone, and the geographical information (pairs of latitude and longitude) for each county is available online. Thus, each bus is assumed to be located at the centered county of that zone. Furthermore, the length of each line can be calculated using the two pairs of latitudes and longitudes. The attributes for transmission lines are summarized in Table B.2.

Table B.2. Benchmark values of impedance for the 11-zone mini-NYISO test system

Interface name	**From Zone**	**To Zone**	**Distance (miles)**	**Resistance (ohms)**	**Reactance (ohms)**	**Reactance (per unit)**
DYSINGER EAST	West	Genessee	76	12.70	35.95	0.03
West Central	Genessee	Central	36	5.95	16.85	0.01
Volney East	Central	Mohawk Valley	62	10.24	29.00	0.02
MOSES South	Mohawk Valley	North	139	23.06	65.30	0.05
Central EAST	Mohawk Valley	Capital	79	13.16	37.26	0.03
UPNY/SENY	Capital	Hudson valley	84	13.91	39.40	0.03
UPNY/CONED	Hudson valley	Millwood	39	6.42	18.17	0.02
MILLWOOD SOUTH	Millwood	Dunwoodie	21	3.43	9.73	0.01
SPRAINBROOK/DUNWOODIE SOUTH	Dunwoodie	NYC	29	4.76	13.46	0.01
CON ED/LILCO	NYC	Long Island	52	8.63	24.44	0.02
Marcy South	Mohawk Valley	Hudson valley	108	17.94	50.80	0.04

B.2. Generator attributes

The next step is to represent the capacity mix in the NYISO. To achieve a reasonable trade-off between generality and complexity, generators with the same technology type and located in the same loading zone is modeled as a single generator, which has the aggregated capacity.

EIA [87] provides the operating generator capacity by state. The generators affiliated to NY state are filtered and are mapped to loading zones based on its geographical location[15]. There are 1038 units located in New York Control Area, and the breakdown by technology type is represented by the pie chart in Fig.B.3. As shown in the pie chart, gas turbines dominate the capacity mix, followed by nuclear power units and hydro units. Biomass, solar PV and storage (flywheel units) are neglected since those units do not have much contribution to the total capacity.

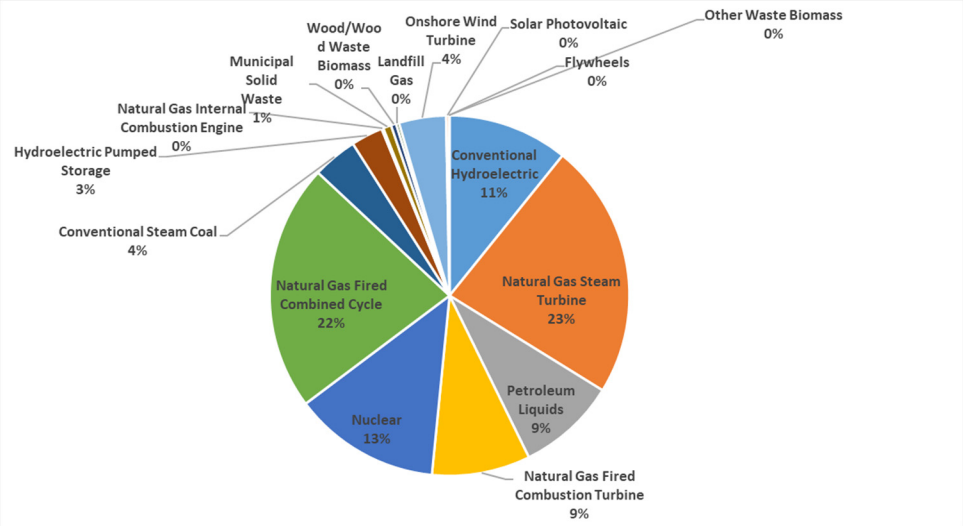

Fig.B.3. Pie chart of generation capacity by technology type in NYISO from EIA

The technology types are re-categorized to common types–natural gas, hydro (conventional hydro or pumped storage), nuclear, coal, wind and oil. Thus, the capacity mix in the mini-NYISO system is provided in Fig.B.4. In comparison with the actual capacity mix of the NYISO system

[15] Since some county are across several load zones, especially in the southeastern area, the zonal information of some units involved are approximated based on the best knowledge available.

[88] from 2016 Power Trend, as shown in Fig.B.4, the capacity mix in the mini-NYISO system is able to reflect the fuel structure for the real-world system. Fig.B.5 represents the capacity proportion by fuel type for each loading zone.

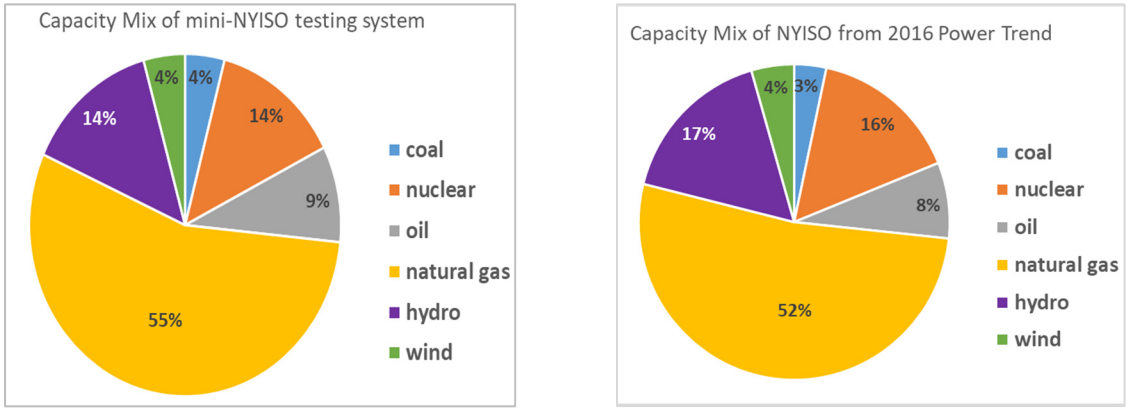

(a) Capacity mix of mini-NYISO testing system (b)Capacity mix of the NYISO from 2016 Power Trend

Fig.B.4. Capacity mix comparison between the mini-NYISO and actual NYISO system

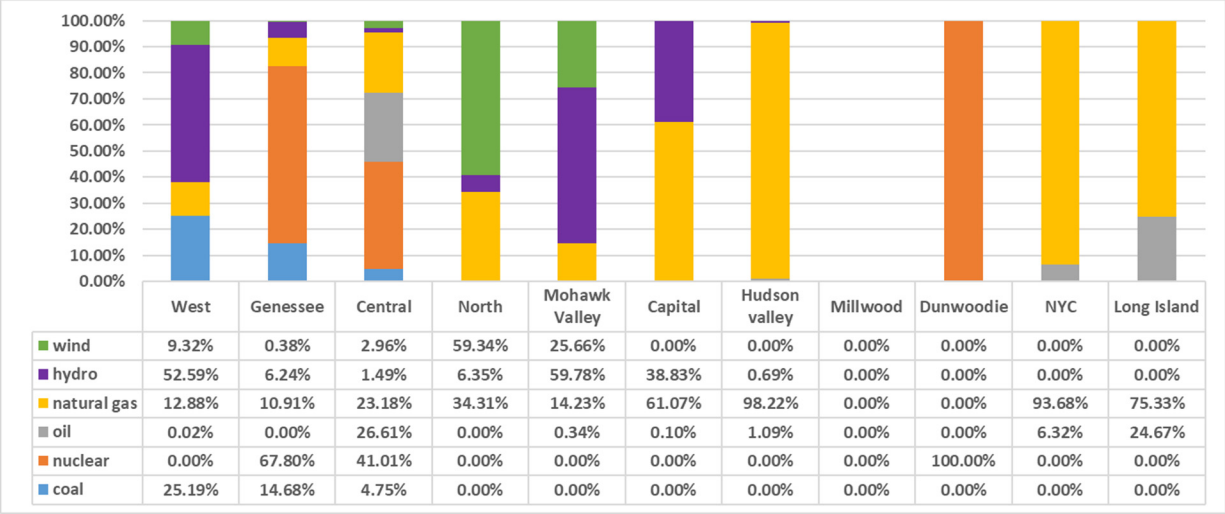

	West	Genessee	Central	North	Mohawk Valley	Capital	Hudson valley	Millwood	Dunwoodie	NYC	Long Island
wind	9.32%	0.38%	2.96%	59.34%	25.66%	0.00%	0.00%	0.00%	0.00%	0.00%	0.00%
hydro	52.59%	6.24%	1.49%	6.35%	59.78%	38.83%	0.69%	0.00%	0.00%	0.00%	0.00%
natural gas	12.88%	10.91%	23.18%	34.31%	14.23%	61.07%	98.22%	0.00%	0.00%	93.68%	75.33%
oil	0.02%	0.00%	26.61%	0.00%	0.34%	0.10%	1.09%	0.00%	0.00%	6.32%	24.67%
nuclear	0.00%	67.80%	41.01%	0.00%	0.00%	0.00%	0.00%	0.00%	100.00%	0.00%	0.00%
coal	25.19%	14.68%	4.75%	0.00%	0.00%	0.00%	0.00%	0.00%	0.00%	0.00%	0.00%

Fig.B.5. Capacity proportion for fuel type by loading zones

To reflect the fact that the capacity of some generators is not fully utilized, the capacity factor is deployed to represent the relationship between the actual generation output and the rated capacity. Those generators participate in SCED and incur production cost; they have the limitations

on ramping capabilities. Table B.3 lists typical values for the generator marginal cost (per EIA data [89]) and ramping rate.

Table B.3. Generator attributes by resource types

Technology type	Nuclear	Coal	Hydro	Gas Turbine	Oil	Wind
Marginal cost ($/MWh)	25.71	37.26	13.42	33.24	45	0
Ramping rate (MW/min)	2.0	2.0	/	6.7	2.0	/

B.3. LSE attributes

Per requirements from the NYISO Tariff, the NYISO publishes hourly zonal load for the next several operating days and posts the actual load on a five-minute basis [90]. Those postings are utilized to generate load data appropriate for the test system.

B.4. Reserve requirements

Reserve products in the NYISO include regulation, 10-minute spinning reserve, 10-minute non-synchronized reserve, and 30-minute reserve. Regulation reserve is necessary to continuously balance load procurement with generation output. The remaining reserve products are responsible for backup generation or demand response, following occurrence of a real-time contingency. The NYISO has a nested requirement for operating reserves [91], as provided in Fig.B.6.

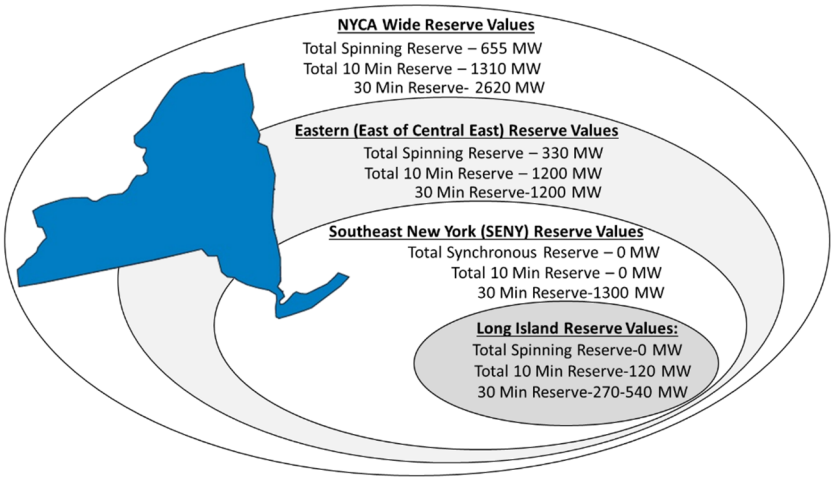

Fig.B.6. NYCA operating reserve requirement

[85] New York Independent System Operator. 2016 Reliability Needs Assessment. http://www.nyiso.com/public/webdocs/media_room/press_releases/2016/Child_2016_RNA/2016RNA_Final_Oct18_2016.pdf

[86] K., Dheepak, W. Li, and L. Tesfatsion. "An 8-zone test system based on ISO New England data: Development and application." IEEE Transactions on Power Systems 31.1 (2016): 234-246.

[87] EIA. Preliminary Monthly Electric Generator Inventory. https://www.eia.gov/electricity/data/eia860M/

[88] New York Independent System Operator. 2016 Power Trend. http://www.nyiso.com/public/webdocs/media_room/publications_presentations/Power_Trends/Power_Trends/2016-power-trends-FINAL-070516.pdf

[89] EIA. https://www.eia.gov/electricity/annual/html/epa_08_04.html

[90] New York Independent System Operator. Actual load, Market & Operations Data Archive. http://www.nyiso.com/public/markets_operations/market_data/load_data/index.jsp

[91] New York Independent System Operator. Ancillary service, training materials for NYMOC courses. http://www.nyiso.com/public/webdocs/markets_operations/services/market_training/workshops_courses/Training_Course_Materials/NYMOC_MT_ALL_201/Ancillary_Services.pdf